

# **Physiology of stem cell-derived cardiomyocytes**

**Fysiologie van stamcelafgeleide hartspiercellen**  
(met een samenvatting in het Nederlands)

Proefschrift

Ter verkrijging van de graad van doctor aan de Universiteit Utrecht op gezag van de rector magnificus, prof. dr. J.C. Stoof, ingevolge het besluit van het college voor promoties in het openbaar te verdedigen op donderdag 18 oktober 2007 des middags te 2.30 uur

door

**Teun Pieter de Boer**

geboren 6 april 1978 te Deventer

Promotor:                    prof. dr. ir. J.M.T. de Bakker  
Co-promotoren:            dr. M.A.G. van der Heyden  
                                      dr. A.A.B. van Veen

The work presented in this thesis was performed at the Department of Medical Physiology of the Division of Heart and Lungs, University Medical Center Utrecht.

The study described in this thesis was supported by a grant of the Netherlands Heart Foundation (NHF-2003B073).

Financial support by the Netherlands Heart Foundation for the publication of this thesis is gratefully acknowledged.

Financial support by the Interuniversity Cardiology Institute of the Netherlands for the publication of this thesis is gratefully acknowledged.



# **Physiology of stem cell-derived cardiomyocytes**

Fysiologie van stamcelafgeleide hartspiercellen  
(met een samenvatting in het Nederlands)

Proefschrift

door

**Teun Pieter de Boer**

geboren 6 april 1978 te Deventer

ISBN: 978-90-393-4671-6

Financial support by the J.E. Jurriaanse Foundation for the publication of this thesis is gratefully acknowledged.

Financial support by the prof. dr. R.L.J. van Ruyven Foundation for the publication of this thesis is gratefully acknowledged.

Financial support by Lead Pharma Holding B.V. for the publication of this thesis is gratefully acknowledged.

Voor Roos en mijn ouders



# Contents

1	Introduction	1
2	Connexin43 repression following epithelium-to-mesenchyme transition in embryonal carcinoma cells requires Snail1 transcription factor	11
3	Inhibition of cardiomyocyte automaticity by electrotonic application of inward rectifier current from Kir2.1 expressing cells	27
4	$\beta$ - but not $\alpha$ - adrenergic stimulation enhances conduction velocity in cultures of neonatal cardiomyocytes	37
5	Pro-arrhythmogenic potential of immature cardiomyocytes is triggered by low coupling and cluster size	51
6	TGF $\beta$ 1 induces efficient differentiation of human cardiomyocyte progenitor cells into functional cardiomyocytes in vitro	69
7	Human fetal cardiac progenitor cells can be efficiently differentiated into cardiomyocytes expressing a cardiac electrical phenotype	89
8	General discussion	105
9	Bibliography	111
10	Nederlandse samenvatting	125
11	List of publications	129
12	Dankwoord	133
13	Curriculum vitae	135



# **Chapter 1**

## **Introduction**

Teun P. de Boer

## Cardiac electrophysiology

From early embryonic development on, the heart provides the body with proper perfusion of the tissue. Starting with peristaltic contractions in the heart tube stage, the mammalian heart develops into a four chambered pump that maintains two circulations; the pulmonary and systemic circulation. Though influenced by innervation (vagal and sympathetic), the heart beats autonomously with a rhythm that is generated by the sinoatrial (SA) node located close to the superior caval vein of the right atrium. In the SA-node spontaneously active cardiomyocytes are present that are able to impose their beating rate on the surrounding atrial tissue. The impulse is propagated via the atrial myocardium toward the atrioventricular (AV) node, located at the border between atria and ventricles, right above the interventricular septum. After a delay generated by the cells of the AV-node that allows proper filling of the ventricles, the impulse is forwarded to the bundle of His. From here, the bundle branches and the Purkinje system are activated allowing rapid propagation of the electrical impulse toward the ventricles. The Purkinje system activates the working myocardium from endo- to epicardium.

This sequence of cardiac activation produces potentials that can be measured at the body surface. The resulting electrocardiogram (ECG), developed by Einthoven et al., proved to be a highly valuable tool in the clinic and laboratory to assess cardiac function non-invasively. In the ECG, activation of the atria gives rise to the P-wave, followed after the AV-delay by the QRS-complex that reflects the activation of the ventricles (see Figure 1.1A). The QRS complex is followed by the T-wave, which is the result of ventricular repolarization. Evaluation of a subject's ECG provides information on impulse formation and propagation in the heart, and can identify a myriad of rhythm disorders. Ultimately, the ECG is the sum of the electrical activity of the smallest functional units of the heart, the cardiomyocytes.

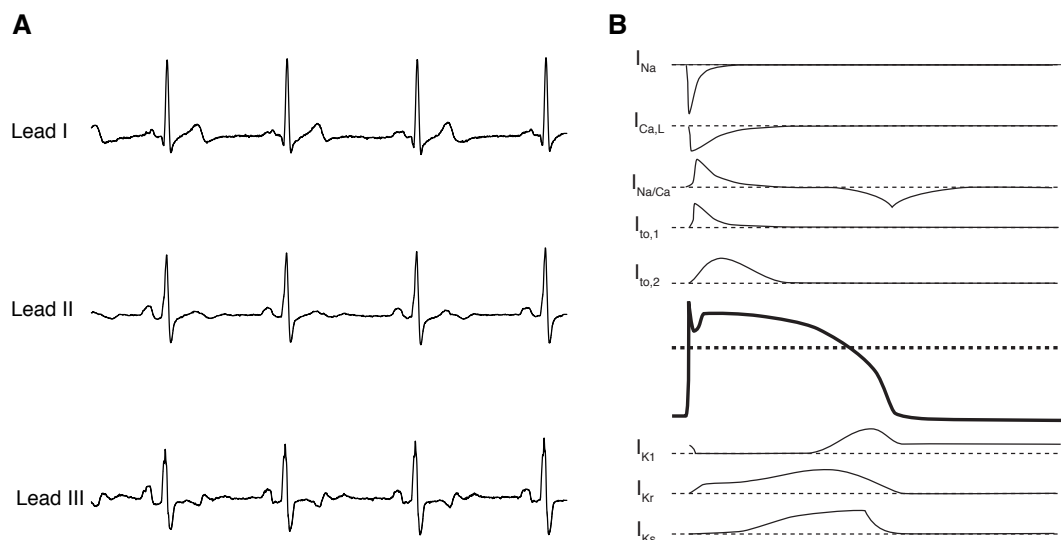


**Figure 1.1:** Electrical activity of the heart. **A:** Electrocardiogram of the author made using the Einthoven configuration. **B:** Schematic depicting ion currents underlying the adult working cardiomyocyte action potential.



*Electrical properties of cardiomyocytes* Cardiomyocytes are excitable cells, i.e. they are capable of producing transient depolarizations, called action potentials (APs), when triggered by a depolarizing stimulus large enough to reach threshold. Firing an AP results in contraction of the cell, a phenomenon called excitation-contraction coupling that depends on intracellular calcium handling (see (1)). The human AP can be divided in several phases that are linked to the activity of several ion channels.

At rest, adult human cardiomyocytes have a stable membrane potential of approximately  $-85$  mV (see Figure 1.1B). When triggered to fire an AP, a rapid depolarization to  $+40$  mV ensues (phase 0), followed by a transient repolarization (phase 1), a slow repolarization called the plateau phase (phase 2) and a relatively fast repolarization to resting membrane potential (phase 3). Finally the resting membrane potential is reached again in phase 4. The underlying mechanism allowing the action potential to occur, is an interplay between different ion channels.

Ion channel proteins form pores in the plasma membrane that selectively conduct one or more ions and their state, i.e. open or closed, is controlled by the membrane potential. It is thought that all voltage-gated ion channels have evolved from a single or small group of prokaryotic potassium channels (see (2)). The archetypical potassium channel is an assembly of four subunits, each containing two transmembrane regions which are joined by a pore-forming region. In eukaryotes, the inward rectifier channels (Kirs) are similar to the archetypical channel. During evolution, potassium channels have evolved that contain six transmembrane regions, again assembling in tetramers. Subsequently, families of calcium and sodium channels evolved that merged four domains containing the six transmembrane regions into a single protein.

The five phases of the human cardiac action potential are the result of the changing balance between the depolarizing and repolarizing current carried by specific ion channels (see Figure 1.1B). Phase 0, the rapid depolarization is caused by a fast increase in sodium conductance, which is attributable to activation of the cardiac sodium channel encoded by the *SCN5A* gene. The initial depolarization is followed by an early repolarization mediated by activation of the transient outward potassium channels, *Kv4.3*. During the plateau phase (phase 2), calcium current via the  $\alpha 1C$  channels is dominant and tries to maintain the membrane potential at a depolarized value. In the last part of the plateau phase, the potassium channels *KvLQT1* and *HERG* become predominant. These channels remain active during the first part of phase 4, which is mostly determined by the potassium conductance resulting from activation of *Kir2.1*, *2.2* and *2.3* inward rectifier channels.

*Impulse propagation in the heart* Impulse propagation in the heart is not only determined by excitability, but also depends on intercellular coupling via gap junction channels. These channels are composed of two hemichannels, which are hexamers of connexin proteins, each contributed by one of the two connected cells. There are twenty-one human connexin isoforms identified (3), but cardiomyocytes mainly express *Cx40*, *-43* or *-45*, that are differentially expressed with regard to location and function in the heart. In the working myocardium of the ventricles, *Cx43* is the main isoform and is expressed predominantly at the intercalated discs.

A third crucial factor influencing impulse propagation is the extracellular matrix. Interspersed between the cardiomyocytes are blood vessels and fibroblasts. The lat-

ter deposit a network of collagen and associated proteins in between and surrounding cardiomyocytes that provides the heart with structure and elasticity. Initially, the extracellular matrix between cells is relatively thin, but upon aging it becomes thicker, although generally this poses no threat to cardiac function. In several pathologies however, such as myocardial infarction, cardiomyocytes become apoptotic or necrotic and are replaced by collagen. This so-called replacement fibrosis may create regions of slow conduction or conduction block that promote the occurrence of arrhythmias.

Coumel was the first who realized that there are three main ingredients required for the production of an arrhythmia, the arrhythmogenic substrate, the trigger factor and the modulation factors of which the most common is the autonomic nervous system. This concept is known as Coumel's triangle (4). The arrhythmogenic substrate may be caused by structural or electrical changes that accompany cardiac disease. When several factors involved in impulse propagation are impaired, the heart becomes less resistant to the occurrence of arrhythmias. Changes in excitability, tissue architecture or intercellular coupling can provide an arrhythmogenic substrate. A related concept is that of wavelength, which is the product of conduction velocity and effective refractory period. If impulse propagation slows or refractory period shortens, wavelength will decrease and therefore the propensity of an arrhythmic event will increase.

Human cardiac diseases often cause changes in one or more than one parameter affecting conduction. As mentioned before, increased collagen deposition is found in cardiac disease, but changes in expression of ion and gap junction channels often accompany the structural alteration. However, abnormalities in ion or gap junction channels also can have a genetic basis, as seen in the long QT-syndromes, Andersen's disease, sick sinus syndromes and Naxos disease. Furthermore, adaptation processes in hearts challenged with heart failure result in so-called electrical remodeling. Depending on the nature of the disease, or the experimental intervention, changes in all cardiac ion channels have been reported. Also calcium-handling in failing hearts is known to be altered. Thorough discussion of the many possible mechanisms involved in arrhythmia are beyond the scope of this discussion, but a distinction can be made between mechanisms involving a change in the inherent excitability of the cardiomyocytes and changes that involve altered impulse propagation.

## Stem cells as a source for newly generated cardiomyocytes

Isolation of murine and later human embryonic stem cells that are capable of forming cell types from all three germ layers of the gastrula provided developmental biologists with an important tool for studying early embryonic development. Furthermore, isolation and culturing of human embryonic stem cells was envisioned as a big step towards creation of tissues that could be used clinically to repair malfunctioning organs. However, many issues such as immune rejection, heterogeneous differentiation, the possibility of tumor-formation and ethical problems have complicated this concept. At the same time, interest in adult stem cells has grown, since these can be obtained from the patient, thereby avoiding both rejection and ethical problems.

*Stem cells and cardiac cell therapy* Loss of cardiomyocytes after myocardial infarction, and therefore a deterioration of cardiac performance, can be the first step in a process

leading to heart failure. Using *de novo* created cardiomyocytes to increase the number of functional cardiomyocytes could improve cardiac performance and may help to decrease the risk of progression towards heart failure. The success of such cell therapy approaches will, excluding the patient's condition, be dependent on at least two factors, cell type and means of administration.

*Stem cell sources* Many stem cell types, ranging from bone marrow cells, skeletal myoblasts to fat cells and embryonic stem cells, have been tested for their cardiogenic potential. Despite the large number of studies conducted that reported in vitro cardiac differentiation of adult stem cells, no irrefutable evidence is obtained yet. Such claims were undermined mostly by the lack of physiological evidence of cardiac phenotype, and depended often solely on biochemical or molecular characterization of a small set of markers.

Various bone marrow-derived cells have been used for transplantation, ranging from crude preparations, cell fractions selected on the presence of a specific surface marker, to cultured cells. The initial finding that bone marrow derived cells can transdifferentiate into cardiomyocytes (5) when injected in infarcted mouse hearts elicited great enthusiasm. Later on these results were questioned because the methods used to retrieve transplanted cells were not reliable enough. Subsequently, it was convincingly demonstrated, using bone marrow from transgenic cardiac reporter mice (MHC-nLAC), that in vivo transdifferentiation into cardiomyocytes does not occur (6). Nonetheless, there are numerous reports of improved cardiac performance following transplantation of bone marrow-derived cells into infarcted heart, both from the lab and clinic (7). The underlying mechanism is unclear, but neovascularization that limits damage caused by myocardial infarction may play a role. Vasculogenesis is conceivable since there is evidence that endothelial progenitor cells are present in bone marrow, although other reports deny the role of vasculogenesis (8). Alternatively, bone marrow-derived cells may secrete factors such as cytokines that stimulate neovascularization. Thus, while cell therapy utilizing bone marrow-derived cells will probably not fulfil the promise of cardiac repair by supplementation of cardiomyocytes, it may very well prove a valuable clinical tool to decrease mortality from myocardial infarction when the positive effects can be maintained long-term.

Skeletal myoblasts are the stem cells in skeletal muscle that contribute to regeneration in vivo and can be obtained autologously from muscle biopsies. They are rather resistant to ischemia and able to proliferate in vitro. Transdifferentiation into cardiomyocytes does not occur but in clinical trials, transplantation of skeletal myoblasts resulted in improved cardiac performance (9; 10). Histologic evaluation of explanted hearts of recipients showed the presence of small patches of skeletal muscle in the myocardial wall. Earlier experimental studies had shown similar findings, along with increased cardiac performance. Unfortunately, the positive effect was accompanied by an increased propensity of ventricular tachyarrhythmias that required treatment with ICDs or anti-arrhythmic medication (11; 12). The increased arrhythmogenicity can be explained by inadequate functional integration of skeletal muscle cells in the myocardium, due to absence of connexin43, and the difference in action potential waveform of skeletal and cardiac myocytes. Given the poor safety of skeletal myoblast transplantation, its clinical application remains problematic.

Embryonic stem cells do have a well-established cardiogenic potential. Using protocols that rely on spontaneous differentiation or induction via endodermal-derived factors, reliable differentiation of cardiomyocytes is possible (13; 14; 15). Differentiation efficiencies range between 5 and 20%, which makes subsequent purification of the cardiomyocytes necessary. The phenotype of cardiomyocytes is most similar to fetal cardiomyocytes with respect to expression pattern of contractile proteins and morphology in culture. Transplantation of differentiated human embryoid bodies into the ventricular wall of pigs with complete AV-block resulted in ectopic pacing (16). Upon transplantation into rodent hearts, several studies showed integration of the embryonic stem cells (17; 18; 19). Undifferentiated embryonic stem cells were found to give rise to teratomas, but selection of cardiomyocytes prior to transplantation precluded this (20). Although technically feasible, the use of embryonic stem cells in treatment of human cardiac disease remains problematic due to ethical and immunological problems.

*Administration of stem cell-derived cardiomyocytes* Present experimental data on cell transplantation to the heart has clearly demonstrated that delivering large amounts of cells at the desired location is difficult. Common methods are intramyocardial injection and intracoronary transplantation. Both techniques are hampered by very low efficiencies; after delivery of millions of cells, the number of retrievable cells most often is dramatically low (up to a few hundred). Most likely, cells are massively lost to the systemic circulation, flow back through the injection tract or die during the procedure due to mechanical stress.

Several tissue-engineering approaches have been devised to overcome these problems. The general concept is that effectiveness should improve if the cells are provided with an extracellular matrix. This idea has been followed in two approaches (21), firstly it is possible to obtain a genuine extracellular matrix by removing cardiomyocytes from myocardial biopsies, or create a matrix *in vitro* using collagen, matrigel, alginate or other biomaterials. Such matrices can subsequently be seeded with cells and applied to the heart (22). Alternatively, liquid matrix components can be mixed with cells and using a cast, tissue construct of defined shape can be created. Employing matrigel and culture medium mixed with a whole heart suspension, Zimmermann et al. created artificial myocardial tissue containing vasculature and demonstrated improved cardiac function and normalized epicardial conduction after transplantation onto infarcted rat hearts (23).

A second approach is to mix cells with extracellular matrix molecules and inject the mixture, thereby creating an artificial tissue *in situ*. A-cellular injections of collagen, fibrin or matrigel into myocardial infarctions resulted in similarly improved angiogenesis, while collagen injection appeared to induce recruitment of myofibroblasts (24). Co-injection of fibrin and skeletal myoblasts, as well as matrigel and murine embryonic stem cells resulted in markedly improved cell retention and survival (25; 26). Using a mixture of collagen, matrigel, culture medium and neonatal rat cardiomyocytes, Zhang et al. demonstrated improved regeneration of myocardial infarction compared to injections with only matrix, cardiomyocytes or control medium (27).

*Electrophysiological characteristics of stem cell-derived cardiomyocytes* Despite the problems described before, replacement therapy using stem cell-derived cardiomyocytes is a promising concept. For a proper evaluation of risks and benefits, it is essential to gain a better understanding of the electrophysiological properties of such cardiomyocytes. While in vivo experiments can help to determine survival of transplanted cells, or help identify pro-arrhythmic risks if the proper animal models are used, it is difficult to directly assess functionality of the graft. Some inroads have been made by Rubart et al., who applied two-photon imaging of calcium transients to study interaction between transplanted myoblast and host myocardium (28). These experiments elegantly demonstrated the possibility to image deeper layers of viable tissue, but information about membrane potential too is essential for the evaluation of pro-arrhythmic risk. Later, Xue et al. demonstrated that this is feasible in a guinea pig model with complete AV-block. Using a voltage sensitive dye, they demonstrated ventricular pacing after transplantation of hESCM (29).

An interesting approach would be to isolate transplanted cardiomyocytes from recipient hearts. However, due to the limited number of surviving cells, this seems a daunting experiment. A more straightforward and informative approach is to study stem cell-derived cardiomyocytes dissociated from their original differentiation culture using cellular electrophysiological and imaging techniques. Since their availability, murine embryonic and embryocarcinoma stem cells have been studied extensively (30; 31; 32) and several excellent reviews on this subject are available (33; 34). Human embryonic stem cell-derived cardiomyocytes (hESCMs) are less well studied. A short overview of the current state of knowledge in this field follows.

Undifferentiated hES cells (H1) express the delayed rectifier potassium current, but no sodium or calcium currents (35). Another study did find  $I_f$  and calcium currents in the same cell line (36). Interestingly, proliferation is markedly reduced by blocking the potassium conductance with various blockers. Upon differentiation, hESCM beat spontaneously and display action potentials resembling nodal, atrial and ventricular-like waveforms (13; 15). Reported resting membrane potentials are around  $-50$  mV, and upstroke velocity is approximately  $7$  V/s, illustrating their immature electrical phenotype, comparable to cultured human fetal cardiomyocytes. Ion currents underlying the action potential have been measured in several studies (13; 36; 37; 35). There is no consensus in literature concerning the origin of spontaneous activity in hESCM. Satin et al. implicated a sodium-window current and found no evidence of involvement of  $I_{Ca,L}$  (37). Experiments with another cell line, however, did demonstrate arrest of spontaneous activity after application of verapamil, a  $I_{Ca,L}$  blocker (15). The upstroke of the action potential is slow, which is compatible with absence or low expression of  $I_{Na}$ . However, voltage clamp experiments by Satin et al. have revealed that hESCMs display significant sodium current. This discrepancy is explained by the relatively depolarized membrane potential of hESCMs that limits sodium channel availability. This concept is supported by the absence or small  $I_{K1}$  currents. Action potentials of hESCM generally show a plateau phase, which is consistent with voltage clamp data demonstrating presence of  $I_{Ca,L}$ . Repolarization after the plateau is sensitive to  $I_{Kr}$  block and voltage clamp data confirm expression of functional  $I_{Kr}$  currents (36). hESCM express KvLQT1 mRNA, but we are not aware of any data demonstrating functional  $I_{Ks}$  expression. Expression of  $I_f$  has been demonstrated at the current level and block of  $I_f$  with za-

tebradine resulted in slowing of spontaneous beating (37; 36). Excitation-contraction coupling in hESCM does not involve intracellular calcium stores, as no increase in intracellular calcium concentration was induced by caffeine, thapsigargin or ryanodine (38). Combined with the observation that verapamil abolishes calcium transients, it is likely that calcium enters the cell primarily via the L-type calcium channel. The absence of a functional sarcoplasmic reticulum is consistent with the immature electrical phenotype.

Undifferentiated embryonic or embryocarcinoma cells are well-coupled via gap junctions and connexin43 expression is considered a marker of undifferentiated state (39; 40). Blocking of gap junctional communication results in decreased growth and increased apoptosis (41). A comparison of six hES lines revealed expression of connexin43 in all tested lines (40) and was confirmed by later studies (42; 43). Other connexin isoforms are also expressed, mRNA was detected for all human isoforms except connexin40.1 and 50 (44). This resulted in high levels of functional gap junctional coupling and gap junction hemichannels. The first step in mesodermal differentiation of hES cells, epithelium-mesenchyme transition, is accompanied by downregulation of connexin43 (45). Once differentiated, cardiomyocytes display a heterogeneous pattern of connexin43 which is probably a reflection of inhomogeneous differentiation. Measurement of conduction velocity in differentiated cultures yielded values lower than observed in monolayers of neonatal mouse or rat cardiomyocytes (46; 47).

## Pro-arrhythmic risk of SDCs and underlying mechanisms

Two aims for transplantation of SDCs can be identified at present. Firstly, the goal of replacement therapy is to increase cardiac performance by replenishing lost cardiomyocytes. Secondly, biological pacemakers are envisioned as a more physiological successor to the currently used electronic pacemakers (48). While very reliable, current electronic pacemakers are not able to respond to increased adrenaline levels by increasing pacing frequency. If biological pacemakers that can respond to adrenaline are reliable enough for clinical use, they may improve quality of life for patients.

These two purposes demand different electrophysiological properties of transplanted cells. Cell replacement therapy requires well-coupled, quiescent cardiomyocytes. The more they resemble the host myocardium, the better. Biological pacemaking however, will have to follow the example set by the SA-node. It requires spontaneously active cardiomyocytes that are electrically coupled with their neighbors, but only at coupling levels that allow them to maintain spontaneously active and pace surrounding myocardium.

*Pro-arrhythmia associated with cell replacement therapy* Several clinical and experimental studies have demonstrated pro-arrhythmic side-effects of cell transplantation. Skeletal myoblast transplantation resulted in ventricular tachycardia, transplantation of hESCM-containing embryoid bodies induces ectopic pacemaking (16; 11; 12). We will consider the probable underlying mechanism for cells used for transplantation in the context of cell replacement.

Mesenchymal or bone marrow stem cell transplantation appears to be safe in most studies. The cells that are introduced have no intrinsic excitability, but can form

connexin43-based gap junctions. It is likely that this explains the absence of clear pro-arrhythmia. There are however some indications that these cells can pose a threat, as in vitro experiments using co-cultures of neonatal rat cardiomyocytes and mesenchymal stem cells have shown. If co-cultures contain more than 10% mesenchymal cells, sustained re-entry in the form of spiral waves is observed (49). A different design using two areas of neonatal cardiomyocytes, bridged by mesenchymal cells, demonstrated synchronization of the areas, but this was accompanied by very slow conduction over the bridge (50; 51). This might provide a threat as slow conduction is proarrhythmic. Furthermore, the incidence of synchronization was markedly decreased with bridges wider than 300  $\mu\text{m}$ . Injection of mesenchymal stem cells into scars of patients with ischemic heart disease did not change the electrophysiological properties of injected regions (52). It appears that inexcitable bone marrow-derived cells pose an electrotonic load that can give rise to conduction slowing, and therefore can cause re-entry.

Also skeletal myoblast transplantation has been found to have pro-arrhythmic effects. However, since differentiated myoblasts are excitable, but do not express gap junctions, they seem unlikely to affect the cardiac rhythm. Experimental studies have shown that myoblasts indeed do not propagate the electrical impulse (50). Forced expression of connexin43 was shown to decrease pro-arrhythmia in mixed cultures of neonatal rat cardiomyocytes and skeletal myoblasts (53). Optical mapping of ventricular wedge preparations that contained transplanted skeletal myoblast demonstrated slowing of conduction that correlated with regions expressing skeletal myosin (54). Present evidence suggests that skeletal myoblasts, while not coupled to host myocardium, exert their pro-arrhythmic effects by increasing tissue heterogeneity and heterogeneity of conduction. Both factors increase the likelihood of developing re-entry based arrhythmias.

Transplantation of human embryonic stem cell-derived cardiomyocytes can result in ectopic pacemaking (16; 29). No purification of cardiomyocytes was done in either study, thus a mixed population of cells was injected. This probably resulted in increased tissue heterogeneity at the transplantation site. Furthermore, embryonic stem cell-derived cardiomyocytes display heterogeneity in action potential waveform and gap junction expression. As a consequence, important factors that impair conduction (decreased excitability, reduced cell-to-cell coupling and tissue heterogeneity) and that are associated with pro-arrhythmia, were present in the studies mentioned above. A combination of purification and increased connexin43 expression may be able to create a configuration in which the grafted cells are electrotonically clamped, i.e. silenced, by the host myocardium. Kolosov et al. transplanted purified murine embryonic stem cell-derived cardiomyocytes into mice with myocardial infarction, and demonstrated a marked decrease in tumor formation after purification, but no references to heart rhythm were made (20). In the case of stem cell-derived cardiomyocytes of human origin, testing for pro-arrhythmic properties requires the use of large animal models. Since human action potentials have a longer duration, they are subject to overdrive suppression in the hearts of species with shorter action potentials, which could lead to an underestimation of the pro-arrhythmic risk.

## Scope of this thesis

All studies described in this thesis were initiated with one common purpose, to deepen our understanding of the electrophysiological characteristics of stem cell-derived cardiomyocytes. For this purpose two research areas in cardiovascular sciences that to date have only limited overlap, being cardiac developmental biology and classical cellular electrophysiology, were integrated.

The first chapter of this thesis concerns the regulation of connexin43 during the earliest step in mesodermal differentiation, the epithelium-to-mesenchyme transition. This is followed in the second chapter by a study investigating the possibility to suppress cardiac automaticity by application of cells expressing Kir2.1. In the third chapter we studied the effects of  $\beta$ - and  $\alpha$ -adrenergic stimulation on conduction velocity in cultures of neonatal cardiomyocytes. In order to get a better understanding of pro-arrhythmic features of transplantation of immature cardiomyocytes, we devised a co-culture model that allowed us to study directly the electrophysiology of the interaction between immature and mature cardiomyocytes. The data obtained from this model are presented in chapter 4. Most recently, we identified a pool of cardiac progenitor cells in human fetal and adult hearts. The initial isolation and characterization of cardiomyocytes differentiated from the cardiac progenitor cells is described in chapter 5. A more thorough investigation of the electrophysiological properties of these cardiomyocytes can be found in chapter 6. Finally, I will reflect on the data presented in this thesis in the concluding general discussion.



## **Chapter 2**

### **Connexin43 repression following epithelium-to-mesenchyme transition in embryonal carcinoma cells requires Snail1 transcription factor**

Teun P. de Boer, Toon A.B. van Veen, Marti F.A. Bierhuizen, Bart J.M. Kok, Martin B. Rook, Kristel J.M. Boonen, Marc A. Vos, Pieter A. Doevendans, Jacques M.T. de Bakker, Marcel A.G. van der Heyden

*Differentiation, Volume 75, Issue 3, March 2007, 208-18*

## Abstract

Embryonic stem (ES) cells and embryonal carcinoma (e.g. F9 EC) cells express high amounts of functional connexin43 (Cx43). During mesoderm formation and subsequent cardiac differentiation, Cx43 is initially down-regulated but is up-regulated again as the emerging cardiomyocytes mature. In this study, we have investigated the regulation of Cx43 expression during early phases of differentiation in F9 EC and P19 EC cells. We found a striking inverse correlation between the expression of Cx43 and that of the transcriptional repressor Snail1. No clear relationship was found with Smad-interacting-protein1 (SIP1), another transcription factor inducing epithelium-to-mesenchyme transition (EMT). Promoter-reporter assays indicated Cx43 repression at the promoter level by ectopically expressed Snail1. To establish whether the Cx43 down-regulation depends on endogenous Snail1, MES-1 cells, differentiated derivatives of P19 EC, were stably transfected by an siRNA construct silencing Snail1 expression. This resulted in a mesenchyme-to-epithelium transition, which was accompanied by increased levels of Cx43 mRNA and protein, and enhanced metabolic and electrical coupling. We conclude that Snail1-mediated EMT results in a Cx43 repression.

## Introduction

Gap junctions allow the direct exchange of small metabolites and ions between adjacent cells. They are indispensable in many biological processes, from action potential propagation in the heart to secretion, development, and tissue repair (55; 56; 57). Gap junctions are formed by two hemichannels on adjacent cells, each consisting of six connexin (Cx) proteins arranged around a central pore. Docking of the two hemichannels results in the creation of a functional cell-to-cell channel. To date, at least 20 Cx isoforms have been identified in the genomes of mouse and humans (3). Although expression is particularly prominent in the working myocardium of the heart, Cx43 is expressed widely in multiple tissues of all mammals.

Cell-cell interactions are formed by different classes of proteins resulting in the formation of adherence junctions, desmosomes, and tight junctions. The functional integrity of cell-cell junctions is critically important for Cx43-mediated gap-junction formation (58). However, the underlying molecular determinants such as the cadherin isoform, may be redundant or interchangeable (59). Furthermore, it was shown that Cx43 interacts with cell-cell junction-associated proteins such as cadherins,  $\alpha$ - and  $\beta$ -catenins, p120ctn, and Zonula Occludens-1 (ZO-1), for a review, see (60). An unexpected finding in stem cell biology has been the observation that undifferentiated pluripotent cells are connected by functional gap junctions. Cx43 was found to be expressed in pluripotent human embryonic stem (ES) cells (61; 44), mouse ES cells (39; 62), and P19 embryonal carcinoma (F9 EC) cells (63). Upon differentiation in aggregates known as embryoid bodies (EBs) in which cardiomyocytes form spontaneously (64), the amount of Cx43 expressed decreased, and many premature embryonic-like cardiomyocytes were nearly devoid of Cx43 (62). Upon cardiomyocyte maturation, Cx43 levels increase again (62). This recapitulates Cx43 expression during embryonic heart formation in vivo (65; 66; 67).

In mouse EB formation, an outer endoderm forms a skin around an ectoderm-like core. Subsequently, gastrulation-like events occur, resulting in mesoderm formation that eventually results in beating cardiomyocytes (68). In some ES cell lines, early mesoderm formation has been described as involving an epithelium-to-mesenchyme transition (EMT), mimicking that in the embryo (69). In general, an EMT is characterized by a dramatic change in cell-cell and cell-matrix interactions, which allow the cells to escape the epithelium and migrate through an extracellular matrix. In parallel, a transcriptional program is initiated to maintain the mesenchymal character of the cells. Many extracellular stimuli can evoke an EMT by activating at least four different transcription factor families. These include Smad-interacting protein1 (SIP1) and Snail1 (70; 71; 72). Among the effects of Snail1 or SIP1 activity are direct transcriptional repression of the cell-cell adhesion genes E-cadherin, claudins, and occludin, which disrupt adherence and tight junctions, respectively (73; 74; 75).

In a previous study, we used F9 EC cells to characterize Cx43 expression during a protein kinase A (PKA) signaling-mediated EMT (76). The F9 EC cells treated with retinoic acid (RA) and cyclic AMP (cAMP) recapitulate the transition made by extra-embryonal visceral endoderm into parietal endoderm in the embryo *in vivo*, one of the earliest developmental EMTs. We found that upon EMT, functional Cx43 expression that was detected decreased dramatically. This EMT was later associated with rapid Snail1 up-regulation (77). This suggests a causal relation between Snail1 and Cx43.

Here, we hypothesize that Snail1-mediated EMT results in Cx43 down-regulation, and therefore could be responsible for low Cx43 levels in the resulting cell population. We have found that Snail1 expression negatively correlates with Cx43 in two different EC cell lines. Furthermore, we demonstrate that the Cx43 promoter is a target for Snail1 repression. Finally, by silencing endogenous Snail1 in MES-1 cells, we showed that Cx43 levels could be restored.

## Materials and methods

*Cell culture and differentiation* P19s18 EC, END-2, MES-1, EPI-7 (78; 79), and F9 EC cells (80) were maintained in DMEM/F12 (1:1; Gibco, Breda, the Netherlands) containing 10% fetal calf serum (Gibco), 2 mM L-glutamine, and 50 U/ml penicillin and 50  $\mu$ g/ml streptomycin. P19s18 and F9 EC cells were cultured on 0.1% gelatin-coated surfaces. F9 EC cells were induced to differentiate using  $10^{-6}$  M all-trans RA (Sigma, St. Louis, MO) for 5 days, with or without dibutyryl-cAMP for the last 24 hr or less, as described previously (Van der Heyden et al., 2000).

*Northern blotting* Total RNA was extracted with Trizol reagent (Gibco) according to the manufacturer's instructions. Thirty microgram RNA was run on a 1.2% formaldehyde-agarose gel and transferred to a Qiabran membrane (Qiagen, Venlo, the Netherlands). Blots were incubated with [ $^{32}$ P]-labeled probes for murine Cx43 (protein-coding region) and GAPDH. Signal detection and analysis were performed using a PhosphorImager and ImageQuant software (Amersham Biosciences, Roosendaal, the Netherlands).

*Semi-quantitative reverse transcriptase polymerase chain reaction (RT-PCR)* RNA was isolated using Trizol and 2  $\mu$ g total RNA was reverse transcribed using oligo-dT and M-MLV-RT (Gibco) in a 20  $\mu$ l reaction volume. Subsequently, 1  $\mu$ l reaction volume (cDNA equivalent of 100 ng total RNA) was used in the PCR reaction. Primers, annealing temperature, product size, and optimized number of PCR cycles are depicted in Table 2.1. RT-PCR for determining Cx43 promoter usage and alternative splicing was performed according to Pfeifer et al. (2004). Products were analyzed in 1%-1.5% agarose, ethidium bromide-stained gels.  $\beta$ -tubulin was used as an internal standard.

**Table 2.1:** PCR primer pairs

Name	Forward/reverse 5'-3'	Annealing ( $^{\circ}$ C)	Product (bp)	Cycles
Cx43	AGCGTGAGGAAAGTACCAAACAGC AAGAAGGCCACCTCAAAGATAGAC	62	666	28
Cx30.3	CACCGTATGTGATCTCCAAAG ATGTTTCCCACCTGACCTG	54	198	31
Cx45	AAAGAGCAGAGCCAACCAA GTCCCAAACCCTAAGTGAAGC	54	313	27
Cx26	AGATGGAGGGAGAGGATGAG TCAGAGGAAGAGAAACAATGTG	54	311	31
$\beta$ -tubulin	TCACTGTGCCTGAACTTACC GGAACATAGCCGTAAACTGC	55	319	25
Snail1	GGAAGCCCAACTATAGCGAGC CAGTTGAAGATCTTCCGCGAC	58	423	30
SIP1	GTCCATGCGAACTGCCATCTGATCCGCTCT GGCTTGCAGAATCTCGCCAC	58	349	33

SIP1, Smad-Interacting-Protein1; Cx, Connexin.

*Immunofluorescent staining* Indirect immunofluorescence was used to determine Cx43 and ZO-1 cellular localization. In brief, cells were washed with PBS, fixed for 25 min with 4% formaldehyde, permeabilized with 0.5% Triton X-100 for 5 min, and quenched with 50 mM glycine. Antibodies were diluted in NET-gel (50 mM Tris pH 8.0, 150 mM NaCl, 1 mM EDTA, 0.2% gelatine) supplemented with 10% normal goat serum. Primary and secondary antibodies were incubated overnight and for 2 hr, respectively, followed by five washes with NET-gel. Primary antibodies used were Cx43 (Clone 2, Transduction labs, Lexington, KY; cat. nr. 610062) and ZO-1 (Zymed, San Francisco, CA; catalog number 61-7300). Secondary antibodies used were Texas Red or fluorescein isothiocyanate (FITC)-conjugated donkey anti-mouse or rabbit (Jackson Immunoresearch, West Grove, PA).

*Western blotting* Cells were lysed in RIPA buffer (20 mM Tris-HCl, pH 7.4, 150 mM NaCl, 10 mM  $\text{Na}_2\text{HPO}_4$ , 1% [v/v] Triton X-100, 1% [w/v] Na-deoxycholate, 0.1% [w/v] SDS, 1 mM EDTA, 50 mM NaF, 1 mM PMSF, 10  $\mu$ g/ml aprotinin). Lysates were clarified by centrifugation at 14,000  $\times$  g for 5 min at 4 $^{\circ}$ C. Twenty microgram protein lysate was mixed with Laemmli sample buffer and proteins were separated

by 7% or 10% sodium dodecyl sulfate-polyacrylamide gel electrophoresis (SDS-PAGE) and subsequently electro-blotted onto a nitrocellulose membrane (Biorad, Veenendaal, the Netherlands). Equal loading was checked by reversible Ponceau staining. Primary antibodies were Cx43 (Zymed; catalog number 71-0700), ZO-1 (Zymed; catalog number 61-7300), Pan-cadherin (Sigma; catalog number C-3678), E-cadherin (Transduction Labs; catalog number 610181),  $\beta$ -catenin (BD Biosciences, Erembodegem, Belgium; catalog number 610153),  $\beta$ -tubulin (Sigma; catalog number T-4026), and HA-tag (Sigma; catalog number H-9658). Proteins were visualized by using peroxidase-labeled secondary antibody (Jackson) and standard ECL procedures (Amersham Bioscience). In attempts to visualize Cx26, Cx30.3, Cx45, and Snail1 at the protein level, we used Cx26 (Zymed #71-0500), Cx30.3 (Zymed #40-0900), Cx45 (a generous gift from Dr. T. H. Steinberg, Institute for Infectious Diseases, St. Louis, MO), and Snail1 (Santa Cruz, sc-10432; Heidelberg, Germany) antibodies. This, however, did not result in signals that unambiguously could be attributed to the presence of the Cx in question or Snail1, either caused by low levels of protein expression, antibody specificity or affinity, or a combination of factors (not shown).

*Electrical and metabolic coupling* A symmetrical setup with two HEKA EPC-7 patch clamp amplifiers (HEKA Elektronik, Lambrecht, Germany) was used to measure electrical coupling between cells. Macroscopic gap junctional currents were recorded using a custom data acquisition program (kindly provided by Dr. J. G. Zegers, AMC, Amsterdam, the Netherlands) running on a G4 Apple Macintosh computer equipped with a 12-bit National Instruments PCI-MIO-16E-4 acquisition card. Current signals were low-pass filtered at 2.5 kHz and acquired at 10 kHz. Macroscopic gap junctional currents were elicited in cell pairs by applying small transjunctional voltage steps (10 mV) from holding potential ( $-50$  mV). By using small pulses, junctional conductances were maximal and not inactivating. Offline analysis was performed using MacDaq 8.0 (kindly provided by Dr. A. C. G. van Ginneken, AMC, Amsterdam) and R 2.0.1 (81). Gap junctional conductance ( $g_j$ ) was defined as  $g_j = I_j/V_j$ , where  $I_j$  and  $V_j$  denote junctional current and transjunctional voltage, respectively. Electrophysiological experiments were conducted at  $20^\circ\text{C}$ . Extracellular buffer used was a modified Tyrode's solution, containing (in mmol/l) NaCl 140, KCl 5.4,  $\text{CaCl}_2$  1.8,  $\text{MgCl}_2$  1, HEPES 15,  $\text{NaHCO}_3$  17.5, glucose 6, pH 7.20/NaOH. Pipette buffer contained (in mmol/l) potassium gluconate 125, KCl 10, HEPES 5, EGTA 5,  $\text{MgCl}_2$  2,  $\text{CaCl}_2$  0.6,  $\text{Na}_2\text{ATP}$  4, pH 7.20/KOH. For dye injections, microelectrodes were filled with 4% (w/v) Lucifer Yellow in 150 mM  $\text{LiCl}_2$ , 10 mM HEPES. Patch pipettes were pulled on a Narishige PC-10 puller and fire-polished. When filled with pipette buffer, pipette resistance ranged between 2 and 5  $\text{M}\Omega$ .

*Luciferase assays* Cells were cultured on 25  $\text{cm}^2$  dishes and subsequently transfected with 2  $\mu\text{g}$  of luciferase reporter construct, either pGL3-rCx43 ( $-1338/+281$ ; Teunissen et al., 2003) or E-cadherin promoter (Batlle et al., 2000), and 1  $\mu\text{g}$  of pSG5-HA-Snail1 (C-terminal HA-tagged murine Snail1 [accession number X67253], a generous gift from Dr. A. Garcia de Herreros, Barcelona, Spain) when indicated, using the Calcium-Phosphate method. As a transfection control, pRL-CMV (Promega, Leiden, the Netherlands) was co-transfected. After  $\sim 20$  hr, cells were washed with phosphate-

buffered saline (PBS) and medium was replaced by normal culture medium. Forty-eight hours post-transfection, cells were washed with PBS and harvested with passive lysis buffer (Promega) and assayed for luciferase activity using the Promega Dual Luciferase Reporter Assay system on a Lumat LB9507 luminometer (EG86 Berthold, Bad Wildbad, Germany). Transfections were carried out in duplicate and repeated at least three times independently. Promoter activity is given as fold activity  $\pm$ SEM, relative to non-promoter containing pGL3-basic.

*siRNA interference* For construction of siRNA vectors, we essentially used the system described by (82). Oligonucleotides were based on murine Snail1 (accession number NM\_011427); for siSna1 5'-GATCCCGCCCACTATAGCGAGCTGTTCAAGAGACAGCTC GCTATAGTTGGGCTTTTTGGAAA-3' and 5'-AGCTTTTCCAAAAAAGCCCACTATAGC GAGCTGTCTCTTGAACAGCTCGCTATAGTTGGGCGG-3'; for siSna2 5'-GATCCCGATCT TCAACTGCAAATATTTCAAGAGAATATTTGCAGTTGAAGATCTTTTTTGGAAA-3' and 5' -AGCTTTTCCAAAAAAGATCTTCAACTGCAAATATTTCTTGAATATTTGCAGTTGAAG ATCGG-3'; and for siSna3 5'-GATCCCACCCACTCGGATGTGAAGATTCAAGAGATCTTC ACATCCGAGTGGGTTTTTTGGAAA-3' and 5'-AGCTTTTCCAAAAAACCCTCGGAT GTGAAGATCTTGAATCTTCACATCCGAGTGGGTGG-3'. For oligonucleotide annealing, 2  $\mu$ g sense and antisense oligo was mixed in a volume of 60  $\mu$ l, heated at 90°C for 3 min, slowly cooled to 37°C and incubated for 1 hr at 37°C. Once annealed, BamHI and HindIII sticky ends were formed at the 5' and 3' part of each double-stranded oligo, respectively. The H1 promoter and Zeocin resistance gene containing pTER+ vector was digested with BglII and HindIII, and double-strand oligos were ligated. The resulting pTER+-siRNA constructs were verified by sequencing. MES-1 cells were transfected with empty vector pTER+, or pTER+ vectors containing siSna1 or siSna3 using Lipofectamine (Invitrogen, Paisly, UK) according to the manufacturer's protocol. Two days following transfection, selection using 500  $\mu$ g/ml Zeocin (Invitrogen) was started. After 3 weeks, stable pools were subjected to limited dilution in 96-well plates (average of 0.5 cell/well). Growing clones were subsequently transferred into 24- and six-well plates. Stable clones were selected for further analysis on the basis of Snail1 expression as detected by RT-PCR.

## Results

### Cx43 down-regulation in F9 EC primitive to parietal endoderm EMT is preceded by Snail1 up-regulation

In a previous study, we observed a strong decrease in Cx43 expression at the mRNA, protein, and functional level in F9 EC cells undergoing EMT (76). In a similar study, it was found that this EMT was associated with a rapid up-regulation of the zinc finger transcriptional repressor Snail1 (77). To investigate the kinetics of these two processes, we differentiated F9 EC cells into primitive endoderm-like cells by addition of RA (Figs. 2.1A, 2.1B). This resulted in up-regulation of Cx43 mRNA and protein expression (Figs. 2.1C, 2.1D). A small increase in Snail1 mRNA was also found, likely the result of spontaneous transdifferentiation into parietal endoderm (Fig. 2.1C). Thirty minutes after

dibutyryl-cAMP addition, which initiates parietal endoderm differentiation (Figs. 2.1A, 2.1B), a massive increase in Snail1 mRNA was observed (Fig. 2.1C). This was maintained for at least 24 hr (Fig. 2.1C). The increase in Cx43 mRNA expression was transient and expression had returned to low levels at 24 hr. Cx43 protein levels were similarly decreased in time (Fig. 2.1D). Although direct interaction of Cx43 with the tight junction protein ZO-1 has been established (reviewed in (60)), we observed an inverse correlation when comparing F9 EC and F9 PrE with respect to Cx43 and ZO-1 expression. From these data, we conclude that F9 EC cells undergoing primitive to parietal endoderm EMT are characterized by Cx43 down-regulation, which is preceded by Snail1 up-regulation.

### Cx43 down-regulation correlates with increasing Snail1 levels in P19 EC cells and their differentiated derivatives

Pluripotent P19 EC cells can be induced to differentiate in derivatives of all three germ layers (reviewed in (32)) recapitulating early differentiation events in embryonic development. We compared undifferentiated P19s18 EC cells with three derivative cell lines of endodermal (END-2), mesodermal (MES-1), and ectodermal (EPI-7) characteristics (78; 79). P19s18 EC, END-2, and EPI-7 display an epithelial-like morphology when grown as monolayer cultures, in contrast to MES-1 cells, which have a mesenchymal-like morphology. mRNA was isolated from all four-cell lines and Cx43 mRNA was detected by Northern blotting and quantified with respect to GAPDH. The highest Cx43 mRNA levels were detected in P19s18 EC cells (100 arbitrary units, a.u.), while lower levels were found in EPI-7 (32 a.u.), END-2 (15 a.u.), and MES-1 (4 a.u.) cells, respectively (Fig. 2.2A). Similar results were found by semi-quantitative RT-PCR (Fig. 2.2B). Furthermore, RT-PCR revealed an almost perfect negative correlation between Cx43 and Snail1 expression. Some positive relation was found between this Cx and SIP1, another transcriptional inducer of EMT, when comparing the three differentiated derivatives. However, by including P19 EC in this comparison, this correlation becomes less clear. Finally, Cx26, Cx30.3, and Cx45 were also detected. A perfect positive correlation between Cx30.3 and Snail1 mRNA was observed, but neither Cx26 nor Cx45 displayed a strong correlation with either Snail1 or SIP1 (Fig. 2.2B).

Cx43 mRNA expression was partially reflected in protein expression, which indicates additional post-transcriptional regulation of expression levels. The lowest levels of Cx43 were found in MES-1 cells (Fig. 2.2C). Here, a positive correlation was found with ZO-1 and to some extent with Pan-cadherins, in contrast to F9 EC cells. Remarkably, E-cadherin was only detected in undifferentiated P19s18 EC cells, and not in its differentiated derivatives. However, E-cadherin is a well-known target of Snail1 repression, and its absence in the differentiated derivatives is in accordance with Snail1 expression in these cell lines. No differences in  $\beta$ -catenin were observed.

We next assessed the cellular localization of Cx43 in the four different cell lines (Fig. 2.3), and to reveal the cell borders, ZO-1 co-staining was performed. In P19s18 EC cells, the majority of Cx43 was located intracellularly; however, Cx43 was also located at the borders between cells in gap-junctional-like structures. In END-2 and EPI-7, Cx43 was mainly localized at the cell borders, apparently in gap junctions. In MES-1 cells, however, Cx43 was mainly intracellular, although some gap-junctional-like

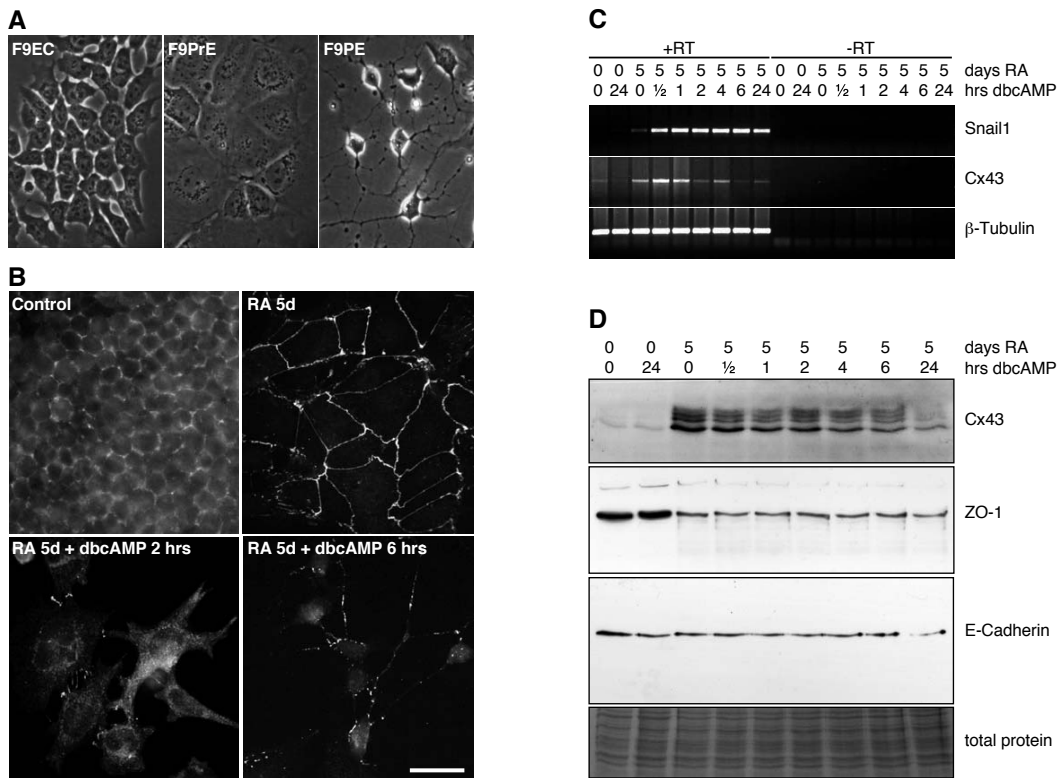


**Figure 2.1:** Epithelium-to-mesenchyme transition (EMT) of F9 embryonal carcinoma (EC) cells from primitive to parietal endoderm is characterized by Snail1 up-regulation followed by connexin43 (Cx43) down-regulation. **A:** F9 EC cells were treated with  $10^{-6}$  M all-trans retinoic acid (RA) for 4 days resulting in primitive endoderm differentiation (F9PrE). Subsequent addition of 1 mM dbcAMP induces differentiation into parietal endoderm (F9PE). **B:** Localization of Zonula Occludens-1 (ZO-1) in differentiating F9 cells. F9 EC (control) were differentiated into PrE (RA 5d). Subsequently, EMT was induced by addition of dbcAMP. Cultures undergoing EMT were analyzed 2 and 6 hr following dbcAMP application (RA 5d+dbcAMP 2 hr and RA 5d+dbcAMP 6 hr, respectively), scale bar=20  $\mu$ m. **C:** Reverse transcriptase polymerase chain reaction (RT-PCR) for Snail1 and Cx43 of differentiating F9 EC cells. F9 EC cells were treated with RA for 5 days. dbcAMP is added at day 5 for the indicated time (hours). In response to RA, resulting F9 PrE cells express Cx43. Subsequent differentiation into PE, characterized by an EMT results in a rapid increase (within 0.5 hr) of Snail1. Maximal down-regulation of Cx43 is observed during the 24-hr period and is most obvious at 6 hr of dbcAMP stimulation. No PCR product was obtained without prior reverse transcriptase reaction (-RT).  $\beta$ -Tubulin serves as input control. **D:** Western blot analysis of Cx43, ZO-1, and E-cadherin in differentiating F9 EC cells. Cell stimulation protocol as in **C**. Cx43, displaying multiple bands of differently phosphorylated states, is up-regulated in response to RA-mediated PrE and down-regulated in response to dbcAMP mediated PE differentiation. ZO-1 expression is strong in F9 EC cells and decreased in PrE and PE cells. E-cadherin is down-regulated following 24 hr stimulation with dbcAMP. Total protein serves as control.



staining could be seen.

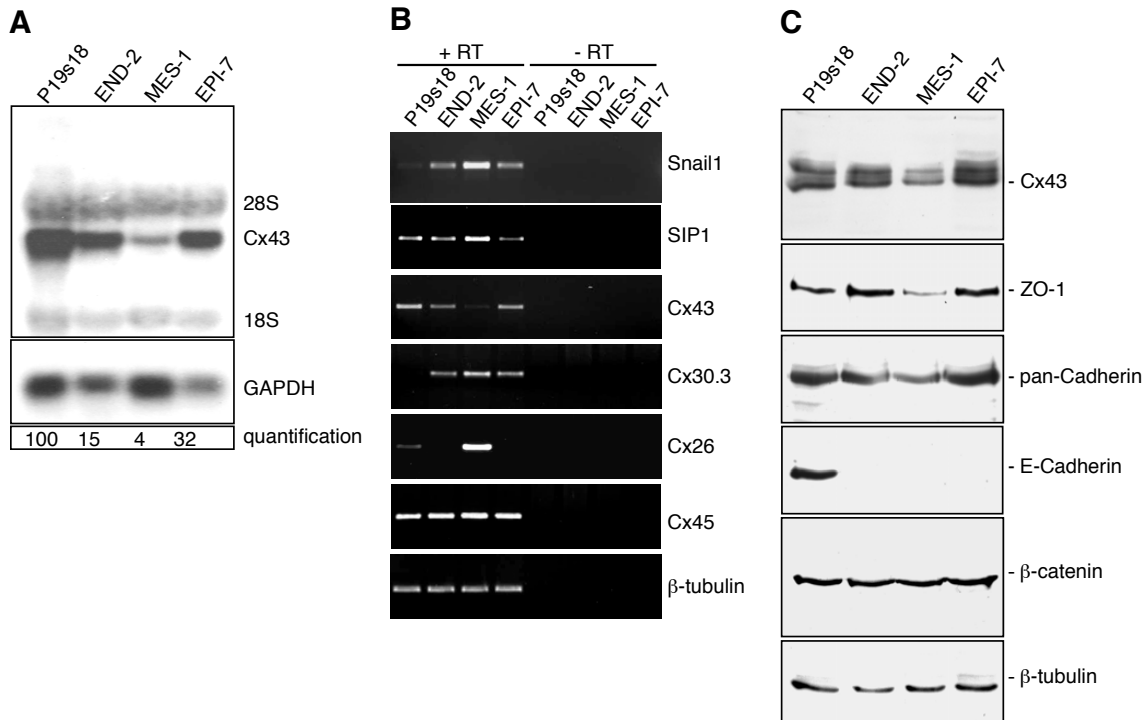


**Figure 2.2:** P19s18 and its derivatives display a negative correlation between Snail1 and connexin43 (Cx43) expression while Cx30.3 is positively correlated with Snail1. **A:** Detection of Cx43 expression in P19s18 embryonal carcinoma (EC) cells and its derivative cell lines by Northern blotting. Signal of 18S and 28S rRNA is visible above and beneath the Cx43 signal. GAPDH serves as input control. Phosphorimager mediated quantification indicates strongest expression in P19s18 EC (100 arbitrary units [a.u.]) and lower expression in END-2 (15 a.u.), MES-1 (4 a.u.), and EPI-7 (32 a.u.) cells respectively. **B:** Semi-quantitative reverse transcriptase polymerase chain reaction analysis of Snail1, SIP1, Cx43, Cx30.3, Cx26, and Cx45 on P19s18 EC and its derivative cell lines.  $\beta$ -tubulin serves as input control. **C:** Western blot analysis of Cx43, ZO-1, pan-cadherin, E-cadherin, and  $\beta$ -catenin expression in P19s18 EC cells and its derivatives.

Finally, functional gap-junctional coupling was established by both Lucifer Yellow dye coupling and electrotonic coupling. Dye spreading assays indicated the strongest gap-junctional coupling in P19s18 F9 EC cells (Figs. 2.4A, 2.4B). Two minutes after dye injection, Lucifer Yellow was visible on average in  $15.8 \pm 2.4$  (SEM; N=20) neighboring cells for P19s18 EC cells. In END-2 and EPI-7 cells, on average dye spread into  $9.1 \pm 1.3$  (N=20) and  $7.4 \pm 1.0$  (N=20) adjacent cells, respectively, while MES-1 cells were poorly coupled with only  $3.0 \pm 0.5$  (N=20) positive cells. As dye-coupling depends to some extent on the Cx isoform involved and on the size of the cells, we next compared electrotonic coupling of P19s18 EC and MES-1 cells. P19s18 EC cell pairs exhibited a significantly higher level of electrical coupling ( $37.3 \pm 7.0$  nS [N=17]) as compared with MES-1 cells ( $17.3 \pm 3.0$  nS [N=17],  $p < 0.015$ ). These results illustrate that upon differentiation of pluripotent P19s18 EC cells, Cx43 expression was decreased at mRNA and protein levels and probably also at the functional level. The strongest decrease was seen in MES-1 cells. Furthermore, Cx30.3 mRNA is reciprocally up-regulated in these cell lines. Finally, a strong correlation was found between the alternate Cx43/Cx30.3 expression and that of Snail1.

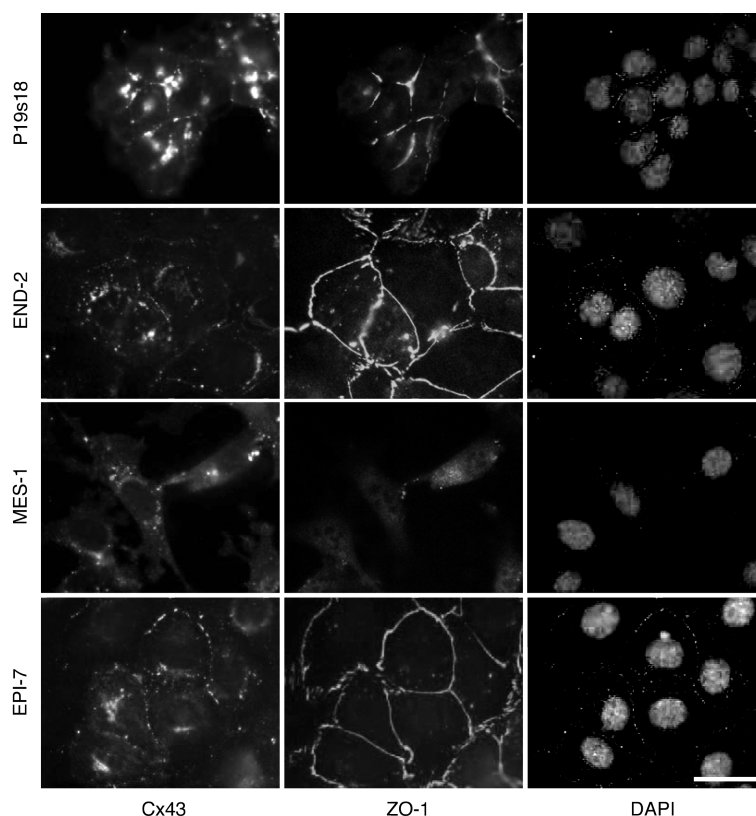


**Figure 2.3:** Connexin43 (Cx43) subcellular localization in P19s18 embryonal carcinoma (EC), END-2, MES-1, and EPI-7 cells. Cx43 is expressed intracellularly and at cell borders in P19s18 EC cells. At the cell borders, Cx43 is partially colocalized with Zonula Occludens-1 (ZO-1). In END-2 and EPI-7 cells most of Cx43 is localized at the cell borders and displays colocalization with ZO-1. In MES-1 cells, Cx43 is mainly intracellular. Cell nuclei are stained with 4,6-diamidino-2-phenylindole (DAPI). Scale bar=20  $\mu\text{m}$ .

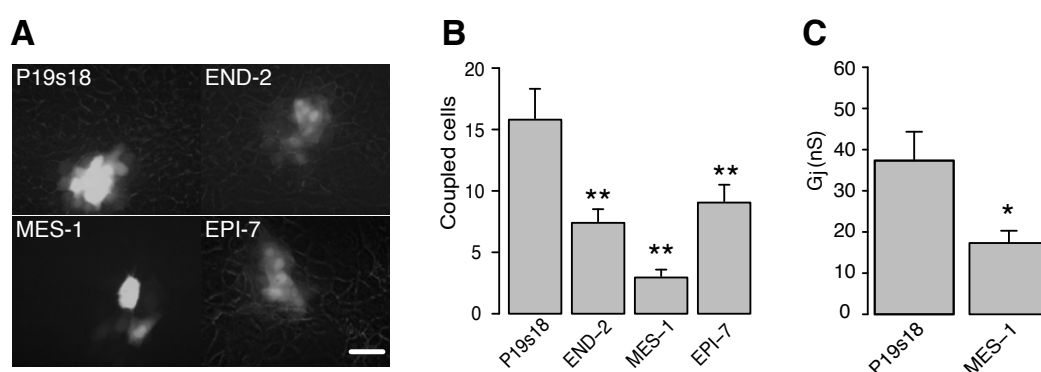


**Figure 2.4:** Gap-junctional coupling of P19s18 embryonal carcinoma (EC) cells and derivatives is correlated with connexin43 (Cx43) expression. **A:** One cell within a large cluster of cells was injected with 4% Lucifer Yellow. The dye was allowed to spread for 2 min and subsequently visualized by epifluorescent microscopy. **B:** Quantification of Lucifer Yellow dye coupling. The number of Lucifer Yellow receiving cells from the dye-injected cell is scored 2 min after initial injection. \*\*  $p < 0.01$  with respect to P19s18 (ANOVA, Holms-Sidak test). **C:** Electrical coupling of P19s18 EC and MES-1 cell pairs respectively as measured by double voltage patch clamp. \* Indicates  $p < 0.05$  (Student's t-test).

## The Cx43 promoter activity matches Cx43 mRNA levels and is repressed by ectopic Snail1

The Cx43 gene was originally considered as a two-exon gene driven by one promoter. Only recently it has been recognized that Cx43 transcription can be mediated by three promoters (P1-P3) and that Cx43 pre-mRNA is subjected to alternative splicing (83). Promoter P1, which was the first identified Cx43 promoter, however, appears superior in activity compared with P2 and P3 (83). Nevertheless, we questioned whether P19s18 EC and its derivatives may use alternative promoters, and/or generate different mRNAs by alternative splicing. Therefore, mRNA was subjected to RT-PCR using different primers to distinguish between promoter usage and alternative splicing. This analysis provided no evidence for alternative promoter use or alternative splicing between the four cell lines (Fig. 2.5A). To further investigate the level at which the negative regulation of Cx43 in P19s18 EC cell differentiation occurred, we determined Cx43 P1 promoter activity in undifferentiated P19s18 EC cells and the differentiated derivatives. The rat Cx43 P1 promoter reporter was transfected into all four cell lines, and the relative reporter activity was determined by luciferase activity (Fig. 2.5B). The strongest promoter activity was found in P19s18 EC cells ( $26.1 \pm 3.2$ , mean  $\pm$  s.e.m.) fold over non-promoter containing luciferase reporter), followed by END-2 ( $12.9 \pm 0.8$  fold) and EPI-7 ( $11.3 \pm 1.0$  fold) cells. The lowest promoter activity was found in MES-1 cells ( $7.3 \pm 0.5$  fold). Therefore, differences in promoter activity may account for the differences in Cx43 mRNA expression.

As a strong inverse correlation was found between Cx43 and the transcriptional repressor Snail1, we next investigated whether Snail1 co-expression would lead to Cx43 P1 promoter down-regulation. Co-transfection of 1  $\mu$ g of Snail1 expression construct resulted in inhibition of the rat Cx43 P1 promoter by  $58.4 \pm 4.3\%$  in P19 EC cells. As a control, we used the E-cadherin promoter as an established Snail1 target gene (84), which was inhibited by  $77.6 \pm 3.1\%$ . As Snail1 is an E-box (CANNTG)-binding transcription factor, we established whether Snail1-specific E-boxes (CA(C/G)(C/G)TG; (84, 74)) were present in the Cx43 P1 promoter. The murine and rat Cx43 promoter contained nine and four E-box consensus sequences, respectively, of which two and one conform to the Snail1-specific E-boxes, respectively (Fig. 2.5D). Therefore, we conclude that the Cx43 promoter is a target gene for Snail1, whose regulation might be by direct Snail1 binding to its E-boxes.

## Silencing of endogenous Snail1 in MES-1 cells results in mesenchyme-to-epithelium transition, Cx43 up-regulation, and enhanced gap-junctional communication

To confirm a causal relationship between Snail1 and Cx43 expression, we investigated whether inhibition of endogenous Snail1 would increase Cx43 expression. We constructed three different Snail1 siRNA-silencing expression constructs. Ectopic expression of HA-tagged Snail1 resulted in detectable Snail1 expression on Western blot (Fig. 2.6A). Co-transfection of silencing construct siSna1 or siSna2 resulted only in a very minor inhibition of Snail1 in this system. In contrast, co-transfection of siSna3 resulted in very efficient silencing of ectopic Snail1 (Fig. 2.6A). Next, MES-1 cells were

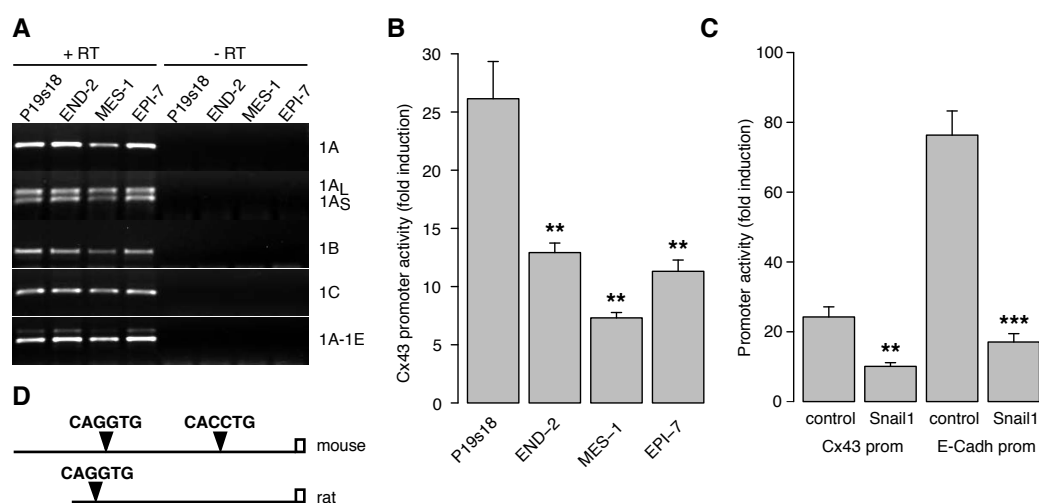


**Figure 2.5:** Connexin43 (Cx43) P1 promoter activity in P19s18 embryonal carcinoma (EC), END-2, MES-1, and EPI-7 cells. **A:** No difference in Cx43 promoter usage or alternative splicing in P19s18 EC cells and its derivatives. Reverse transcriptase polymerase chain reaction on RNA from P19s18 EC, END-2, MES-1, and EPI-7 cells with primer combinations indicative for promoter P1 (1A, 1A<sub>L</sub>, 1A<sub>S</sub>, 1A-1E), P2 (1B) or P3 (1C), and primer combinations indicative for alternative splicing (1A, 1A<sub>L</sub>, 1A<sub>S</sub>, 1A-1E). **B:** P1 promoter activity in P19s18 EC, END-2, MES-1, and EPI-7 cells correlates with Cx43 mRNA expression. Luciferase values are expressed as fold stimulation over non-promoter luciferase reporter (pGL3basic). Results from at least three independent experiments performed in duplicate are shown. \*\*  $p < 0.01$  with respect to P19s18 EC (ANOVA Holms-Sidak test). **C:** Snail1 repression of Cx43 and E-cadherin promoter in P19s18 EC cells. Reporter constructs are transfected in absence and presence of 1  $\mu$ g Snail1 expression vector. Luciferase values are expressed as fold stimulation over pGL3basic. Results from at least three independent experiments performed in duplicate are shown. \*\*  $p < 0.01$  and \*\*\*  $p < 0.001$  with respect to control without Snail1 co-transfection (Student's t-test). **D:** Schematic representation of mouse and rat Cx43 promoters and part of exon 1A. Consensus Snail1 binding sites (triangles) and sequences are indicated.

stably transfected with either empty siRNA expression vector (pTER+), or silencing constructs containing either siSna1 or siSna3. pTER+ overexpression did not change cell morphology (Fig. 2.6B). siSna1 overexpression resulted in a moderate change in cell morphology as the cells appeared larger and more flattened. siSna3a overexpression resulted in a total mesenchyme-to-epithelium transition (Fig. 2.6B). Subsequently, RNA was isolated from stably transfected cells (total pools) or isolated clones from these pools, and subjected to semi-quantitative RT-PCR (Fig. 2.6C). Upon expression of siSna1, Snail1 was only down-regulated to a very limited extent. Expression of siSna3 resulted in a strong reduction of Snail1 expression. Upon silencing of Snail1, Cx43 was up-regulated, which was most obvious in siSna3-expressing cells. Western blot analysis of the same pools and clones revealed a minor up-regulation of Cx43 in siSna1 and stronger Cx43 up-regulation in siSna3 (Fig. 2.6D). Pan-cadherins and ZO-1 were up-regulated in both siSna1 and siSna3 pools and clones, but the strongest effects were seen in siSna3 pools and clones. Restoration of E-cadherin expression was found only in siSna3 pools and clones (Fig. 2.6D). Finally, we found that siSna3 clones exhibited increased levels of gap-junctional communication as measured by dye coupling ( $9.3 \pm 0.9$  [n=10],  $9.4 \pm 1.2$  [n=9], and  $14.7 \pm 1.6$  [n=11] coupled neighboring cells for pTER+cl5, siSna1 cl1, and siSna3 cl2, respectively; Fig. 2.6E) and electrotonic coupling ( $8.6 \pm 1.7$  [n=8] and  $14.8 \pm 2.0$  [n=9] nS for pTER+cl5 and siSna3 cl2, respectively; Fig. 2.6F) when compared with MES-1 cells overexpressing the empty pTER vector or siSna1. From these results, we conclude that there is a causal, reciprocal relationship between endogenous Snail1 and Cx43 expression.

## Discussion

The results presented here indicated the existence of a Cx43 down-regulation during an EMT that is associated with a rapid up-regulation of Snail1. In a recent study, it was shown that ectopic SIP1 induces EMT in human epithelial cells, which is accompanied by direct down-regulation of P-cadherin, Claudin 4, and Cx26 promoter activity (75). In our P19s18 EC and derivative cell lines, SIP1 is endogenously expressed, but there was little correlation between expression levels and Cxs (Fig. 2.2B) in contrast to the effect induced by Snail1. Moreover, Cx26 is most highly expressed in MES-1 cells, which displayed the highest level of SIP1, although we have not determined the functional activity of SIP1 in these cells. Nevertheless, our study and that of (75) indicate that EMT-inducing transcription factors, either ectopic SIP1 or endogenous Snail1, repress a set of genes whose products function in cell-cell adhesion, which now also include cell-cell channel proteins like Cx26 and Cx43.

Dye-coupling studies in the developing mouse embryo gave rise to the concept of communication compartments, in which the early mouse embryo and its extra-embryonic tissues are divided into many discrete regions that display intraregional, but no interregional dye coupling (85; 86). This would enable the exchange of differentiation factors, and eventually determining cell fate, between the cells of one tissue type and excluding the neighboring type. It was established that the visceral extra-embryonic ectoderm expresses high levels of Cx43 (87; 76), while no Cx43 is found in the parietal endoderm (76). Differentiation of F9 EC cells represents the first em-

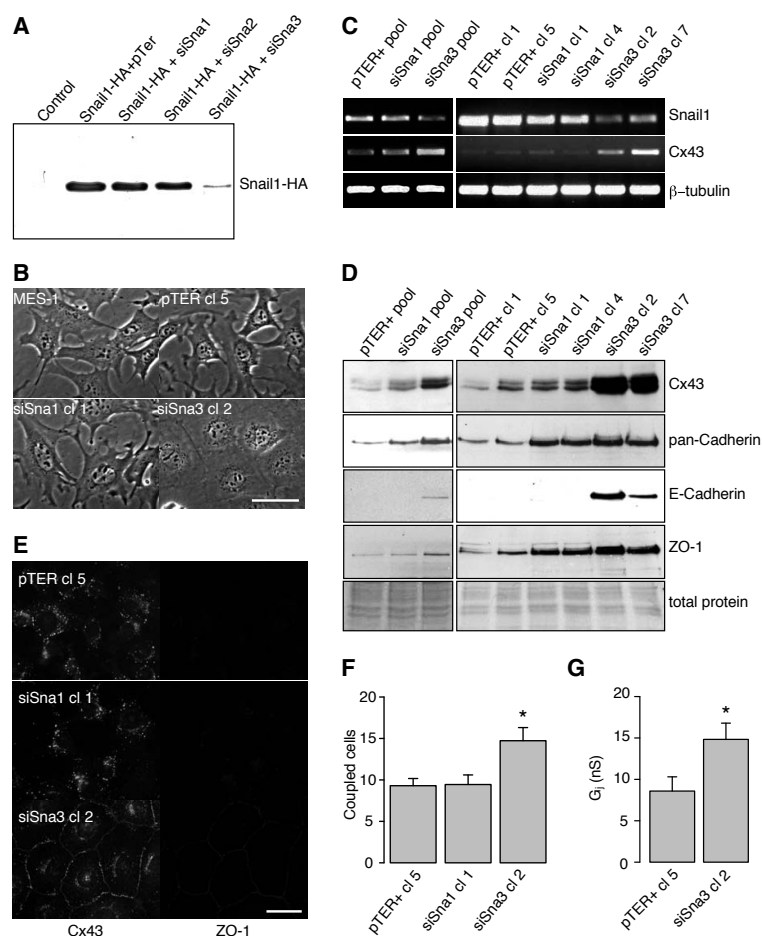


**Figure 2.6:** Snail1 silencing in MES-1 cells induces a mesenchyme-epithelium transition, connexin43 (Cx43) up-regulation and enhanced functional gap-junctional coupling. **A:** Western blot analysis of COS-7 cells co-transfected with HA-tagged Snail1 with empty pTER+ and three different Snail1 silencing siRNA expressing pTER+ constructs. Snail1 expression is detected by anti-HA-tag antibody. Control is non-transfected COS-7 cells. Strongest silencing is observed with siSna3. **B:** Phase-contrast images of native MES-1 cells and MES-1 clones expressing either empty pTER+(clone 5), siSna1 expressing pTER+(clone 1) or siSna3 expressing pTER+(clone 2). siSna3 expressing cells display an epithelium-like morphology. Scale bar = 20  $\mu$ m. **C:** Semi-quantitative reverse transcriptase polymerase chain reaction for Snail1 and Cx43 on MES-1 pools and selected clones expressing pTER+, siSna1, or siSna3. Snail1 expression is strongly decreased in siSna3 expressing pools and clones, while Cx43 is up-regulated. **D:** Western blot analysis of Cx43, pan-cadherin, E-cadherin, and Zonula Occludens-1 (ZO-1) expression on same-cell pools/lines as in (C). **E:** Localization of Cx43 and ZO-1 in clones expressing empty pTER+(clone 5), siSna1 (clone 1), and siSna3 (clone 2). In siSna3 expressing cells, Cx43 is strongly expressed at the cell borders and co-localizes with ZO-1. pTER+ and siSna1 expressing cells display mainly intracellular Cx43 and ZO-1 expression. Scale bar = 20  $\mu$ m. **F:** Lucifer Yellow dye-coupling quantification in MES-1 cell clones expressing pTER+, siSna1 or siSna3. Increased coupling is found in siSna3 clone 2. \*  $p < 0.05$  with respect to pTER+ cl 5 and siSna1 cl 1 (ANOVA Holms-Sidak test). **G:** Electrical coupling of MES-1 cell clones expressing either empty pTER+(clone 5) or siSna3 (clone 2). \*  $p < 0.05$  (Student's t-test).

bryonic EMT, i.e., the transition of visceral (or primitive) extra-embryonic to parietal endoderm, in development. The observed Cx43 down-regulation (Fig. 2.1) may separate the communication capacity between these two tissue types.

With respect to ZO-1 expression in relation to Snail1, our data confirmed the study of (74) in which a redistribution, but no down-regulation of ZO-1, was observed in response to Snail1 expression. A direct interaction of Cx43 and ZO-1 has been observed by several researchers (for a review, see (60)). Our data suggest that the existence of such an interaction strongly depends upon the cell-cell junctional localization of ZO-1. While Snail1-mediated redistribution of ZO-1 (74) seems to depend primarily on the decrease of tight junction proteins claudins and occludins, down-regulation of Cx43 may be a primary effect of Snail1-dependent transcriptional repression.

The role of cadherins with respect to Cx43 expression and localization is still enigmatic. Cx43-mediated gap junctional communication in mouse epidermal cell lines correlates with E-cadherin, but not with P-cadherin expression, and gap-junctional communication (and epithelial morphology) could be restored in E-cadherin negative cell lines by ectopic E-cadherin expression (58). On the other hand, E-cadherin-negative mouse blastocysts display normal Cx43 distribution in the trophectoderm (59). Furthermore, gap-junctional coupling in L cells was inhibited by E-, P-, or N-cadherin overexpression, while in the same study coupling was increased by N-cadherin expression in hepatoma cells (88). It became clear that in regenerating hepatocytes, cadherin-based cell-cell adherence junctions act as foci for gap junctional assembly, although similar foci were observed at sites of tight junction formation (89). Apparently, the relationship between cadherin mediated cell-cell adhesion and gap-junctional communication may be very differentially dependent on the cell type involved. In our study, we see no relationship between E-cadherin and Cx43 expression in F9 EC, PrE, and PE cells (Fig. 2.1C) or P19s18 and its derivatives (Fig. 2.2C), while in the latter cell types, some correlation in expression levels was observed when using a Pan-cadherin antibody (Fig. 2.2C). Also, in MES-1 cells expressing siSna1 and siSna3, a positive correlation is found between Pan-cadherin and Cx43 staining, while a correlation with E-cadherin was less clear. Our observation that Cx43 is repressed by Snail1 and the fact that E-cadherin, and perhaps other cadherins too, form a direct target for Snail1 may explain these discrepancies. Depending on the relative role of Snail1 and other transcriptional regulators of both Cx43 and E-cadherin in a given cell type, different or even opposite effects may be expected.

Although speculative, the Snail1-associated Cx43 down-regulation as observed in F9 EC and P19 EC cells might occur as a general phenomenon in many EMTs during differentiation, organogenesis, and tissue repair mechanisms.

## Acknowledgments

Christine Mummery is thanked for the P19s18 EC, END-2, MES-1, and EPI-7 cells and for critically reading the manuscript. We thank Bas Defize for sharing Snail1 expression and E-cadherin reporter constructs and for his valuable advice. This study is supported by the Technology Foundation (STW program DPTE, Grant #MKG5942, MvdH and Grant UGT.6746, TvV), the Netherlands Heart Foundation (Grant 2003B07304,

TdB, BK), the FP6 (Framework Program LSHB-CT-2004-502988) of the European Committee (BK), and the Netherlands Organization for Scientific Research (NWO, Grant 916.36.012, TvV).



## **Chapter 3**

### **Inhibition of cardiomyocyte automaticity by electrotonic application of inward rectifier current from Kir2.1 expressing cells**

Teun P. de Boer, Toon A. B. van Veen, Marien J. C. Houtman, John A. Jansen, Shirley C. M. van Amersfoort, Pieter A. Doevendans, Marc A. Vos and Marcel A. G. van der Heyden

*Medical and Biological Engineering and Computing, Volume 44, Issue 7, July 2006, 537-42*

## Abstract

A biological pacemaker might be created by generation of a cellular construct consisting of cardiac cells that display spontaneous membrane depolarization, and that are electrotonically coupled to surrounding myocardial cells by means of gap junctions. Depending on the frequency of the spontaneously beating cells, frequency regulation might be required. We hypothesized that application of Kir2.1 expressing non-cardiac cells, which provide  $I_{K1}$  to spontaneously active neonatal cardiomyocytes (NRCs) by electrotonic coupling in such a cellular construct, would generate an opportunity for pacemaker frequency control. Non-cardiac Kir2.1 expressing cells were co-cultured with spontaneously active rat NRCs. Electrotonic coupling between the two cell types resulted in hyperpolarization of the cardiomyocyte membrane potential and silencing of spontaneous activity. Either blocking of gap-junctional communication by halothane or inhibition of  $I_{K1}$  by BaCl<sub>2</sub> restored the original membrane potential and spontaneous activity of the NRCs. Our results demonstrate the power of electrotonic coupling for the application of specific ion currents into an engineered cellular construct such as a biological pacemaker.

## Introduction

Genetically engineered cell based pacemakers may become a valuable alternative for the current electronic pacemakers. The dominant endogenous pacemakers in the mammalian heart, such as the sinoatrial (SA) and atrioventricular nodes, constitute a specific spatially organized population of cardiac myocytes that have no primary contractile function. These cardiomyocytes are characterized by the expression of a specialized electronome, i.e., genes responsible for excitability and action potential propagation. This facilitates regular spontaneous depolarizations that by gradually increasing conductive properties toward the periphery of the node can drive the working myocardium (for review see reference (90)). The four most relevant properties of the nodal cardiomyocytes electronome of most mammals are the expression of pacemaker channels of the HCN type, the absence of fast inward sodium channels, the absence or minimal expression of inward rectifier channels of the Kir2.x type, and finally, the expression of specialized gap-junction protein isoforms (for review see reference (91)). Several studies have elaborated on the use of HCN ion channels in the construction of biological pacemakers, which is covered elsewhere in this issue. Here, we will further emphasize on the role of the inward rectifier potassium current for control of pacemaking frequency.

The inward rectifier current ( $I_{K1}$ ) is predominantly active during the last phase of repolarization and subsequently phase 4 of the atrial and ventricular action potential, where it has its role in both establishing and stabilizing the resting membrane at a rather negative potential between  $-75$  and  $-90$  mV (for review see reference (92)). Inward rectification is established by increasing potassium conductivity at hyperpolarization, while the  $I_{K1}$  channels close upon membrane depolarization. The molecular determinants of  $I_{K1}$  have convincingly been identified as the potassium ion channel constituents Kir2.1 (KCNJ2) and Kir2.2 (KCNJ12) (93), of which the first seems the

predominant isoform in the heart. A tetramer of Kir2.x subunits will form one  $I_{K1}$  channel (94) either as a homomeric (Kir2.1 or Kir2.2 only) or heteromeric (combined Kir2.1 and Kir2.2) channel (95). This molecular built-up enables an efficient dominant negative effect whenever one or more of the four subunits is modified and thereby disturbs the total  $I_{K1}$  channel conformation resulting in non-functional channels.

The absence of strong  $I_{K1}$  from the nodal tissues is a requirement for HCN ion channels to enable gradual depolarization by their pacemaker current ( $I_f$ ), resulting in the nodal action potential. Consistent with the limited expression or even absence from the SA node, no increased sinus rhythm is seen in the Kir2.1 knock-out mouse (93). Mice overexpressing a dominant negative form of Kir2.1 from the  $\alpha$ -MHC promoter surprisingly displayed even a decrease in heart rate (96). Neither ectopic beats nor re-entry arrhythmias were observed in these animals, indicating redundancy for Kir2.1 loss in the intact murine myocardium. However, in isolated cardiomyocytes from both mice, an increased incidence of spontaneous action potentials was observed. In contrast to the two downregulation approaches of  $I_{K1}$ , its upregulation in transgenic mice overexpressing wildtype Kir2.1 in the heart resulted in the expected slowing in heart rate (97).

Mutations in Kir2.1 that result in less or non-functional  $I_{K1}$  channels may be considered as natural knockouts. In recent years, several mutations have been identified, several of which behave as dominant negative, leading to a clinical manifestation known as Andersen syndrome (98; 99). Amongst other features, Andersen syndrome patients may suffer from cardiac arrhythmias. Therefore, unlike mice, large animal species, including man, may be more vulnerable for a loss of  $I_{K1}$  from the heart with respect to the occurrence of arrhythmias. In principle, introduction of a dominant negative form of Kir2.1 in the working myocardium may undermine a stable resting membrane potential (RMP), and thereby increase vulnerability of the cell for membrane potential fluctuations, which may eventually result in a spontaneous depolarization. Dependent upon the size of such an unstable region, a real local pacemaker able to drive the heart may be formed. In guinea pig, where a more prominent role for Kir2.1 in ventricular cardiomyocyte membrane potential stabilization is suspected than in mice, a strong ectopic expression of dominant negative forms of Kir2.1 indeed leads to liberation of pacemaker activity in the ventricle (100).

Although introduction of potent dominant negative Kir2.1 may result in biological pacemaker activity, the disadvantage is its dependence on spontaneous membrane potential fluctuations rather than on pacemaker currents formed by the HCN family. A similar situation can be found in embryonic stem cell pacemaker action. During stem cell differentiation into cardiomyocytes, the developmental program is recapitulated resulting in spontaneously beating cells. In the P19 cell model, only a minority of the cells express functional  $I_f$ , and no  $I_{K1}$  is found in such cells (32) from which can be concluded that pacemaker behavior occurs through RMP fluctuations allowed by the absence of the inward rectifier. Upon maturation, however, some cells start to express  $I_{K1}$ , which is accompanied by stable, more negative RMPs and a cessation of spontaneous beating. The uncontrolled maturation of embryonic stem cell derived cardiomyocytes makes them currently unsuitable to generate biological pacemakers. A promising avenue seems to use a cell-based tissue construct delivering HCN-mediated  $I_f$  to the surrounding myocardium (101). Such a biological pacemaker cell construct

needs to be tightly controlled, and we hypothesized that biologically engineered ion channel expressing cells could attribute to biological pacemaker regulation through electrotonic coupling. Here, we demonstrate, as a proof of principle, that  $I_{K1}$  expressing HEK-293 cells can modulate the beating frequency of spontaneously active neonatal rat cardiomyocytes through electrotonic interaction.

## Methods

*HEK-KWGF cells and neonatal cardiomyocytes* HEK-293 cells (ATCC # CRL-1573) were regularly cultured in DMEM supplemented with 10% fetal calf serum, 2 mM L-glutamine, 50 U/ml penicillin, and 50  $\mu\text{g}/\text{ml}$  streptomycin, all purchased from Cambrex (Verviers, Belgium).

HEK-293 cells stably expressing murine wildtype Kir2.1-GFP (HEK-KWGF) were generated as follows. HEK-293 cells were transfected with a pcDNA3-Kir2.1GFP, producing a C-terminal GFP-tagged Kir2.1 (a generous gift of Anatoli Lopatin (96)) using Lipofectamin (Invitrogen, Paisly, UK) and selected for stable transfectants with 500  $\mu\text{g}/\text{ml}$  G418 (Sigma, St. Louis, MI, USA) for 3 weeks. Complete stable pools of Kir2.1-GFP expressing cells were FACS sorted. The upper 10% of the total population displaying the strongest GFP expression was isolated, proceeded in culture, and denominated as HEK-KWGF cells.

Neonatal rat cardiomyocytes (NRCs) were isolated in accordance with the Guide for the Care and Use of Laboratory Animals published by the US National Institutes of Health (NIH Publication No. 85-23, revised 1996) and was approved by the institutional committee for animal experiments. Isolation and culture procedures were as described before (102), with only slight modifications. Sixty micrograms per milliliter Pancreatine (Sigma) was used instead of 20  $\mu\text{g}/\text{ml}$  DNase, cells were resuspended in culture medium consisting of M199 with Hanks, HEPES, L-AA and L-glutamine (Gibco, Breda, The Netherlands) and 10% neonatal bovine serum (Gibco), and pre-plating was shortened to 2 h. Co-cultures were made by plating NRC on the day of isolation and on the next day, HEK-KWGF cell suspensions were added at the desired concentrations.

*Western blot analysis* Cells were lysed in RIPA buffer (20 mM Tris-HCl, pH 7.4, 150 mM NaCl, 10 mM  $\text{Na}_2\text{HPO}_4$ , 1% (v/v) Triton X-100, 1% (w/v) Na-deoxycholate, 0.1% (w/v) SDS, 1 mM EDTA, 50 mM NaF, 1 mM PMSF, 10  $\mu\text{g}/\text{ml}$  aprotinin). Lysates were clarified by centrifugation at 14,000g for 5 min at 4°C. Twenty micrograms of protein lysate was mixed with Laemmli sample buffer and proteins were separated by 10% SDS-PAGE and subsequently electro-blotted onto nitrocellulose membrane (Biorad, Veenendaal, The Netherlands). Antibodies used: connexin43 (Cx43) (Zymed, San Francisco, CA, USA; cat. nr. 71-0700), Pan-Cadherin (Sigma, St Louis, MI, USA; cat. nr. C-3678), and GFP (Santa Cruz Biotechnology, Santa Cruz, CA, USA; cat. nr. SC-9996). Proteins were visualized by using peroxidase labeled secondary antibodies (Jackson, Soham, UK) and standard ECL procedures (Amersham Bioscience, Roosendaal, The Netherlands).

*$I_{K1}$  and action potential recording* A HEKA EPC-7 patch clamp amplifier was used to measure electrotonic interaction between cells. Voltage and current signals were

recorded using a custom data acquisition program (kindly provided by Dr J.G. Zegers) running on an Apple Macintosh computer equipped with a 12-bit National Instruments PCI-MIO-16E-4 acquisition card. Current signals were low-pass filtered at 2.5 kHz and acquired at 10 kHz. Action potentials were elicited with a brief square current pulse.  $I_{K1}$  was recorded in voltage clamp mode of the whole-cell patch clamp configuration. A conventional mono-exponential fitting procedure was used to derive membrane capacitance from currents elicited by  $-10$  and  $+10$  mV square pulses while holding the cell at RMP. Series resistance was not compensated for.  $I_{K1}$  was elicited by application of 1 s square test pulses ranging between  $-130$  and  $+50$  mV from a holding potential of  $-40$  mV. Steady state currents at the end of the pulse were normalized to membrane capacitance and plotted against test pulse potential. Online analysis was done using MacDaq 8.0 (kindly provided by Dr A.C.G. van Ginneken) and R 2.0.1 (81). Experiments were performed at  $20^{\circ}\text{C}$  on a Nikon Diaphot 300 inverted microscope. Extracellular buffer used was a modified Tyrodes solution, containing (in mM) NaCl 140, KCl 5.4,  $\text{CaCl}_2$  1.8,  $\text{MgCl}_2$  1, HEPES 15,  $\text{NaHCO}_3$  17.5, glucose 6, pH 7.20/NaOH. Gap-junctional coupling was inhibited by applying 4 mM Halothane dissolved in extracellular buffer at the interface between NRC and HEK-KWGF cells with an additional micropipette. Pipette buffer contained (in mM) potassium gluconate 125, KCl 10, HEPES 5, EGTA 5,  $\text{MgCl}_2$  2,  $\text{CaCl}_2$  0.6,  $\text{Na}_2\text{ATP}$  4, pH 7.20/KOH. Patch pipettes were pulled on a Narishige PC-10 puller and fire-polished. When filled with pipette buffer, the pipette resistance ranged between 2 and 5  $\text{M}\Omega$ . Liquid junction potential was calculated using Clampex (Molecular Devices Corp, Sunnyvale, CA, USA) and used for online correction. Beating frequency was determined by counting the number of beats for a period of 30 s under visual inspection. For each condition, at least six independent NRC or NRC/HEK-KWGF clusters were analyzed.

## Results

### Validation of $I_{K1}$ expressing HEK-KWGF cells

To create a co-culture system able to test electrotonic coupling of  $I_{K1}$  expressing cells with spontaneous active NRCs, we first created cells which were in principle able to couple with cardiomyocytes and that expressed functional  $I_{K1}$ . Therefore, HEK-293 cells were stably transfected with a murine Kir2.1-GFP fusion protein expression construct. Upon G418 based selection and FACS assisted enrichment, the resulting HEK-KWGF cells were further characterized. Western blot analysis demonstrated the expression of the Kir2.1-GFP fusion protein in stably transfected cells, while no signal was observed in maternal HEK-293 cells or NRC (Fig. 3.1A). Analysis of the gap-junction protein Cx43 expression demonstrated the presence of Cx43 in HEK-293 and HEK-KWGF cells; however, the levels were fairly low when compared to Cx43 expression in rat NRCs (Fig. 3.1A). In contrast, Cadherin expression, required for mechanical interaction between the two cell types, displayed less difference in expression level between the cell types. Epifluorescence microscopy illustrated the presence of a strong GFP signal at the cell borders of HEK-KWGF cells, and therefore Kir2.1 channels appear to be expressed at the plasma membrane (Fig. 3.1B). Subsequently, electrophysiological measurements

indeed validated the presence of high levels of functional  $I_{K1}$  channels in these cells, displaying an I-V curve characteristic for Kir2.1 channels (Fig. 3.1C, D). Current densities were  $-58.7 \pm 6.6$  pA/pF at  $-100$  mV, which is approximately 6-15 fold higher than in isolated neonatal (approximately  $-4$  pA/pF) (93) and adult murine heart cells ( $-4.68$  and  $-9.3$  pA/pF) (97; 96). In rat neonatal cardiomyocytes,  $I_{K1}$  current densities between  $-7$  and  $-9$  pA/pF at  $-100$  mV have been reported (103; 104). HEK-KWGF cells had a mean membrane potential of  $-75.2 \pm 0.5$  mV ( $N = 20$ ). No  $I_{K1}$  was found in non-transfected HEK-293 cells.

## Co-culture of HEK-KWGF cells with NRCs

Neonatal rat cardiomyocytes share several features with nodal cardiomyocytes, of which their automaticity is the most characteristic. Furthermore, they display a maximal diastolic membrane potential of  $-65$  mV and a prominent phase 4 depolarization. As  $I_{K1}$  is the main determinant of the RMP, we compared RMP of NRC clusters with that of NRC/HEK-KWGF cell clusters. NRC clusters displayed a maximal diastolic membrane potential of  $-65.1 \pm 2.8$  mV ( $N = 4$ ), which significantly decreased to  $-77.6 \pm 3.4$  mV ( $N = 6$ ) ( $p < 0.01$ ; Student's t-test) in NRCs coupled to one or more HEK-KWGF cells. When attached to HEK-KWGF, no spontaneous beating of NRCs was observed, nor could action potentials be recorded from those NRCs. Upon triggering by a depolarizing current, however, action potentials could be elicited that displayed an aberrant morphology when compared to mono-cultures of NRCs (Fig. 3.2A). Application of the gap-junction blocker Halothane to NRC/HEK-KWGF cell pairs decreased RMP of the NRC to its normal value and restored spontaneous action potential formation and beating behavior (Fig. 3.2B).

We next questioned whether HEK-KWGF cells could be used in co-cultures to control beating frequency, i.e., pacing rate, of a NRC culture. Therefore, co-cultures containing 300,000 cells were made with 0, 5, 25, 50 or 75% contribution of HEK-KWGF cells. NRC monocultures displayed a beating rate of approximately 238 bpm (Fig. 3). Co-culture with 5% HEK-KWGF cells dramatically decreased the beating rate to 83 bpm. Increasing the amount of HEK-KWGF cells inhibited beating rates even further. As it has been shown that  $I_{K1}$  can be inhibited by 1 mM  $\text{BaCl}_2$  (105) (Fig 3.3, inset), we tested whether addition of  $\text{BaCl}_2$  to the co-cultures could rescue the original beating rates. In NRC mono-cultures,  $\text{BaCl}_2$  application resulted in a slight increase (12%) in beating rate, suggesting the presence of limited amounts of endogenous  $I_{K1}$ . When applied to co-cultures,  $\text{BaCl}_2$  could strongly inhibit the silencing effect of HEK-KWGF with respect to NRC beating rate (Fig. 3.3).

## Discussion

Our study demonstrates a hyperpolarizing effect of Kir2.1 on the RMP of neonatal cardiac myocytes by electrotonic coupling, which thereby results in inhibition of spontaneous depolarizations of the cardiomyocytes. A remarkably strong inhibition of the beating frequency was accomplished with relatively few HEK-KWGF cells (Fig. 3.3). This may be explained by the large difference in  $I_{K1}$  densities between the two cell

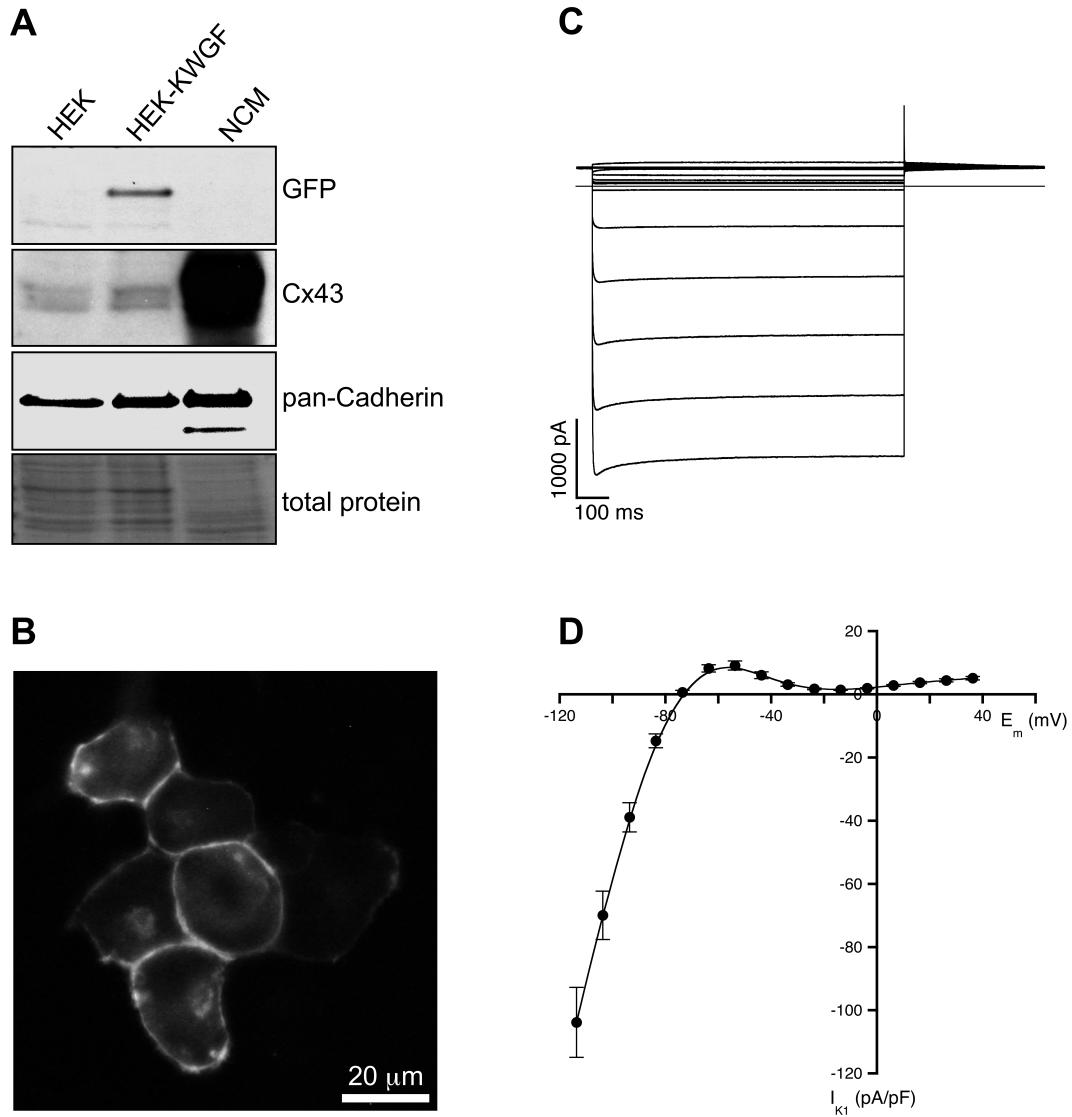


**Figure 3.1:** Characterization of HEK-KWGF cells. **A:** Western blot analysis of non-transfected HEK-293 cells (HEK), Kir2.1GFP expressing HEK-293 cells (HEK-KWGF) and rat neonatal cardiomyocytes (NRCs). Kir2.1-GFP signal (GFP) was only observed in HEK-KWGF cells. Connexin43 is expressed at low levels in HEK and HEK-KWGF cells, and at high levels in NRC. Cadherin adherence junction proteins (pan-Cadherin) are expressed in all three cell types at similar levels. Total protein staining is used as loading control. **B:** GFP fluorescence microscopy displays strong plasma membrane localization of Kir2.1-GFP. **C:** Current traces of HEK-KWGF cells characteristic for  $I_{K1}$ . Scale bars: horizontal = 200 ms, vertical = 500 pA. **D:** Current-voltage relationship of HEK-KWGF cells displaying  $I_{K1}$  characteristics.

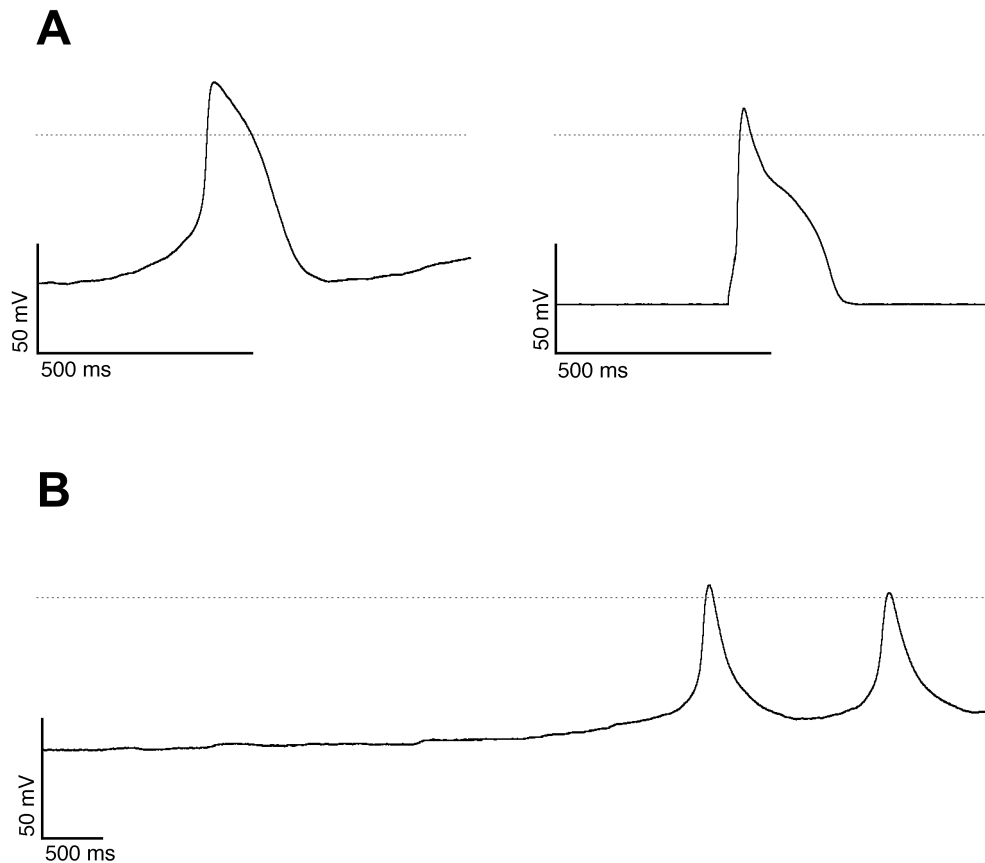


**Figure 3.2:** Electrotonic coupling between HEK-KWGF and neonatal cardiomyocyte (NRC). **A:** Action potential recordings from spontaneous NRC mono-cultures (left panel) and triggered NRC/HEK-KWGF cell pair (right panel) as measured from the NRC. Note the difference in resting membrane potential (RMP), action potential upstroke and duration. **B:** Gap-junction uncoupling by halothane restores RMP and spontaneous action potentials in NRC/HEK-KWGF cell pair as measured from the NRC. Scale bars: horizontal = 500 ms, vertical = 50 mV, dashed line indicates 0 mV.



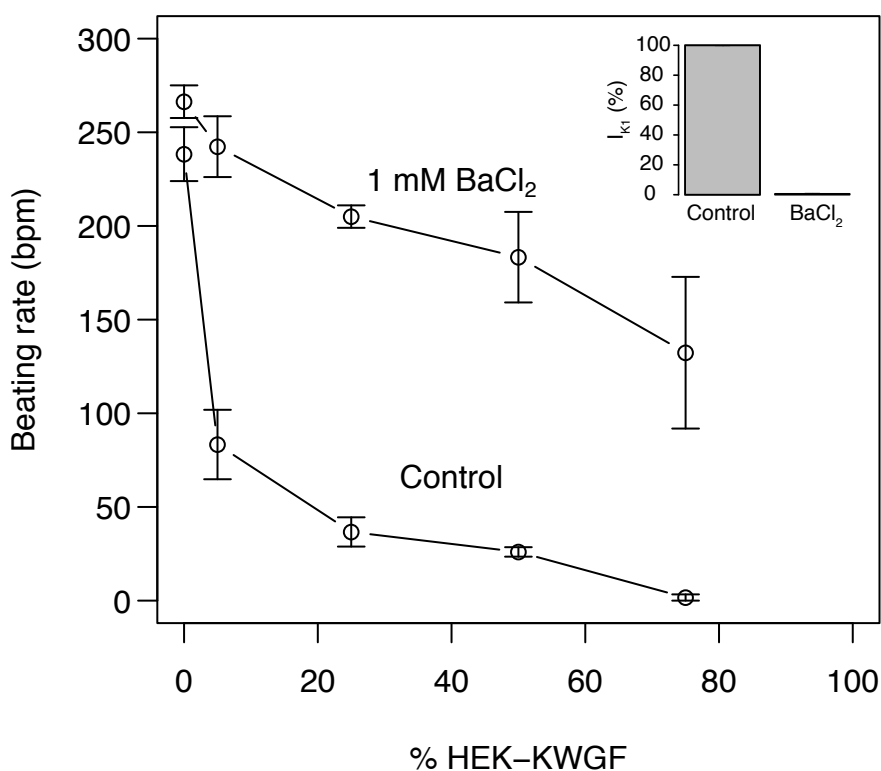


**Figure 3.3:**  $I_{K1}$  dependent regulation of neonatal cardiomyocyte (NRC) beating frequency. NRC and HEK-KWGF cells were co-cultured at a density of 300,000 cells/well with an increasing percentage of HEK-KWGF with respect to NRC cells. Beating frequencies (bpm) of NRC in the co-cultures were determined in the absence (control) and presence of 1 mM BaCl<sub>2</sub> (BaCl<sub>2</sub>). Results from six independent measurements  $\pm$  SEM are given. Significant differences (control vs BaCl<sub>2</sub>) ( $p < 0.01$ ) were found at all points except for 0% HEK-KWGF, and beating rate at 25% HEK-KWGF cells were statistically different ( $p < 0.01$ ) from 0 to 5% HEK-KWGF cells within each condition (two-way ANOVA). Inset: 99% inhibition of peak  $I_{K1}$  by BaCl<sub>2</sub> was determined in HEK-KWGF cells ( $N = 4$ ).

types, which are  $\sim -60$  and  $\sim -8$  pA/pF at  $-100$  mV for HEK-KWGF and NRC cells, respectively. This mechanism would be of support to create cellular constructs consisting of a heterogeneous population of  $I_f$  expressing cells and  $I_{K1}$  expressing cells, which dependent on their relative contribution within the construct might generate a predetermined pacemaker frequency. This approach would obviously benefit from a controlled expression of  $I_{K1}$ . This could be reached by generating clonal cells expressing different amounts of Kir2.1 and thereby  $I_{K1}$ . Alternatively, intervention in natural Kir2.1 regulatory mechanisms could be used, such as PKC or PKA mediated effects on  $I_{K1}$  (106; 91). Furthermore, Kir2.1 channels appear sensitive to intracellular polyamine (107) or PIP<sub>2</sub> regulation (108) which seems to operate at least in part interdependently (109). Obvious drawback of these approaches is the rather limited specificity of the signaling interference which may have many undesired effects on other ion channels in the heart or on  $I_{K1}$  in other tissues than the heart. More specific, and thus in favor, is to produce cells in which Kir2.1 is placed under the control of an inducible promoter, in which the inducing agent has no other physiologically relevant biological function. To achieve this, ecdysone could be an inducer of choice (110). The current promises in cardiac tissue engineering aside, the preclinical research now first has to establish the applicability of proofs of principles studies like this one, for their eventual clinical relevance.

## Conclusion

Electrotonic coupling of Kir2.1 expressing cells to spontaneous depolarizing NRCs results in silencing of the spontaneous beating behavior of the latter. This system is a proof of concept demonstrating the power of electrotonic coupling for the application of specific ion currents into an engineered cellular construct such as a biological pacemaker.

## Acknowledgments

We thank Anatoli Lopatin for sharing Kir2.1-GFP expression construct and Henk Roze-muller for FACS sorting of the HEK-KWGF cells. This study is supported by the Technology Foundation (STW program DPTE, grant #MKG5942, MvdH and grant UGT.6746, TvV), the Netherlands Heart Foundation (grant 2003B073, TdB) and the Netherlands Organization for Scientific Research (NWO, grant 916.36.012, TvV). FP6 (Framework Program LSHB-CT-2004-502988) of the European Committee (BK).

## Chapter 4

### **$\beta$ - but not $\alpha$ - adrenergic stimulation enhances conduction velocity in cultures of neonatal cardiomyocytes**

Teun P. de Boer, Harold V.M. van Rijen, Marcel A.G. Van der Heyden, Bart J.M. Kok, Tobias Opthof, Marc A. Vos, Habo J. Jongsma, Jacques M.T. de Bakker, Toon A.B. van Veen

*Circulation Journal, Volume 71, Issue 6, June 2007, 973-81*

## Abstract

**Background:** Both during cardiac maturation and myopathy, elevated levels of circulating catecholamines coincide with alterations in impulse propagation. We used an in vitro model of cultured cardiomyocytes to study the effects of adrenergic stimulation on conduction characteristics of immature heart cells. **Methods and Results:** Neonatal rat cardiomyocytes were cultured on preparations designed to measure conduction velocity (CV). CV was measured on the same preparation twice: at  $t=0$  and at  $t=24$  hours. Under control conditions ( $N=7$ ), CV at  $t=0$  ( $30.9 \pm 1.9$  cm/s) and  $t=24$  ( $32.4 \pm 4.4$  cm/s) was similar ( $P=0.70$ ). Immunohistochemistry revealed expression of the gap junction proteins connexin40 (Cx40), Cx43 and Cx45 with Cx43 being highly predominant. Stimulation for 24 hours with the  $\beta$ -adrenergic agonist isoproterenol (ISO) significantly increased CV from  $28.0 \pm 2.0$  cm/s at  $t=0$  to  $34.8 \pm 2.2$  cm/s at  $t=24$  ( $P=0.002$ ,  $N=5$ ). Microelectrode recordings showed a faster upstroke of the action potential (AP) of ISO treated cells. RT-PCR showed that ISO increased expression of SCN5a and  $\alpha_{1c}$  ( $\alpha$ -subunit of the cardiac sodium and L-type calcium channel respectively). Stimulation of cells with ISO did not induce alterations in distribution nor in expression of Cx40, Cx43 and Cx45 (both mRNA and protein) but slightly increased phosphorylation of Cx43. Stimulation for 24 hours with the  $\alpha$ -adrenergic agonist phenylephrine did neither affect CV nor the expression of the connexin isoforms, SCN5a and  $\alpha_{1c}$ . **Conclusions:**  $\alpha$ - and  $\beta$ -adrenergic stimulation differently affect propagation of the electric impulse which is primarily not caused by a differential effect on intercellular coupling. RT-PCR analysis and an enhanced AP upstroke velocity indicate a higher functional expression level of  $\alpha_{1c}$  and SCN5a in  $\beta$ -adrenergic stimulated cells, which may explain the observed increase in CV.

## Introduction

In the mature circulatory system,  $\alpha$ -adrenergic stimulation predominantly affects vessel diameter while  $\beta_1$ -adrenergic stimulation determines the adaptation of heart rate and contractility to changing demands. In immature stages of the heart, postnatal maturation coincides with in-growth of sympathetic neurons, elevated levels of released catecholamines and enhanced expression of  $\beta$ -adrenoreceptors (111). Shortly after birth, hyperplasia of the cardiomyocytes ceases which is followed by hypertrophic growth and maturation (112). During maturation, cardiac rhythm becomes slower while conduction velocity of the electrical impulse, which is initially slow (113), increases.

Several factors contribute to cell-to-cell propagation of the cardiac electrical impulse. Cell-to-cell propagation is enabled by specialized membrane structures named gap junctions. Gap junctions are agglomerates of intercellular channels composed of hexagonally arranged connexin proteins. The connexins form a large family of transmembrane proteins, which are expressed in virtually all vertebrate cells (114). Three isoforms, connexin40, (Cx40), -43 and -45, are expressed by mammalian cardiomyocytes. Expression of the isoforms is not uniform within cardiac tissue, differs between the species and is subject to developmental changes (115; 67; 66; 116). Cx43, as expressed between all working myocardial cells, highly predominates. Intercellular gap

junctional communication ( $g_j$ ) is determined by the number and distribution of expressed gap junction channels ( $n$ ), the open probability of each channel ( $P_0$ ) and the single channel conductance ( $\gamma_j$ ).  $P_0$  and  $\gamma_j$  differ between gap junction isoforms and are subject to post-translational modulation (e.g. by phosphorylation) (117).

Propagation further depends on the expression level of protein subunits that constitute the ion channels responsible for the electrical make-up of the action potential. In adult hearts, especially sodium channel availability determines the upstroke velocity of the action potential. In immature hearts, availability of the L-type calcium channel is most important in this respect. The higher the upstroke velocity, the faster a depolarized myocyte is able to trigger adjacent myocytes. Within the syncytium of all connected cardiomyocytes, changes in upstroke velocity thereby reflect on conduction velocity.

A third factor that affects propagation is geometry of the tissue. Differences in cell size and cell shape affect conduction characteristics through differences in cytoplasmic resistance. During cardiomyopathy, heterogeneous presence of discontinuities, as can be induced by fibrosis, can affect impulse propagation by pathway lengthening or through load-mismatch (118).

Both during physiological maturation of the newborn heart and during pathophysiology of the mature heart, elevated levels of circulating catecholamines coincide with changes in conduction velocity of the electrical impulse. In order to address whether adrenergic stimulation directly affects the molecular machinery underlying impulse propagation, we used an *in vitro* model of cultured neonatal rat cardiomyocytes (NRC) and subjected them to  $\beta$ -adrenergic stimulation. Here, we present the observed effects on conduction characteristics as induced by modulation of ion- and gap junction channel functionality.

## Materials and Methods

*Isolation and culture of neonatal rat ventricular cardiomyocytes.* Neonatal rat ventricular cardiomyocytes (NRC) were isolated from hearts of 1-2 day old Wistar rats as described before (102). For cell culture preparations, cells were seeded on collagen-coated substrates (25  $\mu\text{g}/\text{ml}$ , Boehringer) in a density of  $10^5$  cells/ $\text{cm}^2$ . Culture medium (Ham's F10 with L-glutamine, 100 IU penicillin/streptomycin, 10% fetal bovine serum, Life Technologies) was replaced daily.

*Determination of conduction velocity in vitro* To measure conduction velocity *in vitro*, patterned growth of NRCs was performed on custom-made glass dishes (5 $\times$ 5 cm) according to methods developed by (119). The bottom side of such dishes was coated with a layer of indium-tin-oxide (translucent and electrically conductive), platinum electrodes were integrated in the dish and on top cells were grown in channels with a width of 100  $\mu\text{m}$  and a length of 2 mm. This pattern was created by coating the dishes with collagen, which was followed by a KTI Negative Resist KTRF coating (Cassio Chemicals, Wormerveer, NL) preventing cell attachment. Next, the KTRF coating was partially removed by UV radiation and Xylol, using a photo-lithographic mask. From this, a pattern with 8 channels was produced exposing the collagen coating where myocytes could attach. For electrophysiological experiments, the dish was mounted on

a custom built stage on an inverted microscope (Leica) and connected to a custom built 64-channel amplifier. The electrically conductive coating on the bottom side of the dishes enabled heating by applying current through the coating, which was regulated by a thermostat (34°C). Measurements were performed in normal culture medium and gas exchange was prevented by silicone-oil (2 ml) layered on top of the culture medium. The preparation was paced (1 ms stimuli) at the extremity of one of the channels ( $2\times$  threshold, cycle length of 400 ms) using an extracellular bipolar electrode (tip-diameter 50  $\mu\text{m}$ ). Extracellular electrograms were recorded from 24 electrodes (3 electrodes/channel, inter-electrode distance 400  $\mu\text{m}$ ) in unipolar mode at 2 kHz. Local activation times were defined as the point of maximal negative  $dV/dt$  and determined by custom made software based on MatLab (the Mathworks, Inc.). Conduction velocity between electrodes was calculated by dividing the inter-electrode distance by the difference in activation time.

*Adrenergic stimulation of the cells*  $\beta$ -adrenergic stimulation of cells (24 hours) was performed by supplementation of 100 nM isoproterenol (ISO, Sigma) to the culture medium. Control incubations were performed in presence of 1  $\mu\text{M}$  atenolol ( $\beta_1$ -antagonist, Sigma), which was added one hour prior to stimulation with ISO. To further address specificity of the  $\beta$ -adrenergic stimulation,  $\alpha$ -adrenergic stimulation was performed using 10  $\mu\text{M}$  phenylephrine (PE, Sigma). For measurements of conduction velocity, each preparation was measured twice. After a control experiment at  $t=0$ , the floating silicone oil was removed and the preparation was thoroughly rinsed with Hanks Balanced Salt Solution (HBSS), before new culture medium supplemented with stimuli (or without in case of control) was applied. Since the conduction assay is non-invasive, this allowed to measure the same preparation under control conditions ( $t=0$ ), and upon 24h exposure time ( $t=24$ ). For protein and RNA isolation from cultured monolayers, exposure-time was terminated by washing the cells with PBS and addition of lysis buffer.

*Recording of action potentials* Action potentials were recorded using a custom made amplifier and sharp micro-electrodes filled with 3M KCl. Data were recorded at 4 kHz using a data acquisition program (Scope, kindly provided by Dr. J.G. Zegers, Academic Medical Center, Amsterdam) running on a Apple PowerMac G4. Channels were paced as with conduction velocity measurements at a cycle length of 300 ms. In the paced channel, cardiomyocytes were impaled with the micro-electrode and action potentials were recorded. All measurements were done after washout of adrenergic stimuli. Recordings were analyzed using MacDaq 8.0 (kindly provided by Dr. A.C.G. van Ginneken, AMC Amsterdam). Maximal upstroke velocity was determined by differentiation of voltage traces. Membrane capacitance of single cells was measured in whole cell voltage clamp mode, using a HEKA EPC-7 amplifier (HEKA, Lambrecht, Germany). Capacitance was derived by fitting the current elicited by a square test pulse (amplitude 5 mV) with a mono-exponential curve.

*Immunocytochemistry on cultured cells* Glass coverslips with cultured cells were rinsed in serum free medium, fixed in methanol ( $-20^\circ\text{C}$ ), washed with PBS and stored until

use. Immunolabeling was performed as described before (62). The following antibodies were used; rabbit polyclonal antibodies raised against Cx45 (kindly provided by Dr. T.H. Steinberg, Washington University, St.Louis (120)), Cx40 (Alpha Diagnostics), N-cadherin (Sigma) and mouse monoclonal antibodies raised against Cx43 (Transduction Laboratories), desmin (Sanbio),  $\alpha$ -actinin (Sigma), Troponin-T (Sigma) and  $\beta$ -MHC (kindly provided by Dr. A.F.M. Moorman, Academic Medial Center, Amsterdam, The Netherlands). Secondary antibodies for immunohistochemistry (Texas Red and FITC conjugated whole IgG) were purchased from Jackson Laboratories. HRP-conjugated secondary antibodies for Western blotting were purchased from Biorad.

*Protein isolation, SDS-PAGE and Western Blotting* Total cellular protein was isolated from confluent beating cultures by collecting them in lysis buffer (400  $\mu$ l/10 cm dish; 50 mM Tris-HCl pH 7.4, 150 mM NaCl, 0.5% Nonidet-P40, 0.5% Sodium deoxycholate, 0.1% Sodium dodecyl sulfate (SDS), 2 mM Phenyl-methylsulfonyl Fluoride (PMSF), protease-inhibitor-cocktail: 2 mM phenylmethylsulfonyl fluoride, 1 mM iodoacetamide, 1 mM phenantroline, 1 mM benzamidine, 0.5 mM pefabloc, 5 mM sodium bisulfate, 20  $\mu$ g/ml pepstatin A). After centrifugation, total cellular protein in the supernatant was determined using the BCA protein assay. Equal amounts (50  $\mu$ g/lane) of each sample were separated on 10% SDS polyacrylamide gels, and electrophoretically transferred to nitrocellulose membrane (0.45  $\mu$ m, Biorad). Protein transfer was assessed by Ponceau S staining. Prior to primary antibody incubation, blots were blocked with 5% dried milk powder. After incubation with Horse-Radish Peroxidase conjugated secondary antibodies, signals were visualized using Enhanced Chemo Luminescence reagent (ECL, Amersham) and exposure to XB-1 film (Kodak).

*RNA isolation and semi-quantative RT-PCR* Total RNA was isolated using Trizol (Gibco) according to the manufacturers protocol and 0.5  $\mu$ g RNA was reversed transcribed using M-MLV-RT (Gibco). PCR reactions were performed in 50  $\mu$ l reaction mixtures (cDNA equivalent of 50 ng total RNA). DNA was denatured for 5 minutes at 94°C followed by a repetitive program used for x-cycli: 45 second denaturation at 94°C, 30 seconds annealing of primers at appropriate temperature and 1 minute DNA extension at 72°C. Number of cycles was optimized and resulted in non-saturated PCR reactions. Reactions were terminated with 5 minutes extra DNA extension at 72°C and cooling down to 20°C. Obtained PCR products were run on 1.5% agarose gels and stained with ethidium bromide. Table 4.1 shows the number of cycles and characteristics of the primers used.

*Statistics* All values are given as mean  $\pm$ S.E.M. Multiple group comparison was performed using ANOVA, followed by a Fishers Post-hoc test using StatView 4.5 for Macintosh. P-values 0.05 were regarded as statistically significant. For two-group comparisons, Student's t-test was used.

**Table 4.1:** PCR primer pairs

Name	Forward/reverse 5'-3'	Annealing (°C)	Cycles	Product (bp)
rSCN5a	CCCTGCGCCACTATTACTTCACCA CACCTCTTGGTGAAAGCGAACAG	60	30	842
r $\alpha_{1c}$	TTCCAGATGAGACCCGCGAGCAG TGTCTGCGGCGTTCTCCATCTC	58	30	750
rCx40	CCCACCCCGTCAACTGTTATGTCT CACTGACAGGTCATCTGACCTTGC	60	35	500
rCx43	AGCGTGAGGAAAGTACCAAACAGC AAGAAGGCCACCTCAAAGATAGAC	62	30	666
rCx45	GGCTATAACATTGCTGTCAAACCA AGCCAACAGCATCCCTGAAGATAA	60	35	444
GAPDH	ATGGTGAAGGTCCGGTGTCAAC TTACTCCTTGAGGCCATGTA	55	30	1002

## Results

### Cell culture of isolated cardiomyocytes

A seeding density of 100,000 NRC/cm<sup>2</sup> resulted within 24 hours in confluent and synchronically beating monolayers of myocytes. Purity of the cultures was assessed by immunolabeling against  $\alpha$ -actinin, a marker strongly expressed in cardiomyocytes but not in non-myocytes. Co-staining with the nuclear dye Hoechst 33258 allowed for evaluation of the content of non-cardiac cells in the cultures, which appeared to be lower than 10% (data not shown). Treatment of cultures for 24 hours with isoproterenol (ISO) did not induce changes in cell size and shape (see Figure 1A), but increased beating rate within minutes. Pre-incubation with the  $\beta_1$ -antagonist atenolol prevented this increase in beating rate. Membrane capacitance, as a measure of cell size, revealed no significant difference between control cells ( $16.7 \pm 1.9$  pF, N=6) and ISO treated cells ( $18.6 \pm 2.0$  pF, N=5).

### Effect of ISO on impulse propagation and AP upstroke velocity

Extracellular electrograms recorded at three subsequent electrodes of a channel are shown in Figure 4.1B. The first large deflection (in between the lines indicated with a star) represents the stimulus artefact, which is followed by the electrical activity of the preparation. Figure 4.1C shows the conduction velocity (CV) as determined from preparations with myocytes grown in the channels. Under control conditions (N=7), CV at t=0 h ( $30.9 \pm 1.9$  cm/s) and t=24 h ( $32.4 \pm 4.4$  cm/s) were statistically similar (P=0.70). Stimulation for 24 hours with the  $\beta$ -adrenergic agonist ISO significantly increased CV from  $28.0 \pm 2.0$  cm/s at t=0 to  $34.8 \pm 2.2$  cm/s at t=24 h (P=0.002, N=5). In addition, action potentials were recorded from myocytes within the paced channels. Figure 4.2A shows representative examples of action potentials recorded at t=24 h from myocytes under control conditions (CON) and upon treatment with ISO. Figure 4.2B shows that at t=24 h, maximal upstroke velocity in (untreated) control



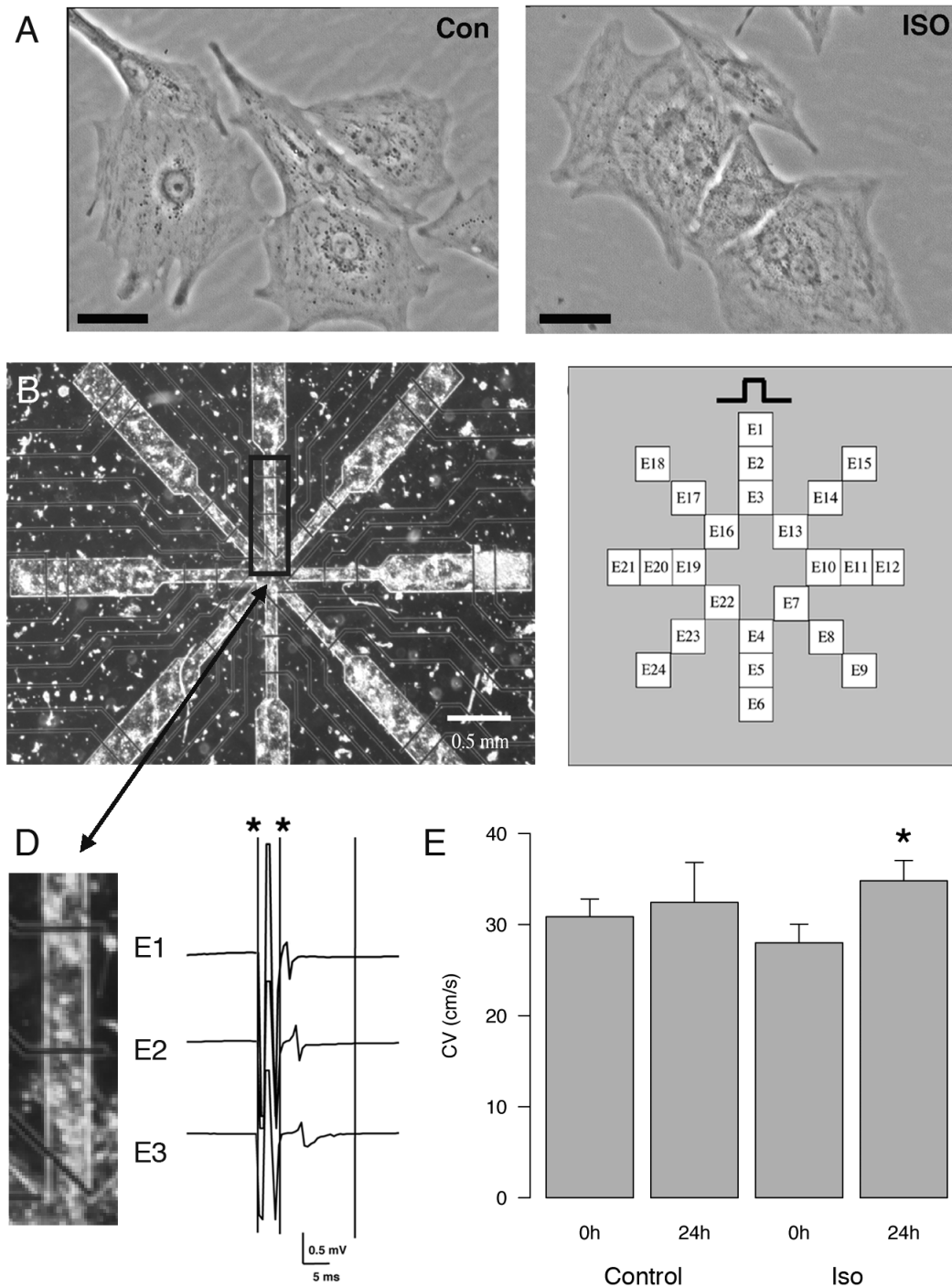


**Figure 4.1:** **A:** Representative morphology of cultured neonatal rat cardiomyocytes under control (Con) conditions or after treatment with isoproterenol (ISO). Bar=20  $\mu\text{m}$ . **B:** Patterned growth of cells on top of the preparations with the inserted electrodes. **C:** Schematic representation of the inserted electrodes. **D:** Unipolar electrograms recorded at 3 subsequent electrodes in a channel. The first large deflections in between the lines marked with a star represent the stimulus artefact. Local activation is determined by maximal negative  $dV/dt$ . **E:** Bar plot showing the conduction velocity in cm/s. Conduction velocity (CV) was measured at t=0h and at t=24h for both control preparations with untreated cells and for preparations that were stimulated with ISO after the measurement at t=0h.

preparations was  $33.9 \pm 3.6$  V/s (N=12) while stimulation with ISO significantly increased maximal upstroke velocity to  $52.6 \pm 7.7$  V/s (N=11, P=0.04). ISO did not affect the maximal diastolic potential of the cells.

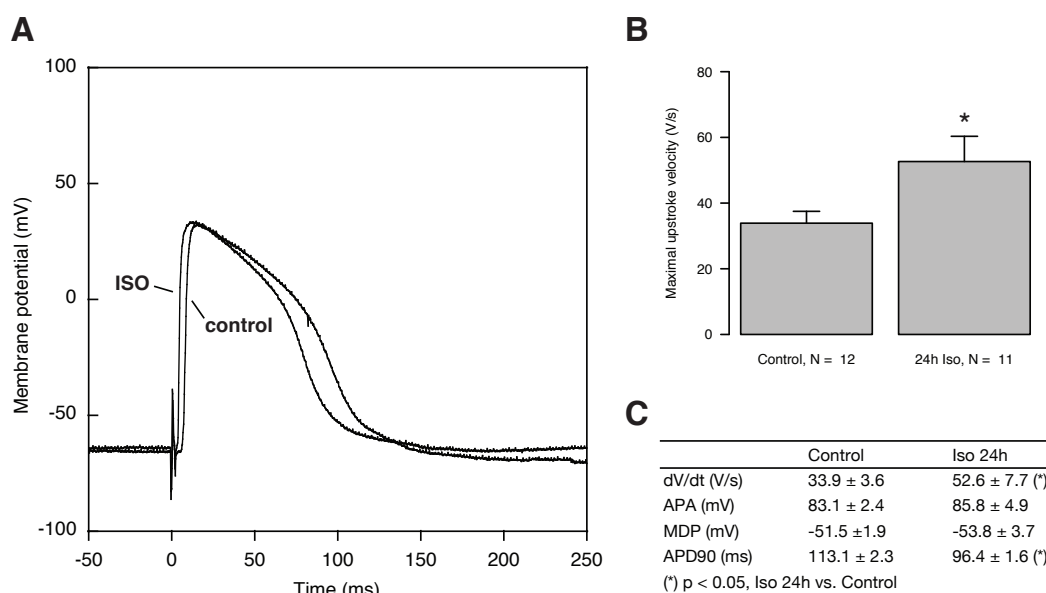


**Figure 4.2:** **A:** Representative examples of APs recorded at  $t=24$  h from myocytes cultured on the preparations under control conditions or upon treatment with ISO. **B:** Statistics of upstroke velocity from the recorded APs. \* = significantly different from control. **C:** Table summarizing the effects of 24 h ISO stimulation on action potential parameters.

## Immunohistochemistry

Labelling of the cultures (N=6) with antibodies against desmin (Fig. 4.3A),  $\alpha$ -actinin (Fig. 4.3B),  $\beta$ -MHC (Fig. 4.3C), and Troponin-T (Fig. 4.3D) revealed a pattern of cross-striations characteristic for immature cardiomyocytes. Cultures were also positive for N-cadherin, a component of the adherence junction, which labelled the complete sarcolemma (Fig. 4.3E). In a similar pattern, extensive Cx43 staining was found (Fig. 4.3F). At a much lower level, Cx40 appeared present at the sarcolemma and only in a minority of cells heterogeneously distributed throughout the culture (Fig. 4.3G). Using a high magnification, Cx45 was detected only sparsely between some cells (Fig. 4.3H). Treatment of the cells with ISO for 24 hours, did neither alter the formerly described expression patterns of the connexin isoforms nor their subcellular distribution (data not shown).

## Western blot analysis of Cx43 and contractile markers

In order to reveal the effects of 24 hours  $\beta$ -adrenergic stimulation with respect to possible changes in expression level of contractile proteins and gap junction proteins, Western blot analysis was performed. Compatible with the results of the immunohistochem-

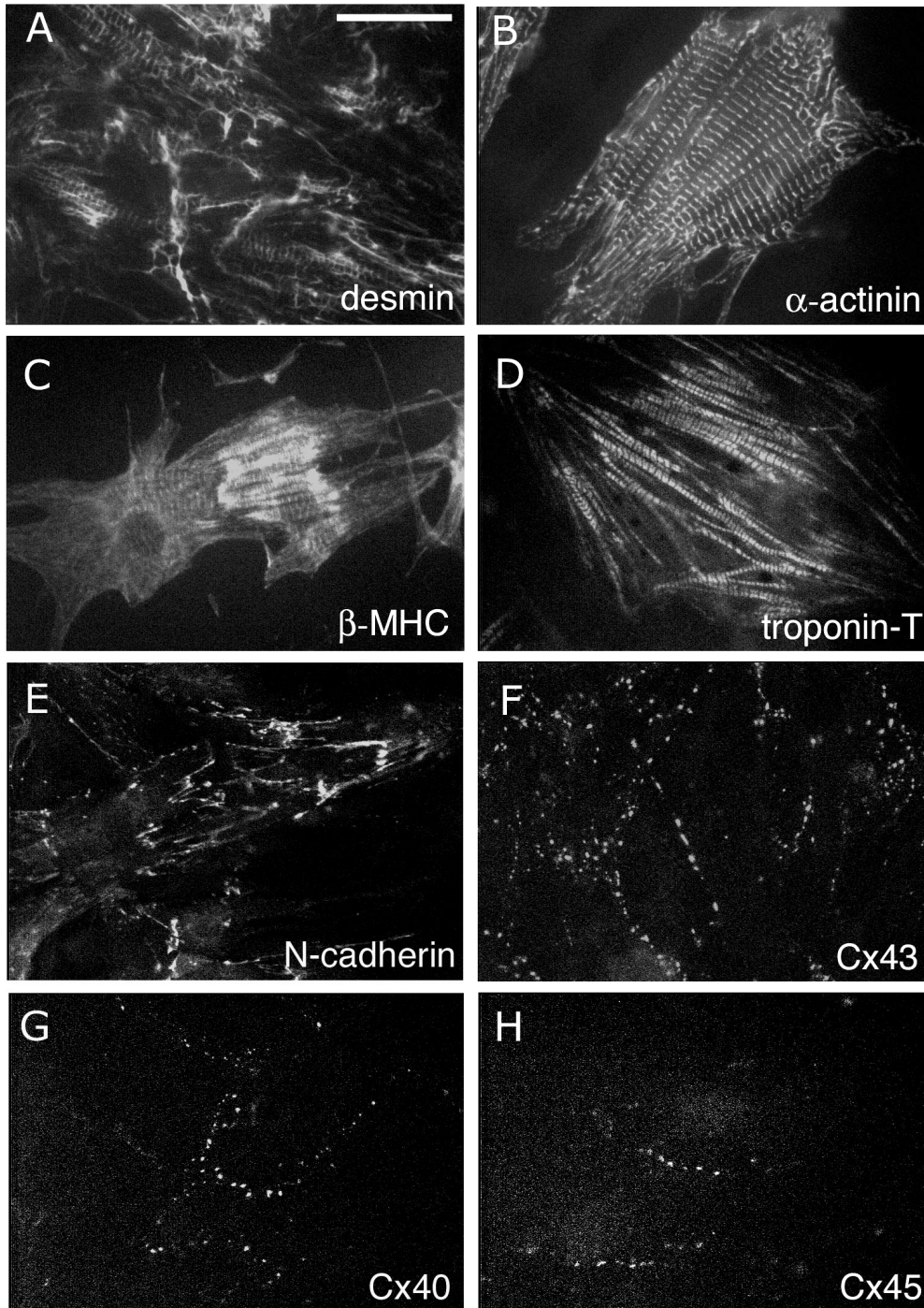


**Figure 4.3: A-H:** Immunohistochemical labelling of isolated and cultured NRCs grown on collagen coated slides. Bar (in A) = 40  $\mu\text{m}$  in B,D,E, 30  $\mu\text{m}$  in A,C,F,G and 20  $\mu\text{m}$  in H.

istry, no immunoblot signals were detected for Cx40 and Cx45 which is most likely due to their very low expression. Immunoblots of Cx43 (typical example shown in Figure 4.4A), exhibited the characteristic three-banded pattern of  $\sim 41$  kD,  $\sim 43$  kD and  $\sim 45$  kD representing one non-phosphorylated (NP) and two phosphorylated forms (P1 and P2), respectively (121). Upon stimulation with ISO, no obvious changes were found in the total density of the three bands suggesting equal expression levels. However, the P2 band of Cx43 (Figure 4.4A, arrow) consistently (N=4) showed a higher density as compared to the P2 band of control cells and of ISO treated cells pre-incubated with atenolol. In addition, no differences in expression level were found for the muscle markers desmin and  $\alpha$ -actinin, and the adherence junction component N-cadherin (Figure 4.4B).

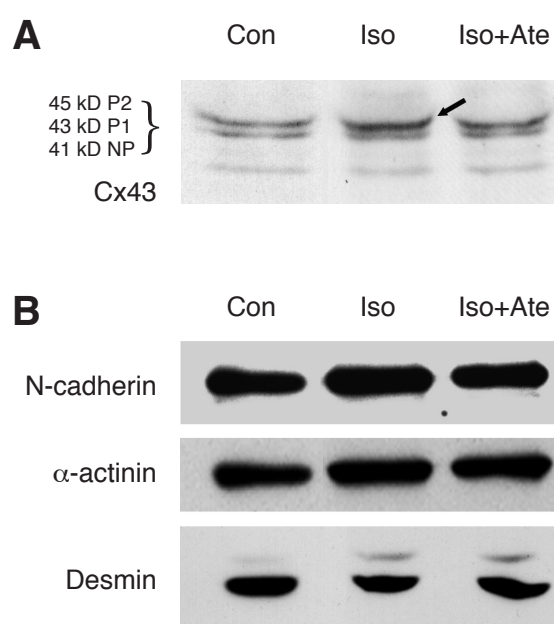


**Figure 4.4:** Western blot of total cellular protein isolated from (un)treated NRCs and stained with antibodies raised against Cx43 (**A**), desmin, N-cadherin and  $\alpha$ -actinin (**B**). P2, P1 and NP in the Cx43 blot represent the double-, single- and non-phosphorylated states of the protein respectively. CON=control, ISO=isoproterenol, Ate=atenolol.

## RT-PCR analysis of Cx40, Cx43, Cx45, SCN5a and $\alpha_{1c}$ mRNA

Semi quantitative RT-PCR analysis was performed to evaluate the effect of ISO on the mRNA level. The expression level of all three connexin isoforms was comparable under control conditions (N=4) and upon stimulation with ISO (N=4) (Figure 4.5). However, RT-PCR performed with specific primers for  $\alpha_{1c}$  ( $\alpha$ -subunit L-type Ca channel,  $I_{Ca,L}$ ) and SCN5a ( $\alpha$ -subunit Na channel,  $I_{Na}$ ) revealed that expression of  $\alpha_{1c}$  and to a lower extent also that of SCN5a was increased upon stimulation with ISO (Figure 4.5). Signals for GAPDH indicate that equal amounts of input cDNA were analyzed. Specificity of the reactions was indicated by the negative controls (no signals in right panels) in which reverse transcriptase was omitted (-RT).

## $\alpha$ -Adrenergic stimulation does not change CV

In order to evaluate whether the above described effects appeared specific for  $\beta$ -adrenergic signalling, analogue experiments were performed with myocytes cultured for 24 hours in presence of 10  $\mu$ M phenylephrine (PE), an  $\alpha$ -adrenergic specific agonist. In contrast to ISO, PE appeared ineffective in changing CV as CV at  $t=0$  ( $29.3 \pm 5.8$  cm/s,  $N=4$ ) and  $t=24$  ( $26.3 \pm 1.8$  cm/s) were statistically similar ( $N=4$ ,  $P=0.57$ ). Furthermore, upon stimulation, no alterations were detected in protein level of Cx43 and desmin, although expression of N-cadherin and  $\alpha$ -actinin appeared upregulated (Figure 4.6A). At the level of mRNA, both expression of all three connexin isoforms, and of SCN5a and  $\alpha_{1c}$  were comparable between control cells and PE-treated cells (Figure 4.6B). Taken together, these data support the absence of alterations in CV upon stimulation with PE.

## Discussion

This study shows that; 1) Stimulation of cultured NRCs for 24 h with ISO increased CV by  $\sim 25\%$  while stimulation with PE did not alter CV. 2) Upstroke velocity of the action potential was increased upon stimulation with ISO. 3) ISO induced no marked alterations in expression and distribution of Cx43 although phosphorylation of Cx43 seemed slightly increased. 4) Semi-quantitative RT-PCR showed an increase in expression of  $\alpha_{1c}$  and SCN5a upon exposure to ISO which fits well with the increased upstroke velocity of the AP. 5) The observed effects appeared specific for  $\beta$ -adrenergic stimulation since  $\alpha$ -adrenergic stimulation with PE revealed results similar to control conditions.

*Cell model* Conduction of electrical activity over the cardiac compartments is roughly determined by three parameters: 1) Intercellular communication through gap junction channels, 2) action potential (AP) characteristics, 3) tissue (and cellular) geometry including factors as cytoplasmic resistance and presence of fibrosis. The dependence of impulse propagation on several interrelated factors often complicates an appropriate interpretation which parameter is causative during alterations in conductance. Therefore, an in vitro model of reduced complexity is a common chosen approach. Cultures of isolated NRCs are routinely used to study different aspects of cardiac cell biology. The high reproducibility of isolation procedures and culture principles, and the large yield of myocytes that can be obtained mainly underlie this fact. However if pathophysiological processes are studied, an experimental limitation of the used model might be the rather immature status of the myocytes as compared to that of adult cardiomyocytes. In this study however, we have evaluated the effect of adrenergic stimulation on electrical impulse propagation; an aspect which embeds a reasonable relevance for both the adult and immature myocardium. The rationale is that under pathological conditions in the adult heart, high levels of circulating catecholamines trigger receptor desensitisation and cardiac malfunctioning eventually leading to cardiac failure (122; 123). On the other hand, in the neonatal heart, catecholamines contribute to physiological growth and maturation (124). In addition, the distribution of gap junction channels under neonatal conditions resembles the expression pattern of gap junctions in the myopathic

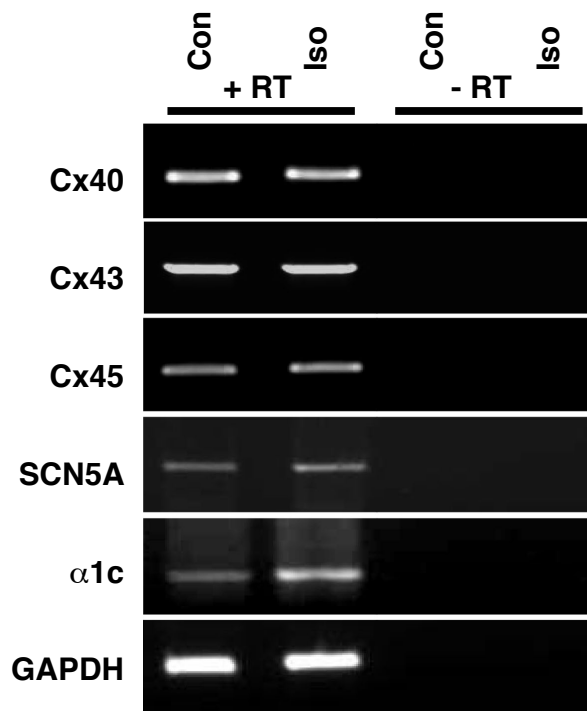


**Figure 4.5:** RT-PCR on the mRNA levels of Cx40, Cx43, Cx45, SCN5a and  $\alpha_{1c}$  after 24 hours of stimulation with ISO. Equal amounts of input cDNA were used as indicated by GAPDH signals. The first two lanes (from left) are showing the specific products obtained, the last 2 lanes are negative controls (RT omitted). CON=control, ISO=isoproterenol.

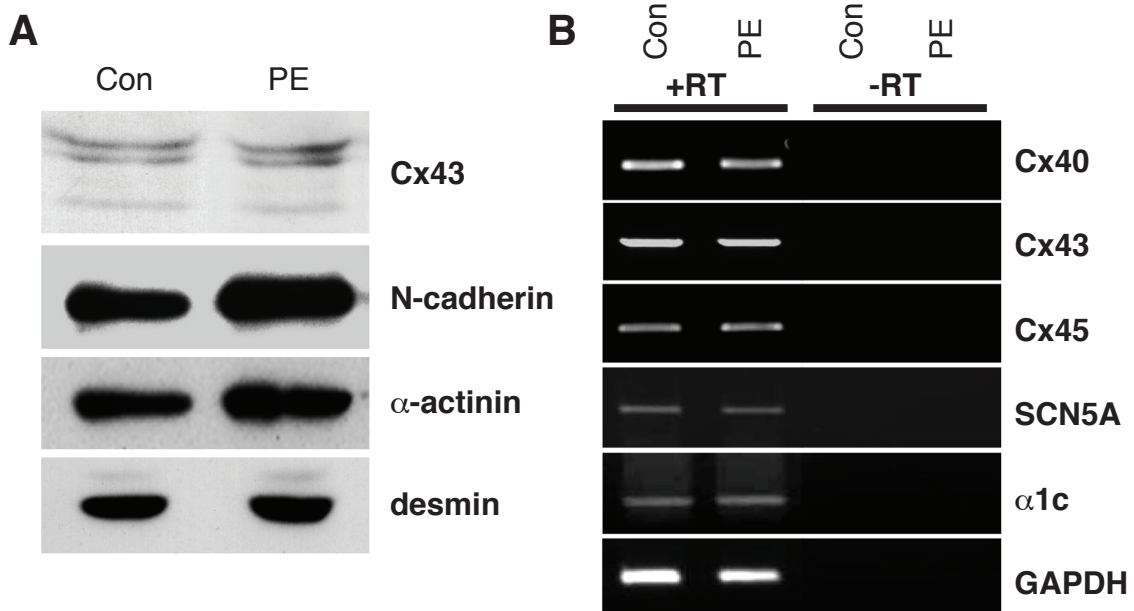


**Figure 4.6: A:** Western blot of total cellular protein isolated from (un)treated NRCs and stained with antibodies raised against Cx43, desmin, N-cadherin and  $\alpha$ -actinin. **B:** RT-PCR on the mRNA levels of Cx40, Cx43, Cx45, SCN5a and  $\alpha_{1c}$  after 24 hours of stimulation with PE. Equal amounts of input cDNA were used as indicated by GAPDH signals. The first two lanes (from left) are showing the specific products obtained, the last 2 lanes are negative controls (RT omitted). Con=control, PE=phenylephrine.

adult heart where gap junctions partially have redistributed to lateral cell sides. In our *in vitro* approach we observed that exposure of cultured NRCs for 24 hours to ISO, but not PE, increased conduction velocity (CV) by 25%. To explain this increase, we subsequently investigated the contribution of possible alterations in cell size, gap junctional coupling and action potential generation.

*Cell size* Upon the rather short stimulation with ISO, hypertrophic growth of the cultured myocytes was excluded because no differences in cell shape or in expression level of contractile proteins were observed. In line with this, membrane capacitance, as a measure of cell size, revealed no significant difference between control cells and ISO treated cells. Based on these observations, no modulatory role for differences in cytoplasmic resistance is expected to participate in the observed effect on CV.

*Gap junctions* In the cell-cultures, expression of Cx40 was low and heterogeneous since some cells initially did express Cx40 while others did not. This might be due to the fact that in the immature ventricle, a gradient exists from cells with relatively high Cx40 expression at the endocardial site to very low or absent Cx40 expression in the sub-epicardial layers (125). After 2 days of culture time, Cx40 expression was further reduced to negligible levels. Together with the hardly detectable expression level of Cx45 (similar as found *in vivo*) this facilitated conditions where cultured cells were almost exclusively coupled by Cx43 gap junctions. On the protein level, exposure of the cells for 24 hours to ISO did not markedly alter expression level and distribution of Cx43, nor reinduced expression of Cx40 and Cx45. Therefore, the observed change in CV presumably can not be explained by changes in the amount of inserted gap junction channels, mislocation of channels (intracellularly) nor by an altered contribution of Cx40 or Cx45 channels which have different conductive characteristics (117). RT-PCR analysis of all three connexin isoforms confirmed the lack of alterations in expression. ISO, however, slightly but consistently increased Cx43 (P2) phosphorylation. Our results are in line with a study reporting disorganization of Cx43 without change in expression level in patients with chronic atrial fibrillation (126), but are in contrast with an earlier and similar *in vitro* study reporting increased Cx43 expression after adrenergic stimulation (127). This discrepancy is explained by important differences in protein isolation procedure used, yielding different protein pools. We have used a method devised by (121) that was shown to isolate functional connexin protein involved in cellular communication. Most (but not all) reports on Cx43 describe an increase in electrical coupling between cells upon phosphorylation by PKA (summarized in (117)). Whether this increased intercellular coupling contributes to the observed increase in CV can't be excluded and might in addition be affected by possible alterations in open time of the phosphorylated Cx43 gap junction channels. On the other hand, alterations in intercellular coupling have to be very robust to affect CV. Both in the intact mouse heart (128), and in strands of cultured NRCs (129), CV was not affected even when the expression of Cx43 gap junction channels was reduced by 50% and 43% respectively.

*Ion Channels* Besides potential changes in gap junctional conductance, we investigated whether changes in action potential characteristics could explain the observed

alterations in CV. In immature cardiomyocytes, the rate of rise of the AP is primarily determined by the density of the calcium current ( $I_{Ca}$ ) and to a lesser extent, the sodium current ( $I_{Na}$ ). The rather small contribution of  $I_{Na}$ , as compared to upstroke characteristics in adult cardiomyocytes, can be explained by the (unstable) maximal diastolic potential of neonatal cardiomyocytes, which is less negative ( $\sim -60$  mV) than the stable resting membrane potential in adult cells ( $\sim -90$  mV). This less negative diastolic potential in neonatal cardiomyocytes limits sodium channel availability and favours calcium channels to facilitate the upstroke of the AP. Since ISO did not alter the maximal diastolic potential as compared to that in control cells, this factor is not expected to influence availability of sodium and calcium channels. RT-PCR analysis revealed that ISO treatment clearly increased the expression levels of  $\alpha_{1c}$  and to a lesser extent of SCN5a, which might potentiate a higher calcium and sodium current density. As has been reported, ISO treatment of neonatal cardiomyocytes increased expression of  $\alpha_{1c}$  which resulted in a functional increase in calcium current density (130; 131). We suggest that in our study, the increased expression of sodium and calcium channels contributes to the measured increase in upstroke velocity of the action potential. In summary, in this study we have shown that stimulation with catecholamines differentially affects CV of the electrical impulse. Whereas  $\alpha$ -adrenergic stimuli appeared rather ineffective,  $\beta$ -adrenergic stimuli increased CV. This effect seems primarily not to depend on alterations in cell-to-cell coupling but most likely can be explained by an elevated upstroke velocity of the action potential as mediated by an increased sodium and calcium current density.

## Acknowledgements

S.J.A. Tasseron and S.C.M. van Amersfoorth (Dept. Experimental Cardiology, AMC, Amsterdam) are kindly acknowledged for their contribution in coating of the specific preparations and for isolation and culture of the cardiomyocytes on these preparations. This study was supported by the Netherlands Heart Foundation (grant 2003B07304, TdB), the Technology Foundation (STW program DPTE, grant #MKG5942, MAGvdH and grant UGT.6746, TABvV) and the Netherlands Organization for Scientific Research (NWO, grant 916.36.012, TABvV).



## **Chapter 5**

### **Pro-arrhythmogenic potential of immature cardiomyocytes is triggered by low coupling and cluster size**

Teun P. de Boer, Marcel A.G. van der Heyden, Martin B. Rook, Ronald Wilders, Renske Broekstra, Bart J.M. Kok, Marc A. Vos, Jacques M.T. de Bakker and Toon A.B. van Veen

*Cardiovascular Research, Volume 71, Issue 4, Pages 704-14*

## Abstract

*Objective* Cell transplantation strategies to regenerate compromised myocardium take advantage of in vitro generated cardiomyocytes. Common in those immature myocytes is spontaneous impulse formation and a restricted ability to establish proper electrical interaction. Spontaneous impulse formation and impaired cell-to-cell coupling have been shown to be arrhythmogenic. To investigate whether these features harbour a pro-arrhythmogenic potential for cell transplantation, a co-culture of spontaneously active neonatal rat cardiomyocytes (NRC) and quiescent adult dog cardiomyocytes (ADC) was used.

*Methods* ADCs and NRCs were isolated and cultured on laminin-coated substrates. Connexin43, N-cadherin and  $\alpha$ -actinin expression was evaluated with immunohistochemistry. Intercellular coupling was measured in cell pairs using the dual voltage clamp technique and fluorescent dye injection.

*Results* One day after isolation, NRCs were beating spontaneously, while ADCs remained quiescent in monoculture. ADC resting membrane potential was  $-80.3 \pm 0.2$  mV (mean  $\pm$  SEM, N = 24) and did not change significantly over time. NRCs had a maximal diastolic potential of  $-65.0 \pm 2.8$  mV (N = 4). After one day of co-culture, pseudopodia-like extensions developed at the former intercalated discs of ADCs, contacting the NRCs. Only ADCs that contacted three or more NRCs started to beat in synchrony. Expression of connexin43 and N-cadherin indicated presence of electrical and mechanical junctions at the interface between the two cell-types. Transfer of Lucifer Yellow demonstrated junctional permeability between ADCs and NRCs. Junctional conductance between ADC-ADC ( $31.9 \pm 5.1$  nS, N = 10) and NRC-NRC ( $35.0 \pm 9.6$  nS, N = 6) pairs was significantly higher compared to ADC-NRC pairs ( $9.7 \pm 2.9$  nS, N = 8). Gap-junctional blockade with halothane reversibly abolished NRC-triggered beating of ADCs. Computer simulations demonstrated that within a delicate window of gap junctional conductance small clusters of spontaneously active cells are able to induce triggered activity in quiescent mature myocytes but also in a two-dimensional sheet of ventricular cells.

*Conclusion* Spontaneously active immature cardiomyocytes are able to trigger mature cardiomyocytes depending on their level of electrical coupling and the amount of coupled immature myocytes.

## Introduction

Spontaneous depolarization of autorhythmic myocytes within the sinoatrial (SA) node triggers each subsequent heartbeat. These nodal myocytes have no primary contractile function but are crucial in impulse formation. They lack a stable resting membrane potential and exhibit a spontaneous diastolic depolarization. This electrical instability is primarily stable due to the low amount of channels conducting the (stabilizing) inward

rectifier current ( $I_{K1}$ ). In the SA node, the level of intercellular electrical coupling, as mediated by gap junction channels, is low between myocytes within the compact node but this gradually increases towards the border zone with the atrial working myocardium (132). This configuration allows the impulse of the spontaneously beating cells to exit the node and prevents clamping of the membrane potential of spontaneously active cells to the membrane potential of the atrial cells. In the working myocardium, a proper and timely activation of all composing cardiomyocytes is effectuated by high levels of rather homogeneously expressed ion channel and gap junction channel constituents. Cardiomyocytes of the working myocardium are non-autorhythmic due to a high expression level of channels conducting  $I_{K1}$ . Automaticity, however, can be introduced by severe downregulation of Kir2.1 protein; the major constituent of the  $I_{K1}$  channel (100). Electrical coupling is facilitated by gap junction channels which predominantly are constituted from hexagonally arranged connexin43 (Cx43) protein subunits (117). Pathophysiological conditions, however, initiate irregularities in expression and distribution of gap junctions throughout the heart (meaning that part of the myocytes are not or poorly coupled to each other). Next to uncontrolled automaticity, these changes have been recognized as an important factor predisposing the heart to arrhythmias (133; 128). In order to ameliorate cardiac performance of hearts compromised by infarction or myopathy, transplantation strategies using in vitro generated donor (non)-cardiomyocytes have gained major interest. Several sources of stem cells have successfully been differentiated into stem cell derived cardiomyocytes (SDCs) but transplantation has also been performed using mesenchymal stem cells, skeletal myoblasts or even neonatal cardiomyocytes. In vitro generated cardiomyocytes share important features with nodal cardiomyocytes. Both neonatal cardiomyocytes and SDCs are spontaneously beating immature myocytes. This automaticity can be beneficial if a biological pacemaker is requested, as demonstrated by Kehat et al., who successfully introduced an ectopic pacemaker in AV-block pigs using SDCs (16). Potapova et al. showed that transplantation of mesenchymal stem cells overexpressing HCN2, a member of the HCN ion channel subunit family underlying the cardiac pacemaker current  $I_f$ , were similarly potent to induce pacemaking activity in a dog model (101). However, if there is no need for new pacemaking, automaticity of immature cells may disturb the vulnerable impulse propagation and enhance the propensity to generate arrhythmias. Besides automaticity, studies on SDCs consistently report low levels of connexin expression, both in vitro and in vivo, with some cells that do and others that do not express connexins (134; 62). In clinical trials, autologous transplantation of skeletal myoblasts which also do not express Cx43 upon differentiation into excitable myotubes, resulted in ventricular tachycardia in several patients (11). An in vitro study showed that this could be overcome by genetically induced overexpression of Cx43 (53). From those studies, we suggest that the potential of immature myocytes to trigger the mature working myocardium not only depends on their spontaneous activity, but also on the level of established electrical coupling in analogy with the pacemaking behaviour of autorhythmic cells in the cardiac conduction system (132). To study those features in detail, we generated an accessible in vitro approach in which we co-cultured immature and mature cardiomyocytes. Furthermore, we performed computer simulations to investigate the basic electrophysiological characteristics of their interaction. Our data show that the ability of immature cardiomyocytes to trigger quiescent mature

cardiomyocytes depends on the amount of connected cells and the level of electrical coupling.

## Materials and methods

*Cell culture* Neonatal rat ventricular cardiomyocytes (NRCs) and left ventricular myocytes from adult dogs (ADCs) were isolated as described before (102; 135). The investigations conformed to the Guide for the Care and Use of Laboratory Animals published by the US National Institutes of Health (NIH Publication No. 85-23, revised 1996) and was approved by the institutional committee for animal experiments. Isolated ADCs, collected in Tyrode supplemented with 0.2 mmol/L  $\text{CaCl}_2$ , were centrifuged at 400 rpm for 3 min. All but the last 10 mL supernatant was removed and 10 mL Tyrode supplemented with 0.6 mmol/L  $\text{CaCl}_2$  was added. Cells were gently resuspended and centrifuged again. These steps were repeated with Tyrode containing 0.8 mmol/L and 1.0 mmol/L  $\text{CaCl}_2$ , respectively. Finally, cells were resuspended in DMEM without additives and gently loaded on top of 10 mL DMEM supplemented with 4% BSA in order to pellet rod-shaped ADCs by gravity. After 5 min, supernatant was removed and cells were resuspended in culture medium: DMEM supplemented with 10% fetal calf serum, 100 IU penicillin/mL and 100  $\mu\text{g}$  streptomycin/mL. After a last centrifugation, cells were collected in 4-8 mL culture medium and seeded on glass coverslips coated with laminin (20  $\mu\text{g}/\text{mL}$ ). For co-cultures, isolated ADCs were added (4000/ $\text{cm}^2$ ) to cultures of NRCs which were seeded one day before ADC isolation. To generate different ratios between NRCs and ADCs, NRCs were seeded at densities of 3250, 6500 and 13000 cells/ $\text{cm}^2$ . Medium was replaced the next day and every second day thereafter.

*Immunohistochemistry* Cells were fixed with methanol at  $-20^\circ\text{C}$  for 2 min and rinsed three times with PBS. Immunolabelling was performed as described before (62). Primary antibodies used were anti-Cx43 (Zymed), anti- $\alpha$ -actinin (Sigma) and anti-N-cadherin (Sigma).

*Reverse transcriptase-polymerase chain reaction* RNA was isolated by use of Trizol (Invitrogen, Breda, The Netherlands) and DNase-I treated RNA was reverse transcribed using oligo-dT Superscript 3 (Invitrogen). The following primer pairs and PCR conditions were used: GAPDH; forward ATGACAACCTCCCTCAAGATTGT, reverse CATTGT CATAACAGGAAATGAG, annealing temperature  $53^\circ\text{C}$ , 30 cycles; KCNJ2; forward CC CGAGAAGGTCAACATCTTGG, reverse TCGTACGAGATCTTGGACGGG, annealing temperature  $60^\circ\text{C}$ , 35 cycles; SCN5A; forward CCGAGAAGGTCAACATCTTGG, reverse TC GTACGAGATCTTGGACGGGT, annealing temperature  $60^\circ\text{C}$ , 35 cycles. Products were analyzed on ethidium bromide-stained 1% agarose gel. GAPDH was used as RNA input control.

*Electrophysiology* A symmetrical setup with two HEKA EPC-7 patch clamp amplifiers was used to measure electrical coupling between cells. All measurements were done on cells cultured for 2 days. Macroscopic gap junctional currents were recorded using

a custom data acquisition program (kindly provided by J.G. Zegers, AMC, Amsterdam) running on a G4 Apple Macintosh computer equipped with a 12-bit National Instruments PCI-MIO-16E-4 acquisition card. Current signals were low-pass filtered at 2.5 kHz and acquired at 10 kHz. Macroscopic gap junctional currents were elicited in cell pairs by applying small transjunctional voltage steps (+ 10 mV) from holding potential (– 50 mV). By using small pulses, junctional conductances were maximal and not inactivating. Offline analysis was done using MacDaq 8.0 (kindly provided by Dr. A.C.G. van Ginneken, AMC, Amsterdam) and R 2.0.1 (81). Gap junctional conductance ( $g_j$ ) was defined as  $g_j = I_j/V_j$ , where  $I_j$  and  $V_j$  denote junctional current and transjunctional voltage, respectively. Action potentials were elicited with a brief square current pulse. Maximal upstroke velocities were determined by differentiating the voltage traces. Resting membrane potential, maximum upstroke velocity and  $I_{K1}$  density of single isolated ADCs were measured using the whole-cell mode of the patch clamp configuration. A conventional mono-exponential fitting procedure was used to derive membrane capacitance from currents elicited by –10 and +10 mV voltage clamp steps from resting membrane potential.  $I_{K1}$  was elicited by applying 1-second square test pulses ranging between –80 and +90 mV from a holding potential of –40 mV. Steady state currents at the end of the pulse were normalized to membrane capacitance and plotted against test pulse potential. Resulting current densities in the –130 to –80 mV voltage range were fitted with linear regression to obtain  $I_{K1}$  conductance density. All electrophysiological experiments were done at 20 °C. Extracellular buffer used was a modified Tyrode's solution, containing (in mmol/L) NaCl 140, KCl 5.4, CaCl<sub>2</sub> 1.8, MgCl<sub>2</sub> 1, HEPES 15, NaHCO<sub>3</sub> 17.5, glucose 6, pH 7.20/NaOH. Gap junctional coupling was inhibited by halothane (136). Halothane dissolved in extracellular buffer (final concentration 4.25 mmol/L) was applied at the interface between ADC and NRCs with an additional micropipette. Pipette buffer contained (in mmol/L) potassium gluconate 125, KCl 10, HEPES 5, EGTA 5, MgCl<sub>2</sub> 2, CaCl<sub>2</sub> 0.6, Na<sub>2</sub>ATP 4, pH 7.20/KOH. For dye injections, microelectrodes were filled with Lucifer Yellow in 150 mmol/L LiCl<sub>2</sub>, 10 mmol/L HEPES. Patch pipettes were pulled on a Narishige PC-10 puller and fire-polished. When filled with pipette buffer, pipette resistance ranged between 2 and 5 MΩ. Liquid junction potential was calculated using Clampex (Axon Instruments) and used for offline correction.

*Computer simulations* Computer simulations were performed to assess the conditions that allow a cluster of spontaneously beating NRCs to trigger beating of an intrinsically quiescent ADC. We used our previously published rabbit SA nodal cell model as a tentative membrane model of a spontaneously active NRC (137). To match the membrane capacitance of a single NRC, membrane capacitance of the model was reduced by a factor of 2 to 16 pF while retaining its membrane current densities. 'NRC cluster size' was varied by increasing the membrane capacitance of the SA nodal cell model in steps of 16 pF instead of adding individual 16-pF cells. The rationale for doing so is that the experimentally observed gap junctional conductance between NRCs is so high that the cells of an SA nodal cell cluster show complete waveform entrainment (138). The phase-2 Luo-Rudy mammalian ventricular cell model (139), with a membrane capacitance of 153.4 pF, was used as membrane model for ADCs. The 'NRC cluster' was coupled to the 'ADC' at a variable ohmic coupling conductance. For numerical integra-

tion, we used an Euler-type scheme with a fixed time step of  $10 \mu\text{s}$ . All simulations were run for a sufficiently long time to reach steady-state behaviour. In addition, computer simulations were performed with a two-dimensional sheet composed of  $27 \times 27 = 729$  cells with a spontaneously active 'focus' located in the centre of the sheet, as previously described in detail (140). Each cell of the square grid was connected to its neighbours through an ohmic coupling conductance. In the present study, the 'focus' represents a cluster of spontaneously beating NRCs. For this simulation, similar settings were used as the above described triggering of single ADCs.

*Statistics* Group comparisons were made using one-way ANOVA with the Holm-Sidak post-hoc test for multiple comparisons. Statistical significance was assumed if  $P < 0.05$ . All data are presented as mean  $\pm$  SEM.

## Results

### Characterization of ADC phenotype in culture

To validate usefulness of isolated ADCs in the in vitro co-culture model system, their phenotype in culture was followed. During the first 3 days, ADCs remained rod shaped with exception of small pseudopodia-like extensions that developed after 1-2 days at the former intercalated disks (IDs) on the longitudinal cell ends. ADCs developed these structures both in mono-culture and in co-culture with NRCs. Up to 3 days,  $\alpha$ -actinin staining revealed a sharply demarcated pattern of cross-striations while former IDs largely remained intact as shown by labelling against N-cadherin (Fig. 5.1A, days 1 and 3). While original IDs still were abundantly positive for ID-associated proteins, like in this case N-cadherin, (Fig. 5.1A, day 3, arrow 1), the pseudopodia-like extensions contained additional diffuse labelling (Fig. 5.1A, day 3, arrow 2). At day 7 however, myocytes largely had lost their rod-shaped phenotype and compact bundled cross-striations, while IDs appeared disorganized as demonstrated by labelling against N-cadherin (Fig. 5.1A, day 7). Insets in Fig. 5.1A represent morphology of myocytes as visualized with phase contrast microscopy.

Up to 7 days, ADCs in monoculture remained quiescent. Resting membrane potential of cultured ADCs was  $-80.3 \pm 0.2 \text{ mV}$  ( $N = 24$ , average of 0, 1, 3 and 7 days culture-time) which did not significantly change over time (Fig. 5.1B). Maximal upstroke velocity of the action potential (AP) was not significantly different during the first three days but was significantly lower at day 7 (Fig. 5.1C).  $I_{K1}$  conductance density, the main determinant of resting membrane potential and its stability (141), tended to decline with prolonged culture although this did not reach significance (Fig. 5.1D). Since upstroke velocity is mainly determined by sodium channel availability, we evaluated the expression level of SCN5a, the  $\alpha$ -subunit of the cardiac sodium channel. Semi-quantitative RT-PCR revealed comparable levels of SCN5a expression at days 0, 1 and 3 while expression was slightly decreased at day 7. The expression profile of the KCNJ2 gene encoding Kir2.1 (the pore-forming unit of the  $I_{K1}$  channels) revealed comparable levels throughout the culture period (Fig. 5.1E). In contrast to ADCs, one day after isolation, NRCs were beating spontaneously with a maximal diastolic potential of  $-65.0$

$\pm 2.8$  mV (N = 4). As shown previously (125), and illustrated in Fig. 5.3C below, cultured NRCs did not change morphology in time. Organization of their contractile apparatus revealed strands of cross-striations as indicated by  $\alpha$ -actinin while intense Cx43 expression was found at intercellular contacts (see Fig. 5.3C, right panel, below). As expected from the difference in cell size, cell membrane capacitance of ADCs was much larger than that of NRCs ( $184 \pm 9.7$  pF, N = 18 versus  $19.6 \pm 1.4$  pF, N = 19, respectively ( $P < 0.05$ )). During culture time, membrane capacitance of NRCs did not change significantly. Membrane capacitance of ADCs did not change during the first 3 days but was significantly increased at day 7 ( $336.0 \pm 47$  pF, N = 6).

### Small clusters of immature cardiomyocytes can trigger a mature cardiomyocyte

Within 2 days of co-culture, through their pseudopodia-like extensions, ADCs contacted single cells or clusters of NRCs. ADC-NRC cell pairs were quiescent with slightly different membrane potentials: ADC  $-79.0 \pm 2.2$  mV, NRC  $-74.3 \pm 2.8$  mV (N = 4). In contrast, ADCs contacting clusters composed of at least 3-4 spontaneously beating NRCs contracted in synchrony. Current clamp recordings of ADCs coupled to NRC clusters showed that NRCs depolarized first, indicating that the ADC was paced by the beating cluster (Fig. 5.4, inset). Additionally, co-cultures composed of increasing NRC-seeding densities (giving rise to larger clusters and an increased likelihood to contact ADCs) showed increasing numbers of beating ADCs. Whereas no beating ADCs were detected in co-culture with 3250 NRCs/cm<sup>2</sup> (N = 6), ADCs co-cultured with 6500 (N = 4) and 13000 NRCs/cm<sup>2</sup> (N = 5) showed a significantly increased incidence of beating ADCs of  $28 \pm 10\%$  and  $56 \pm 8\%$ , respectively (Fig. 5.4).

### Interaction between immature and mature cardiomyocytes results from de novo gap junction formation

Synchronous beating of ADCs and NRCs in our co-cultures suggested formation of functional gap junctions at the cellular interface. To confirm this, immunohistochemical labelling of  $\alpha$ -actinin (marking cardiomyocytes) and Cx43, the predominantly expressed gap junction-constituent in ventricular myocytes, was performed. In addition, labelling of N-cadherin representing the mechanical interaction between cells was assessed. Some diffuse Cx43 label was found in the core of the pseudopodia-like extension (Fig. 5.2A, arrow 1) where  $\alpha$ -actinin was expressed in a typical striated pattern although the organization was not comparable to that found in the remaining rod shaped part of the ADC. More importantly, at the interface between pseudopodia-like extensions from the ADC and the membrane of the NRC, a punctuate expression pattern for Cx43, indicative for genuine gap junctions, was detected (Fig. 5.2A, arrow 2). Even more outspoken expression patterns of N-cadherin were found at the interface between ADC and NRC. Again, diffuse labelling for N-cadherin was present in the core of pseudopodia-like extensions (Fig. 5.2B, arrow 1) while strong junctional labelling was found at the interface (Fig. 5.2B, arrow 2).

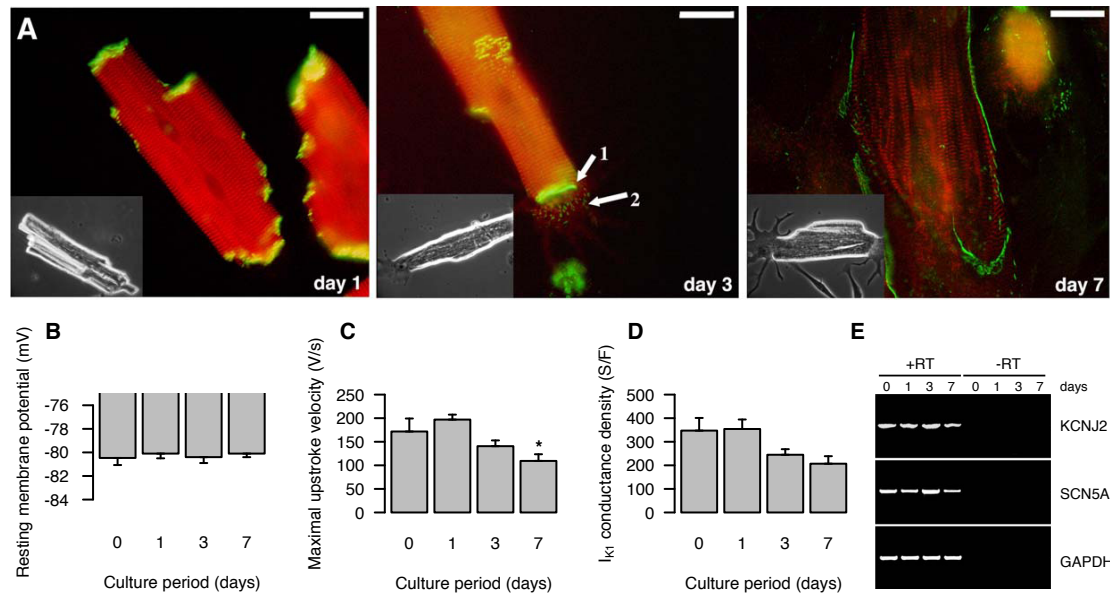


**Figure 5.1:** **A:** Immunohistochemical labelling of cultured ADCs at days 1, 3 and 7 with antibodies against  $\alpha$ -actinin (red) and N-cadherin (green). Insets represent the morphology with phase-contrast. Scale bar = 25  $\mu$ m. **B:** Resting membrane potential of ADC does not change during prolonged culture. **C:** Maximal upstroke velocity of triggered action potentials of ADCs in monoculture. Upstroke velocity at day 7 is significantly reduced compared to days 0 and 1 (asterisk). **D:** Prolonged culture did not significantly reduce  $I_{K1}$  conductance density in ADCs. N = 6 for each parameter at the subsequent days measured. **E:** Semi-quantitative RT-PCR data showing RNA expression levels of SCN5a and KCNJ2 at days 0, 1, 3 and 7 of cultured ADCs. GAPDH was used as RNA input control.

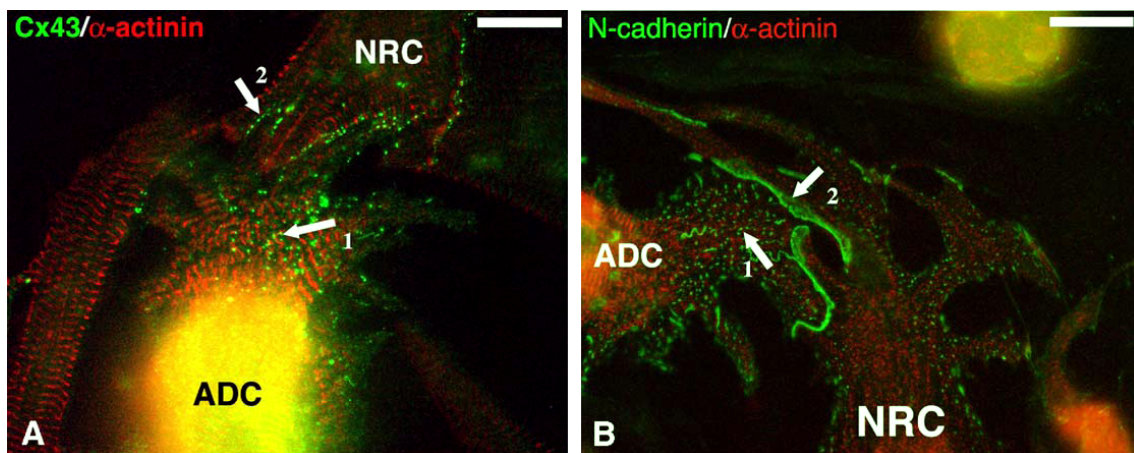


**Figure 5.2:** **A, B:** Immunohistochemical labelling of  $\alpha$ -actinin (A, B, red), Cx43 (A, green) and N-cadherin (B, green) at the interface between ADCs and NRCs. Pseudopodia-like extensions of the ADC contain  $\alpha$ -actinin positive cross striations. Both Cx43 (A) and N-cadherin (B) show diffuse expression in the core of the pseudopodia-like extensions (arrows 1 in A and B) while junction-like labelling is present at the interface between ADC and NRCs (arrows 2 in A and B). Scale bar = 25  $\mu$ m.



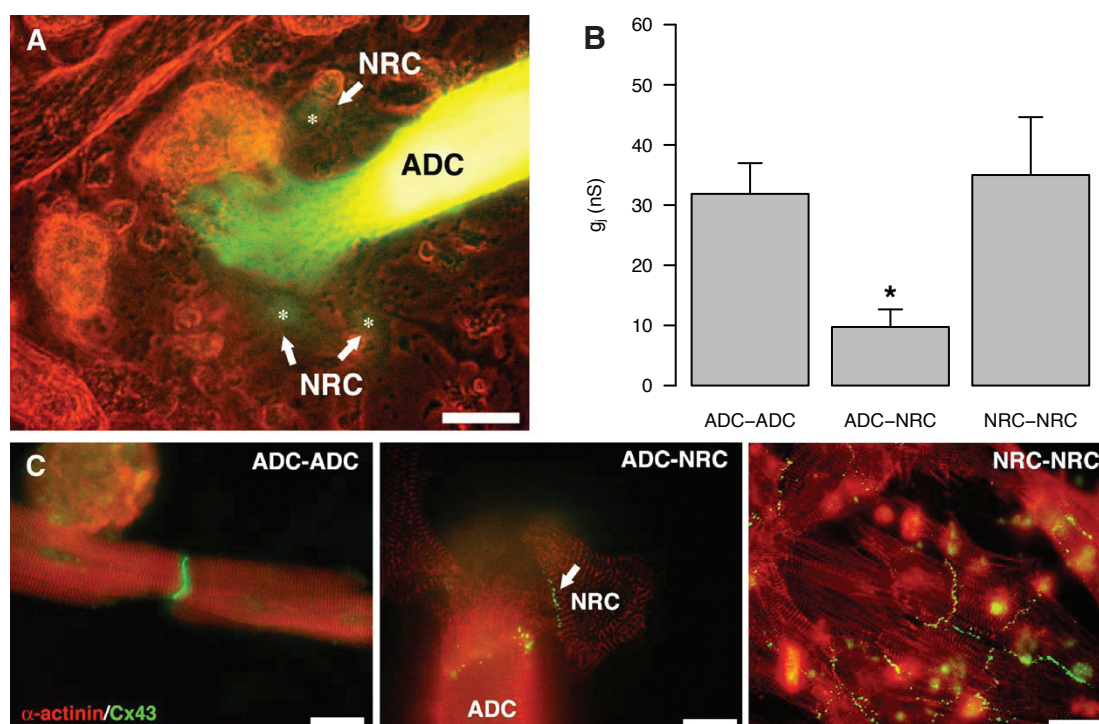


**Figure 5.3:** **A:** Lucifer Yellow dye transfer from the injected ADC to neighbouring NRCs (indicated with asterisks and arrows). **B:** Average gap junctional conductance ( $g_j$ ) between homotypic and heterotypic pairs of cardiomyocytes. Asterisk indicates that conductance between ADC-NRC is significantly lower as compared to that between ADC-ADC and NRC-NRC. **C:** Representative immunohistochemical labelling of  $\alpha$ -actinin (red) and Cx43 (green) of homotypic and heterotypic interactions suggests that Cx43 levels are higher in NRC-NRC and ADC-ADC combinations as compared to the ADC-NRC combination. Scale bar = 25  $\mu$ m.

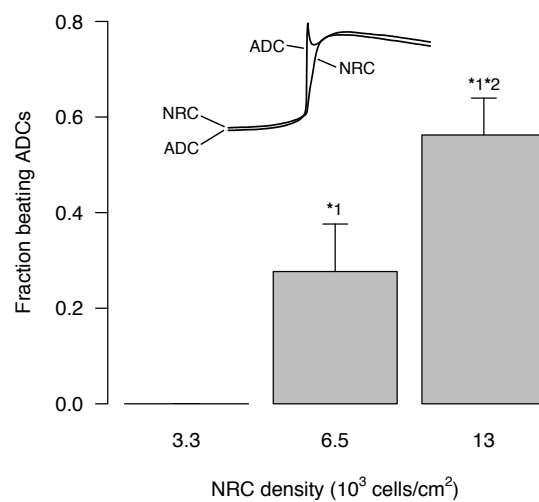


**Figure 5.4:** Incidence of beating ADCs is positively correlated with NRC seeding density. Identical numbers of ADCs were cultured in presence of increased densities of NRCs. Beating rod shaped ADCs were counted on day 2 of co-culture and expressed as fraction of total rod shaped ADCs. Inset shows that the action potential of the NRC precedes that of the ADC but that upstroke velocity of the ADC is much higher. Asterisk 1 means significantly different from density 3.25, asterisk 2 means significantly different from density 6.5.

## Triggered activity of ADCs occurs with poor gap junctional conductance

To test functionality of the de novo generated ADC–NRC Cx43 gap junctions, Lucifer Yellow (a 443 dalton dye which transfers through Cx43 channels) was injected into ADCs. Dye spreading was observed to adjoining NRCs ( $N = 4$ ), confirming functional coupling of ADCs and NRCs (Fig. 5.3A). In order to quantify electrical conductance of gap junctions formed between NRCs and ADCs, the dual whole cell voltage clamp technique was used (142; 143). Gap junctional conductance ( $g_j$ ) between NRC–NRC, ADC–ADC and ADC–NRC cell pairs was compared. Average  $g_j$  between NRC–NRC and ADC–ADC pairs was  $35.0 \pm 9.6$  nS ( $N = 6$ ) and  $31.9 \pm 5.1$  nS ( $N = 10$ ), respectively, which was not significantly different. Average conductance in heterotypic pairs was  $9.7 \pm 2.9$  nS ( $N = 8$ ), which was significantly lower than in both homotypic combinations (Fig. 5.3B). Immunohistochemical evaluation of Cx43 expression suggested that Cx43 labelling at ADC–NRC junctions (Fig. 5.3C, midpanel, arrow) was less pronounced as compared to that in ADC–ADC or NRC–NRC junctions (Fig. 5.3C, left and right panel respectively).

As mentioned, ADCs contacting sufficiently large clusters of NRCs beat in synchrony. To confirm a role for gap junctional communication in such pacing, and to exclude coupling by cytoplasmic connections, beating ADCs were uncoupled from coupled NRCs by application of halothane ( $N = 4$ ). Current clamp experiments showed that when uncoupled, ADCs stopped beating in synchrony with NRCs. Meanwhile their membrane potential became more negative approaching values comparable to those recorded in single cell ADCs. At the same time, the membrane potential of uncoupled NRCs became less negative but they remained spontaneously active (Fig. 5.5). Uncoupling also restored action potential shape of NRCs to that observed in single cells. After withdrawal of halothane, gap junctional coupling was restored and the initial synchronous activity reappeared while membrane potentials of both ADC and NRC returned to values as recorded before exposure to halothane (Fig. 5.5). Upstroke velocities of the triggered ADC action potentials as recorded during the wash-in and wash-out of halothane appeared not significantly different.

## Determinants of triggered activity in ADCs assessed by computer simulation

To validate dependence of triggered activity in ADCs on NRC cluster size and gap junctional conductance, a cluster of spontaneously active cells (SA nodal cells representing NRCs) was coupled to an intrinsically quiescent ventricular cell. Both NRC cluster size and gap junctional coupling conductance between the NRC cluster and the ADC were varied. Fig. 5.6, A–C, illustrates the outcome of the simulation for a cluster of 10 NRCs. At low coupling, the NRC cluster is beating spontaneously but it cannot pass enough current to the ADC to have it reach threshold (pace-but-not-drive (PND); Fig. 5.6A). At high coupling, the spontaneous activity of the NRC cluster becomes suppressed by the electrotonic interactions with the ADC (not-pace (NP); Fig. 5.6C). At intermediate values of coupling conductance, the NRC cluster is beating spontaneously and can pass enough current to the ADC to have it reach threshold (pace-and-drive (PD); Fig. 5.6B). Figure 5.6D shows the outcome for all combinations of NRC cluster size and NRC–ADC

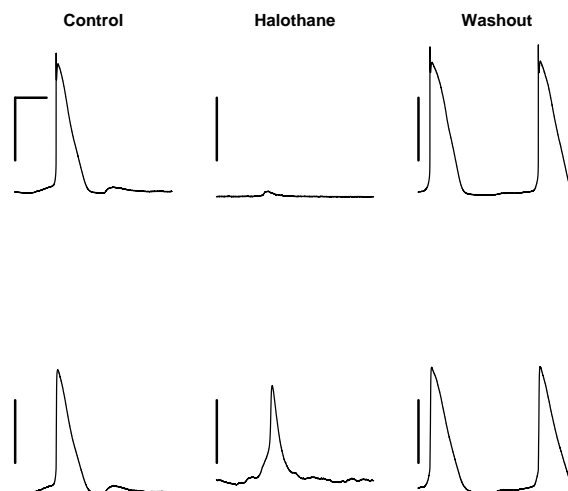


**Figure 5.5:** Electrical communication between a small cluster of NRCs and one ADC shows that the NRCs trigger the ADC to reach threshold and generate an action potential (AP). Suppressing gap junctional communication with halothane blocks AP-formation of the ADC while NRCs remain spontaneously active. Note that the diastolic potential of the cells changed upon uncoupling; NRCs become less negative while the ADC becomes more negative thereby regaining their native resting membrane potential. Horizontal scale bar = 500 ms, vertical scale bar = 50 mV.

coupling conductance. The asterisks indicate the parameter settings of Fig. 5.6, A and B. The solid line with closed circles marks the coupling conductance at which beating of small NRC clusters becomes suppressed (transition from PND to NP). The solid line with open circles marks the minimum coupling conductance at which large NRC clusters trigger beating in the ADC (transition from PND to PD). The solid line with closed squares marks the transition from PD to NP that can occur for NRC clusters of intermediate size when electrotonic interactions become too strong. For clusters comprising 7 or 8 cells, an additional transition (from NP to PD), near 6.5 nS, is observed, which is related to the time course of the junctional current. Above 6.5 nS, the ADC approaches threshold more rapidly and the electrotonic load of the ADC is removed (by reaching threshold and firing an action potential) just before spontaneous activity of the NRC cluster ceases, as occurs below 6.5 nS.

## Computer simulations show a vulnerable window for triggered activity of ADCs

In order to validate whether these observations could be extrapolated to a higher level of complexity, additional simulations were performed. In those simulations we mimicked the approach as described by Kehat et al. in which a spontaneously active human ES embryoid body is transplanted in a mature ventricular tissue which is activated only at a low frequency due to a chronic AV-block (16). In our simulation, a cluster of spontaneously active cells (SA nodal cells representing NRCs) was incorporated into a two-dimensional sheet of intrinsically quiescent ventricular cells. NRC-cluster size

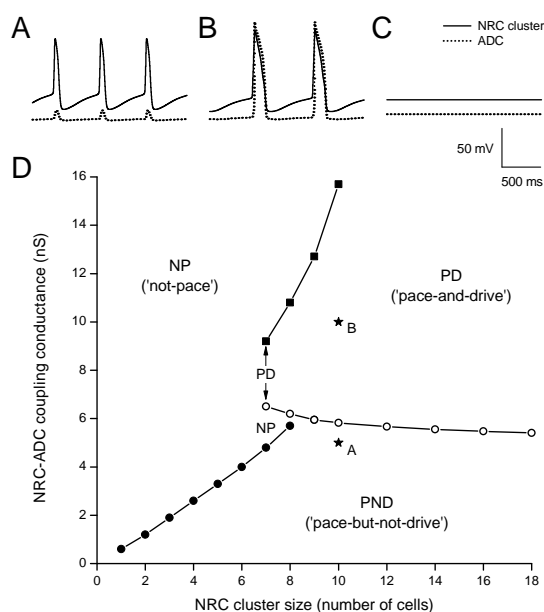


**Figure 5.6:** Simulated electrical activity of an NRC cluster coupled to an ADC. **A-C:** Electrical activity of a cluster of 10 NRCs coupled to an ADC with a gap junctional conductance of (A) 5 nS, (B) 10 nS, or (C) 20 nS. **D:** Effect of NRC cluster size (abscissa) and NRC–ADC coupling conductance (ordinate) on electrical activity. Lines with symbols separate regions where (1) the NRC cluster beats spontaneously, but does not trigger beating of the ADC ('pace-but-not-drive'), (2) spontaneous beating of the cluster is suppressed by the ADC ('not-pace'), or (3) the cluster beats spontaneously and triggers beating of the ADC ('pace-and-drive').

was varied, either using a small cluster of 50 cells or a large cluster of 100 cells. Gap junctional conductance between the NRC cluster and surrounding ventricular cells was varied also and set to 10, 20 or 40 nS. If uncoupled (Fig. 5.7A), the NRC cluster beats spontaneously at a frequency of 2.6 Hz, and surrounding ventricular cells are quiescent with a stable resting membrane potential of  $-86$  mV. At low coupling conductance (Fig. 5.7B), junctional current flows from the NRC cluster to the surrounding cells, resulting in a decrease in beating frequency of the NRC cluster and subthreshold depolarizations in the surrounding ventricular cells. The large cluster is less affected by the electrotonic interactions with the surrounding myocardium than the small cluster, as demonstrated by a smaller decrease in beating frequency (from 2.6 to 2.1 Hz for the large cluster versus 1.6 Hz for the small cluster), and is able to supply more current to neighbouring cells, as demonstrated by the larger amplitude of the subthreshold depolarizations (from  $-86$  mV to  $-68$  mV for the large cluster versus  $-71$  mV for the small cluster). At moderate coupling conductance, spontaneous activity is suppressed in the small cluster (Fig. 5.7C, left), but the large cluster continues to beat at a frequency of 1.6 Hz, and is able to supply enough current to the surrounding myocardium to reach threshold and generate triggered activity (Fig. 5.7C, right). At high coupling conductance, spontaneous activity is suppressed in both clusters (Fig. 5.7D). These simulations confirm that also at a level of increased complexity, a window of gap junctional conductance values exist that allow a sufficiently large cluster of spontaneously active cells to generate

triggered activity in the surrounding ventricular myocardium.

## Discussion

This study shows: (1) ADCs in culture remain quiescent and largely retain their morphology and electrical phenotype. (2) In co-culture with spontaneously active NRCs, de novo generated gap junctions between ADCs and NRCs facilitate functional coupling within two days as shown by electrical conductance and dye transfer. (3) Electrical conductance between homotypic cell pairs is much larger than that between heterotypic cell pairs. (4) Small clusters of spontaneously active NRCs are able to trigger a poorly electrically coupled ADC to beat in synchrony. (5) Triggering occurs within a delicate window of gap junctional conductance and is further influenced by the size of the coupled cell-cluster.

*Role of cell-to-cell coupling* Electrical activity of the heart as initiated within the SA node depends on a delicate interplay between spontaneous electrical impulse formation and propagation. The morphological organization of the SA node supports the generated impulse to be conducted out of the node in order to activate the connected atrial working myocardium (132). The low level of electrical coupling between myocytes within the node is a major determinant of proper pacemaker function since it prevents clamping of the small SA node by the surrounding atrial mass. Differences in expression level and distribution of gap junction channels explain the differential degree in coupling. The delicate balance of the coupling between spontaneously active cardiomyocytes and surrounding quiescent cells may also play a role in arrhythmogenicity of cell transplantation. Multiple approaches focus on the regeneration of compromised hearts by means of transplantation strategies using in vitro generated donor cells. As mentioned, these cells can originate from various sources. Although completely different in origin, such cells exhibit common electrophysiological features in that they are spontaneously active (SDCs, NRCs) or can be stimulated to elicit undesired electrical activity (skeletal myoblasts). Furthermore, these cells express gap junction proteins at a low level and in a distribution pattern comparable to nodal cells. Those features suggest that such cells might harbour the ability to induce pacemaking activity which was experimentally confirmed in a study by Kehat et al. (16). Not much is known about the actual electrical interaction between engrafted immature cardiomyocytes and mature host cardiomyocytes. Measuring this interaction in vivo is experimentally complicated if not impossible. Although functional coupling between donor myocytes and the recipient environment has been suggested by the propagation of calcium waves (28), this does not allow determination of the degree of electrical communication. NRCs exhibit an important prerequisite for impulse formation: the absence of a stable resting membrane potential and a slow diastolic depolarization which triggers spontaneous action potential formation. On the other hand, during the first 3 days after isolation cultured ADCs retain their morphology and electrical phenotype. In co-culture, ADCs and NRCs rapidly (within 48 h) developed gap junctional communication as shown by synchronous beating, dye transfer and electrical coupling. Measurements of electrical conductance between the heterologous cell-pairs revealed that the level of coupling was

rather poor. Because of a very high amino acid homology of Cx43 proteins in general (144), this low conductance is unlikely to result from species differences. In our model no docking problems have to be expected since rat Cx43 and canine Cx43 showed an overall identity of 97.1%, with only one residue differing in the extracellular domain (data not shown). More likely, low conductance results from the de novo formation of gap junctions as suggested by the pattern of Cx43 labelling at the interface between pseudopodia-like extensions of the ADC and connected NRCs. Theoretically, coupling could increase upon aging of the cultures. Because it appeared that after 3 days of culture time ADCs changed both structurally (disorganized contractile apparatus, increased membrane capacitance, lateralization of junctional proteins) and electrically (decrease of AP upstroke velocity, trend to decreased  $I_{K1}$ ), we were restricted to compare the interaction between cultured ADCs and NRCs only during the first 3 days.

*Balance between cluster size and coupling* Most striking, this study shows that pacing of the ADCs is dependent on spontaneous activity of the NRCs, NRC cluster size and low coupling conductance between ADC and NRCs. This relation depicts a pro-arrhythmic source-sink effect which partially can be explained by the low coupling conductance between ADC and NRCs, and the large difference in cell membrane capacitance (ADC:  $184 \pm 9.7$  pF, NRC:  $19.6 \pm 1.4$  pF). Experimental uncoupling of the ADC–NRC interaction clearly demonstrates that: (1) action potential formation of ADCs is triggered by the adjoining NRC cluster, (2) de novo formed gap junctions are responsible for pacing of mature ADCs by immature NRCs, (3) ADC–NRC syncytia display averaged electrical characteristics of the individual cell types. Our computer simulations underline that this delicate source-sink relation between NRCs and ADCs in co-culture is favouring pro-arrhythmia. The parameter space diagram of Fig. 5.6D illustrates the interaction between intrinsic automaticity and intercellular coupling and reflects a generic behaviour that occurs regardless of specific ionic mechanisms as recently set out by Pumir et al. (their Fig. 7 in (145)). For the experimentally observed NRC–ADC coupling conductance of  $\sim 10$  nS, our simulations predict two possible outcomes: suppression of spontaneous activity for clusters up to 7 cells and triggered beating of the ADC for clusters of 8 or more cells. The quantitative difference from our experimental results, where triggered activity was already observed for clusters of three or more cells, can be explained by the smaller depolarization reserve of our model NRC (only calcium current system available) compared to real NRCs (both calcium and sodium current systems available) as well as the more negative resting potential of our model ADC. Interestingly, our simulations demonstrate that this observation can be extrapolated to the tissue level: a relatively small amount of spontaneously active cells with a moderate level of electrical coupling can also drive an intrinsically quiescent sheet of ventricular tissue.

*Possible consequences for cell transplantation* The low conductance between NRCs and ADCs in co-culture might reflect a possible outcome of stem cell transplantation. The in vitro interaction shown in this study demonstrated that interactions between mature and immature myocytes arise at the former ID of the mature cell. In vivo, it remains open whether a comparable plasticity of the mature ID region is also present to facil-

itate a de novo interaction. Apart from a compromised electrical coupling, the aspect of cluster size in relation to arrhythmogenesis is relevant to the field of stem cell transplantation. The dominant form of stem cell delivery is to inject cells intramurally into the myocardium. This is bound to increase the likelihood of settlement of clumps of SDCs in the injected areas. In hearts where the intrinsic pacing rate of the transplanted cells exceeds the endogenous frequency, such clumps could become an arrhythmogenic substrate when electrical integration with the host myocardium starts to develop giving rise to a low coupling conductance. The fact that injection of embryoid bodies initiates ectopic pacemaking in porcine hearts (29) probably involves both the aspect of cluster size and a low effective coupling to the host myocardium.

*Limitations of the study* In this study we have evaluated the underlying mechanism through which spontaneously active cardiomyocytes are able to trigger intrinsically quiescent adult cardiomyocytes. As source of spontaneously active cardiomyocytes we used neonatal rat ventricular myocytes. These cells partly resemble SDCs in that both cell types display spontaneous activity and have a cell size and coupling characteristics aberrant from adult ventricular myocytes. Whether a broader comparison between SDCs and NRCs allows a stronger implication for stem cell therapy requires additional experimental evidence. We were unable to study the interaction between a cluster of spontaneously active NRCs and a sheet of cultured ADCs in an in vitro co-culture of NRCs and ADCs. The reason is that ADCs cannot be cultured in monolayers without losing their endogenous morphology and electrophysiological characteristics. The latter aspect was shown to change after 3 days of culture time which limited the time period in which experiments could be conducted.

## Acknowledgements

The authors like to express their gratitude towards A.T. Jansen, S. Tasseron, S.C. van Amersfoort, H.D.M. Beekman, Dr. G. Antoons and Dr. M.B. Thomsen for their indispensable support during the cell isolations. This study is supported by the Netherlands Heart Foundation (grant 2003B07304, TdB, BK), the Technology Foundation (STW program DPTE, grant #MKG5942, MAGvdH and grant UGT.6746, TABvV), the FP6 (Framework Program) of the European Committee (BK, JMTdB) and the Netherlands Organization for Scientific Research (NWO, grant 916.36.012, TABvV).



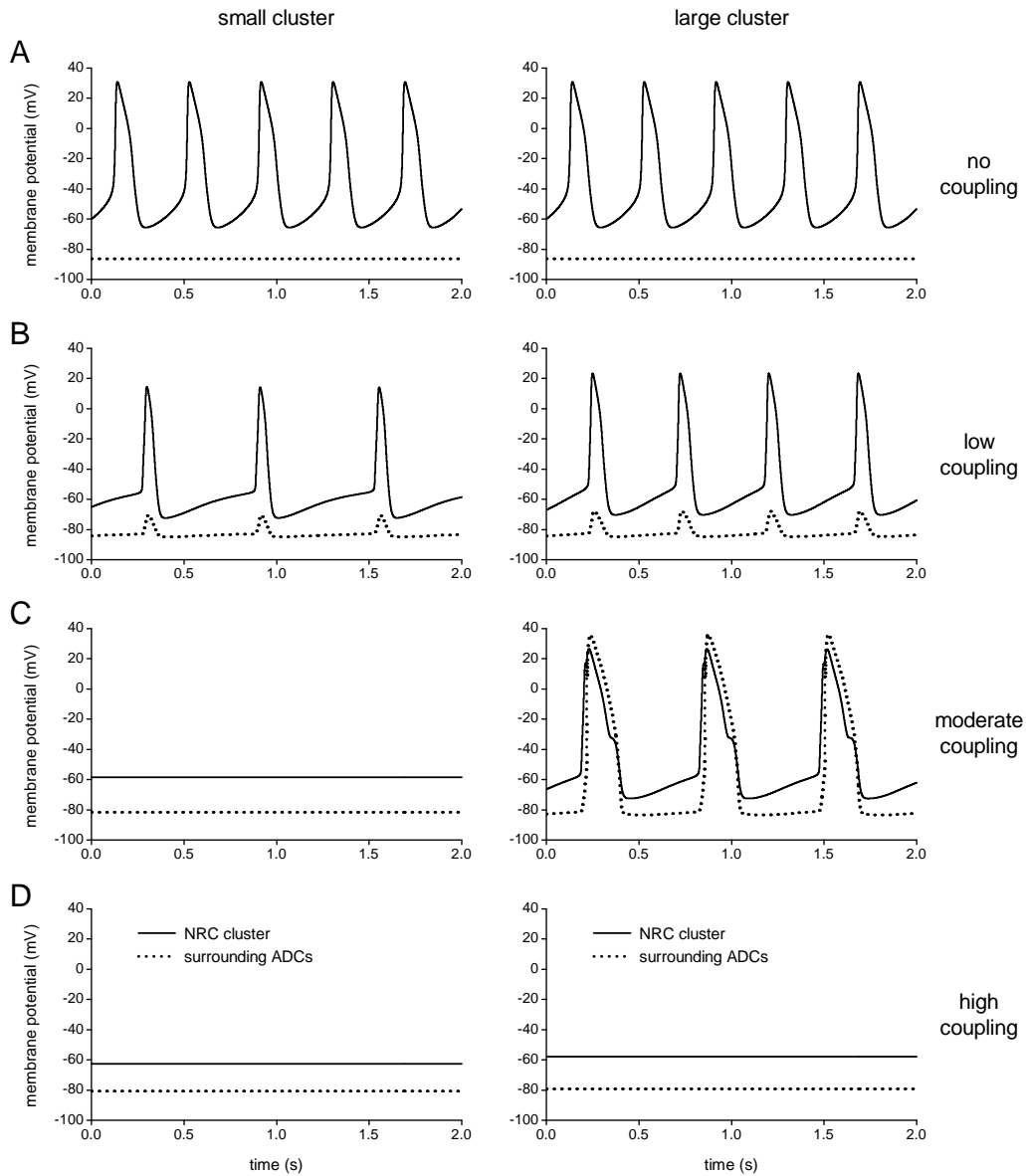


**Figure 5.7:** Simulated electrical activity of a small cluster (50 cells, left panels) or large cluster (100 cells, right panels) of spontaneously active NRCs incorporated into a two-dimensional sheet of ADCs. Membrane potentials of the NRCs and ADCs at the border between the simulated NRC cluster and the surrounding ventricular myocytes are shown as solid and dotted lines, respectively. Gap junctional conductance is set to (A) 0 nS ('no coupling'), (B) 10 nS ('low coupling'), (C) 20 nS ('moderate coupling'), or (D) 40 nS ('high coupling').



## Chapter 6

# **TGF $\beta$ 1 induces efficient differentiation of human cardiomyocyte progenitor cells into functional cardiomyocytes in vitro**

Marie-José Goumans, Teun P. de Boer, Anke M. Smits, Linda W. van Laake, Patrick van Vliet, Corina Metz, Tom Korfage, K.P. Kats, Ron Hochstenbach, Marcel A.G. van der Heyden, Gerard Pasterkamp, Christine L. Mummery, Joost P.G. Sluijter, Toon A.B. van Veen, Pieter A. Doevendans

*Submitted for publication*

## Abstract

The adult mammalian heart has limited regenerative capacity and was generally considered to contain no dividing cells. Recently, however, a resident population of progenitor cells has been identified, which could represent a new source of cardiomyocytes. Here we describe the efficient isolation and propagation of cardiomyocyte progenitor cells (hCMPCs) from human fetal heart and patient biopsies. Establishment of hCMPC cultures was remarkably reproducible with over 70% of adult atrial biopsies resulting in robustly expanding cell populations. Following addition of transforming growth factor  $\beta$ , almost all cells differentiated into spontaneously beating myocytes with characteristic cross striations. hCMPC-derived cardiomyocytes showed gap-junctional communication and action potentials of maturing cardiomyocytes. These are the first cells isolated from human heart that proliferate and form functional cardiomyocytes without requiring co-culture with neonatal myocytes. Their scalability and homogeneity is unique and provide an excellent basis for developing physiological, pharmacological and toxicological assays on human heart cells in vitro.

## Introduction

Myocardial infarction is a severe cardiovascular disorder and a major cause of heart failure and cardiac death. Mature cardiomyocytes do not divide and those lost in an infarcted ventricle are gradually replaced by fibroblasts to form scar tissue, which eventually leads to heart failure. Restoration of contractile activity by transplantation of cultured cardiomyocytes represents an elegant approach to ameliorate damage in the myocardium and preventing progressive loss of cardiac function. However, the realization of cell-based cardiac repair depends on producing human cardiomyocytes in sufficient numbers to provide many grams of cardiac tissue in the scar (146; 147; 148; 149) and with properties that will allow them to couple to the remaining viable tissue without forming arrhythmic substrates. The cells should therefore show a precise degree of maturity that will allow them to survive yet not exhibit autonomous pacemaker activity and they should express high levels of functional cardiac gap junction channels (53; 150). If such cells were available, they would also be useful for the study of human cardiac muscle function and pathophysiology, something that has been hampered by the lack of suitable in vitro models. Multiple stem cell types have been studied as a potential source of cardiomyocytes but so far only human embryonic stem cells (hESC) have been shown unequivocally to differentiate to the cardiomyocyte lineage; they then have characteristic structural and functional properties consistent with early-stage cardiomyocytes (15). hESC-derived cardiomyocytes offer unprecedented opportunities for genetic manipulation, drug discovery and toxicity studies in vitro but despite recent improvements in protocols, the differentiation of hESC is not homogenous (151; 152), which still limits their usefulness even in these areas.

The paradigm that the adult mammalian heart has no intrinsic capacity for repair because it has no dividing cells has been questioned by recent evidence that myocardium in fact contains a resident progenitor cell population that does proliferate in vitro and is capable of giving rise to new myocytes. These observations suggested new options

for the generation of cardiomyocytes and led to the identification of several different cardiac stem cell populations in the heart (148). These have included cells expressing stem cell factor receptor (c-Kit (153)) or stem cell antigen-1 (Sca-1 (154)) on their cell surface, or expressing the homeodomain transcription factor (islet-1 (155)), side population cells (SP (156)) and cells able to grow in cardiospheres (157). In rodents, these cardiac progenitor cell populations (CPCs) have been shown to be capable of differentiating into cardiomyocytes, either in vitro or in vivo, but so far, human CPCs have only been shown to be able to differentiate into cardiomyocytes in vitro when co-cultured with neonatal cardiomyocytes (157).

In this report, we describe the isolation, expansion and differentiation of cardiomyocyte progenitor cells (hCMPCs) from human heart tissue both of fetal origin and derived from tissue samples taken during by-pass surgery as the auricle is routinely removed. We demonstrated that using the method we have developed, CMPCs robustly and reproducibly differentiate into cardiomyocytes and, for the first time, independent of any feeder-cells in the culture. These hCMPCs differentiated electrophysiologically and immunologically into relatively mature cardiomyocytes in vitro. With the simple addition of TGF $\beta$ , a multifunctional growth factor involved in the cardiac differentiation of ESCs (158; 159), the efficiency of differentiation increased to nearly 100%. hCMPC-derived cardiomyocytes displayed excitation-contraction coupling that involved L-type calcium channel activity and they responded to  $\beta$ -adrenergic stimulation. Interestingly, besides myogenic differentiation, CMPCs are also able to form vascular sprouts when cultured on matrigel, showing their progenitor potential. In summary, this report provides first evidence for cardiomyoblasts in pre- and postnatal human hearts that are scalable in culture and differentiate homogeneously in vitro. hCMPCs may thus not only serve as a population of human cardiomyocytes for functional pharmacology but also as a source of autologous transplantable cardiomyocytes which may be collected during routine cardiac surgery and stored for future use.

## Results

### Human cardiomyocyte progenitor cells from human heart tissue

hCMPCs were cloned from human heart tissue, by performing limited dilutions using single cell suspensions from collagenase/protease digested fetal heart tissue and seeding 0.5 cell per well. 1.8% of the single cells grown in a 96-well plate generated clones with high growth potential. These clones contained small spindle-shaped cells with high nucleus-to-cytoplasm ratio (Figure 6.1A), characteristic of progenitor or stem cells, with a normal karyotype after analyzing 50 mitotic cells (Figure 6.1B). FACS analysis of the clones revealed negative staining for the hematopoietic stem cell markers CD34 or CD45 but significant expression of CD105, CD31, moderate levels of c-kit and binding of an antibody recognizing the (rodent) stem cell marker Sca-1 (Supplementary figure 6.9A,B). To characterize these cells further, we analyzed their expression of genes specific for early cardiac development by RT-PCR. These cultured cells expressed c-Kit and Islet-1 (Isl-1) as well as the early cardiac transcription factors GATA-4, Nkx2.5 and Mef2C (Figure 6.1D), suggesting that they are a progenitor cell

population already committed more to the cardiac lineage. We therefore designated them hCMPCs. In addition to mRNA, they also expressed Isl-1 and GATA-4 protein (Figure 6.1F). Although the proliferating hCMPCs did express transcripts of progenitor cells and early cardiac mesoderm, they did not express markers of differentiated cardiomyocytes (Figure 6.1D). mRNA expression of Cx37, 43, 45 and 46 was found in undifferentiated fetal hCMPCs (Figure 6.1G). Some isolations yielded hCMPCs expressing Cx37 and relatively few Cx43, 45 and 46, while other hCMPCs predominantly expressed Cx43 and 45, with less or no expression of Cx46 and 37, respectively.

To improve hCMPC purification, we made use of the ability of the hCMPCs to bind the anti-Sca-1 antibody on their cell surface. We sorted cells, bound to a ferrous-labeled Sca-1 antibody, magnetically from cell suspensions of both fetal hearts and adult auricles. After a lag phase of 3 days (Figure 6.1E), the Sca-1-purified fetal hCMPCs started to proliferate and the small spindle-shaped cells had the same characteristics as the hCMPCs derived clonally by limiting dilution (Supplementary figure 6.9C). 24 out of 33 adult heart tissue samples gave rise to growing hCMPCs after Sca-1 purification. These adult hCMPCs had the same stem-cell-like morphology with a large nucleus and little cytoplasm (Figure 6.1C) as those from fetal tissue; no loss of proliferation potential was noted for 23 passages. Adult hCMPCs had a similar gene-expression profile as fetal-derived hCMPCs (Figure 6.2D). Immunofluorescent staining revealed that almost all of the adult cells were Islet-1+, although this expression was predominantly cytoplasmic ( $78.99 \pm 9.1\%$ ;  $n=6$ ) (Figure 6.1F).

## hCMPCs can form vascular tubes in vitro

To test the differentiation potential of the hCMPCs to vascular cell types in vitro, cells were plated on matrigel. When kept in culture for 24 hours, hCMPCs were able to reorganize in cord-like structures composed of endothelial- and smooth muscle-like cells (Figure 6.4A). Interestingly, while only 4 out of 6 clones formed myocytes, their capacity to form capillary-like structures was evident in all clonally isolated cell lines (supplementary figure 6.6).

## hCMPCs have cardiomyogenic potential

To assess the potential of hCMPCs to adopt a myocytic phenotype, hCMPCs were grown in differentiation medium (DM) containing ascorbic-acid and treated with 5'-azacytidine, a cytosine analog that causes demethylation of DNA. hCMPCs gradually changed morphology and increased in size one week after stimulation. Three weeks after treatment, hCMPCs formed elongated aggregates and showed spontaneously beating areas. Analysis of gene expression showed that only GATA-4 and Nkx2.5 mRNA were expressed in undifferentiated cells, while after 5'-azacytidine stimulation both fetal (Figure 6.2A) and adult hCMPCs (Figure 6.2D) additionally expressed the cardiomyocyte-associated genes MLC-2V, cardiac Troponin-I and sarcomeric  $\alpha$ -actinin. Myo-D mRNA was not detected, indicating that there was no differentiation towards skeletal myocytes (Figure 6.2A). Immunofluorescent staining for sarcomeric proteins showed that differentiated hCMPCs, from both fetal (Figure 6.2B) and adult (Figure 6.2E, F) heart, exhibited sarcomeric striations organized in separated bundles. Analyzing the cells for

other components of the contractile apparatus revealed a pattern of cross striations positive for titin, MLC-2v, and  $\beta$ -MHC (Figure 6.2B). Double staining  $\alpha$ -actinin with intercalated disk related proteins like N-cadherin or ZO-1 resulted in strong positive signals at the cell boundaries of nearly all cardiomyocytes, indicating stable mechanical coupling (Figure 6.2C). Interestingly, only 3 out of 6 clonally-derived cell lines differentiated into spontaneous beating cells, while 1 clone did form myocytes, but without spontaneously beating (supplementary figure 6.6). Furthermore, we were able to freeze fetal and adult hCMPCs, thaw and expanded them, and successfully differentiated the thawed hCMPCs in cardiomyocytes.

## TGF $\beta$ 1 enhances the differentiation potential of hCMPCs

Although transient treatment with 5'-azacytidine induced differentiation of hCMPCs in vitro, the efficiency with which cardiomyocytes expressing well-organized sarcomeres or spontaneously beating clusters were formed was rather low (<15% of the culture). Adding ascorbic-acid to the differentiation medium enhanced the efficiency to more than 35%. For most applications however, we would need to improve the differentiation efficiency and population homogeneity even further. Apart from ascorbic-acid (160), TGF $\beta$  family members, including TGF $\beta$ 1 and BMP, have been found to promote cardiomyogenic differentiation in ESCs, and been critical for the expression of cardiac specific markers (158; 159; 161; 162). Therefore, we explored the possibility that TGF $\beta$ 1 might improve cardiomyogenic differentiation of hCMPCs.

TGF $\beta$  exerts its effect by binding to a complex of type I and type II receptor and phosphorylating Smad proteins (163). TGF $\beta$  phosphorylates Smad2 and 3 while BMP phosphorylates Smad1 and 5. First we determined whether hCMPCs were capable of responding to TGF $\beta$  ligand by examining their ability to phosphorylate Smad proteins. hCMPCs show clear BMP induced Smad1/5 phosphorylation (Figure 6.5A) as well as TGF $\beta$ 1 induced Smad2 phosphorylation indicating that they express the appropriate TGF $\beta$ 1 and BMP receptor combinations to respond to ligand stimulation. To examine the effect of TGF $\beta$ 1 on cardiomyocyte differentiation, hCMPCs were plated in DM, treated with 5'-azacytidine for 24 hours and cultured for up to 3 weeks in DM supplemented with TGF $\beta$ 1. The expression of cardiac genes like Troponin-I, ANP, cardiac-actin and desmin was already observed 7 days after initiation of differentiation in the presence of TGF $\beta$ 1. Without TGF $\beta$ 1, these genes were not detectable at 7 days although expression of cardiac-actin and desmin was present at 14 days (Figure 6.5B). MLC2v was normally detected in cultures without TGF $\beta$ 1 only after 3 weeks but was already present after two weeks in its presence. The expression of Nkx2.5 and  $\alpha$ -actinin protein showed a similar pattern and increased dramatically in hCMPCs after 7 days of culture in the presence of TGF $\beta$ 1 (Figure 6.5C). Addition of an ALK5 kinase inhibitor to the cell cultures, known to block TGF $\beta$  signaling (164), inhibited differentiation of hCMPCs into cardiomyocytes (Figure 6.5D). Immunofluorescent staining demonstrated that 3 weeks after stimulation, the  $\alpha$ -actinin/nuclei ratio was  $34.1 \pm 5.7\%$  in the absence of TGF $\beta$  (n=12), while with TGF $\beta$  in the DM,  $97.7 \pm 9.1\%$  of the cells was expressing  $\alpha$ -actinin (n=12) (Figure 6.5E). Flow cytometry analysis revealed that more than  $94.7 \pm 4.1\%$  (n=3) of the cells were positive for  $\alpha$ -actinin (data not shown).

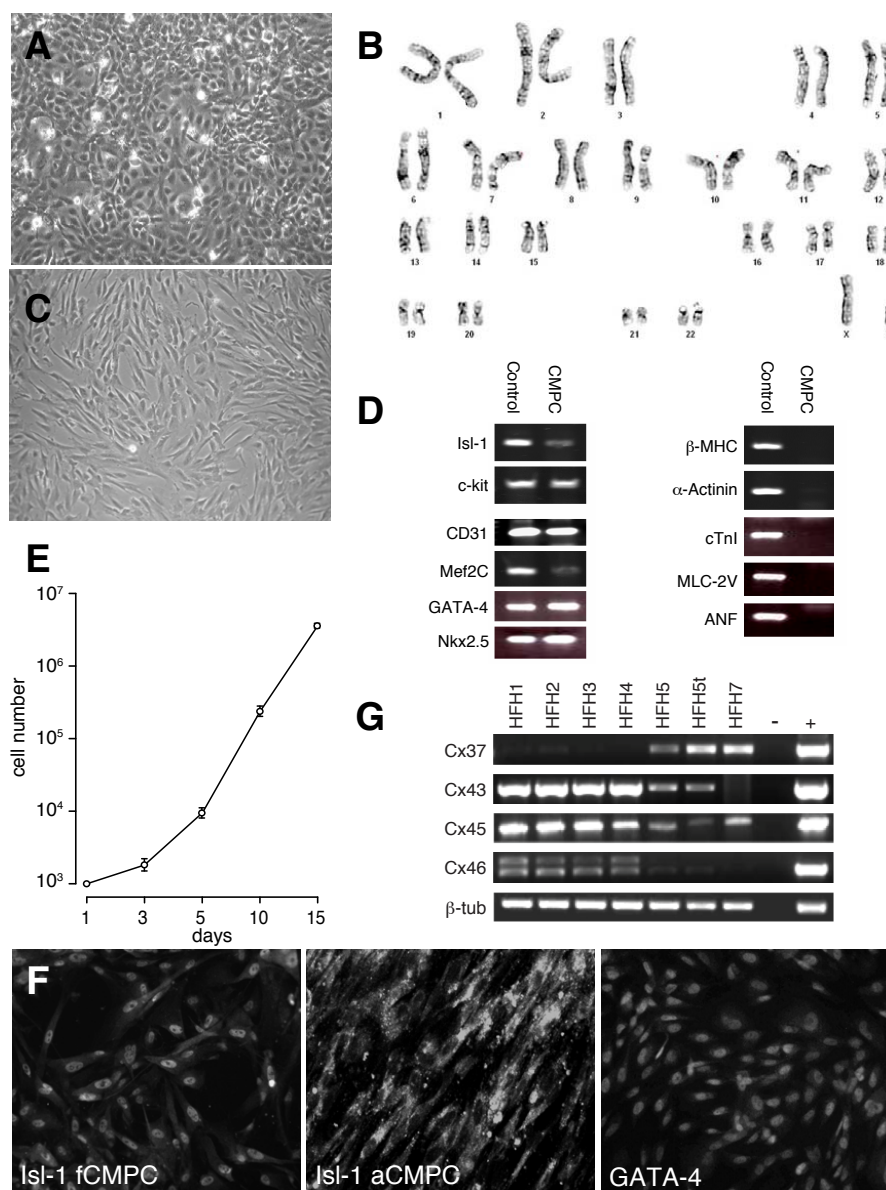


**Figure 6.1:** **A:** Bright field images of fetal hCMPC cultures. **B:** Karyogram showing chromosomes of late passages hCMPCs (>100 population doublings). Quality of the banding is 300-400 visible bands. **C:** Bright field images of adult hCMPC cultures. **D:** Semi quantitative RT-PCR on RNA isolated from undifferentiated hCMPCs probed for the expression of the indicated genes. Fetal heart tissue was used as a positive control for the PCR. **E:** Growth curve of freshly isolated hCMPCs. Total number of cells per well were counted at the indicated day after plating. **F:** Immunostaining of transcription factors Islet-1 in fetal hCMPC, adult hCMPC and GATA-4 in fetal hCMPC. **G:** Semi-quantitative RT-PCR on RNA from undifferentiated fetal hCMPCs obtained from several isolations probed for expression of human connexins.



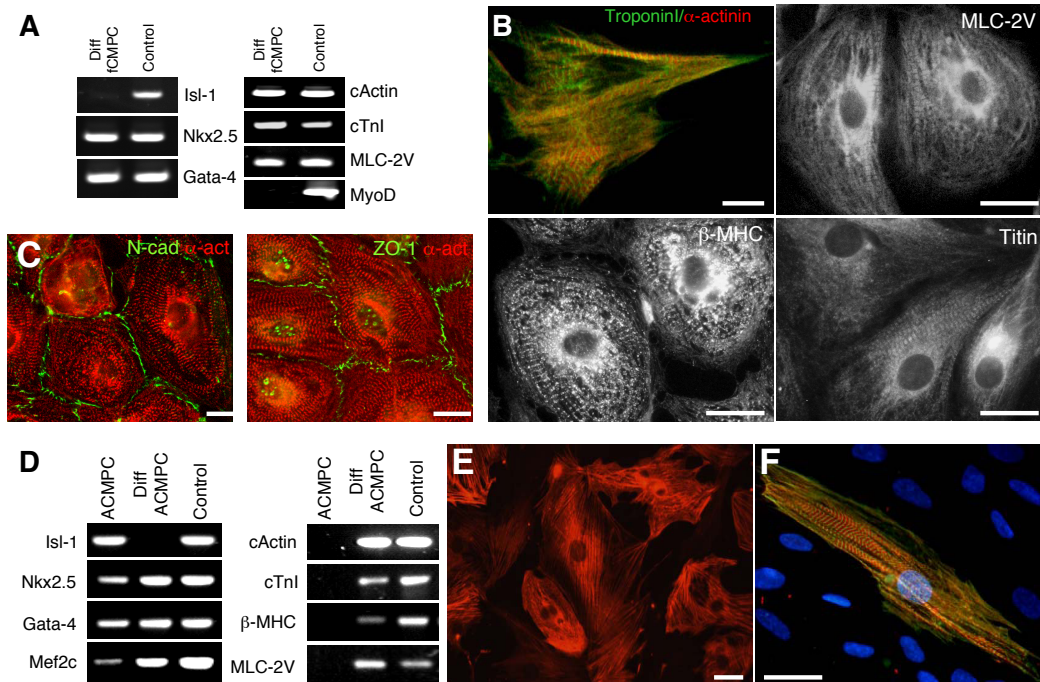


**Figure 6.2:** **A:** Semi-quantitative RT-PCR on RNA isolated from differentiated fetal hCMPCs (diff fCMPC) for the expression of Islet-1, early cardiac transcription factors Nkx2.5 and GATA-4, the contractile proteins cardiac actin, cardiac Troponin I, MLC-2v, and the skeletal myoblast transcription factor Myo-D. Fetal heart tissue was used as a positive control for the PCR. Only for Myo-D, skeletal muscle tissue was used as a positive control **B:** Immunostaining of the contractile proteins desmin, titin, MLC2v,  $\beta$ -MHC and  $\alpha$ -actinin as expressed in fCMPCs differentiated into cardiomyocytes. **C:** Expression profile of the intercalated disk related proteins ZO-1 and N-cadherin. Bar = 20  $\mu$ m. **D:** Semi-quantitative RT-PCR on RNA isolated from undifferentiated adult hCMPCs (aCMPC) and differentiated adult hCMPCs (diff aCMPC) for the expression of Islet-1, early cardiac transcription factors Nkx2.5, GATA-4 and Mef2c, the contractile proteins cardiac actin,  $\beta$ -myosin heavy chain, cardiac Troponin I, and MLC-2v. **E, F:** Immunolabeling of differentiated aCMPC cell culture 3 weeks after 5'-azacytidine treatment for the contractile protein  $\alpha$ -actinin (E) and  $\alpha$ -actinin and Troponin I (F).

## hCMPCs and hCMPC derived-cardiomyocytes form highly conductive gap-junctions

A minimum requirement for cardiomyocytes to be suitable for transplantation is the ability to couple correctly and propagate action potentials. We therefore examined hCMPCs for the presence of gap-junctional communication. Both undifferentiated and differentiated hCMPCs express Cx40, Cx43 and Cx45 mRNA (Figure 6.7B). Immunohistochemical analysis showed that while undifferentiated hCMPCs express Cx40, Cx43 and Cx45 in a diffuse and predominantly intracellular pattern (Figure 6.7A), hCMPCs-derived cardiomyocytes express Cx40 and Cx43 at the cell borders in a typical gap-junctional pattern. Cx45 was found both intracellularly and at the cell membrane. Metabolic coupling was measured by Lucifer Yellow injection in monolayers of undifferentiated and differentiated hCMPCs, resulting in spreading of dye to  $6 \pm 1$  ( $n=14$ ) and  $17 \pm 3$  ( $n=8$ ) cells, respectively (Figure 6.7B and C). The difference in dye spreading was statistically significant ( $p<0.007$ ).

Macroscopic gap-junctional conductance in cell pairs of undifferentiated and differentiated hCMPCs was  $48 \pm 21$  nS ( $n=5$ ) and  $31 \pm 4$  nS ( $n=5$ ), respectively (Figure 6.7D). Differences in average conductance were not statistically significant. A representative recording of differentiated hCMPCs (Figure 6.7E) shows a mild voltage dependent inactivation of gap-junctional conductance starting at a  $V_j$  of +30 mV indicative for Cx43 channels to be the predominantly expressed isoform.

## hCMPC-derived cardiomyocytes generate ventricle-like action potentials, display excitation-contraction coupling and are responsive to adrenergic stimulation

To characterize hCMPC-derived cardiomyocytes, we performed patch-clamp electrophysiology. Action potentials recorded from single cardiomyocytes and small clusters ( $n=11$ ) had a ventricular morphology (Figure 6.3A), as confirmed by quantification of action potential parameters (Figure 6.3B). Average maximal diastolic potential was  $-67 \pm 8$  mV and average maximal upstroke velocity was  $39 \pm 4$  V/s. Average APD<sub>50</sub> and APD<sub>90</sub> were  $258 \pm 38$  and  $483 \pm 51$  ms, respectively. Furthermore, diastolic membrane potential was rather stable, unlike cardiac pacemaker cells. Excitation-contraction coupling was demonstrated using combined calcium-imaging and current clamp experiments (Figure 6.3C). Average time to peak of the transients ( $n=7$ ) was  $447 \pm 54$  ms, time of half-inactivation was  $568 \pm 42$  ms.

Since spontaneous beating of hCMPC-derived cardiomyocytes was accompanied by calcium transients, the response to pharmacological modulation of L-type calcium channels as well as  $\beta$ -adrenergic stimulation with isoproterenol (ISO) was determined. Blocking L-type calcium channels with nifedipine ( $1 \mu\text{M}$ ) completely stopped beating ( $n=7$ ), while application of the L-type calcium channel opener BayK 8644 ( $0.1 \mu\text{M}$ ) significantly increased the beating rate from  $40.4 \pm 2.5$  ( $n=7$ ) under control conditions to  $71.4 \pm 6.7$  ( $n=6$ ) beats per minute immediately after addition (Figure 6.3D), implying a role for the L-type calcium channel in excitation-contraction coupling in differentiated hCMPCs. Application of ISO ( $0.1 \mu\text{M}$ ) increased the beating rate to  $52.1 \pm 4.5$  ( $n=7$ ) beats per minute. The chronotropic responses displayed by differentiated hCM-

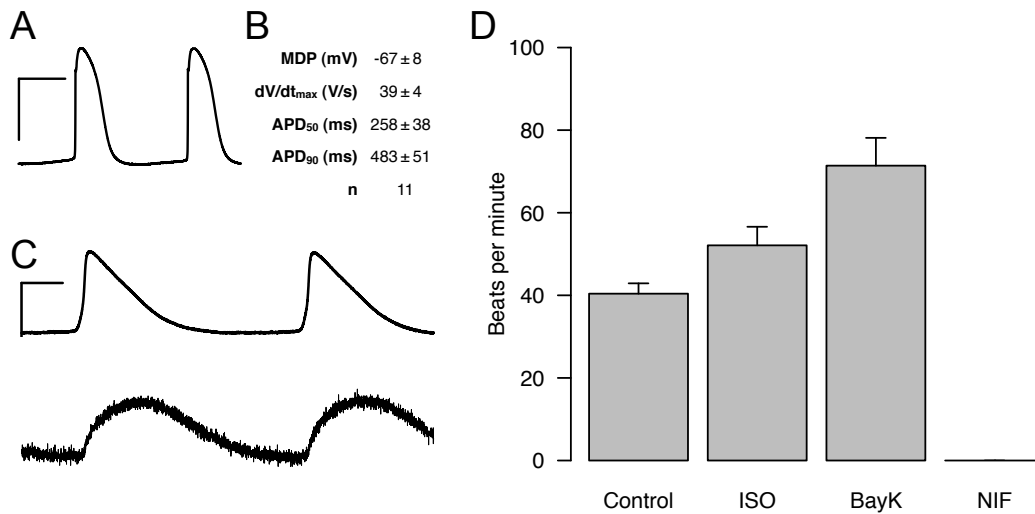


**Figure 6.3:** **A:** Current clamp recording from a hCMPC cardiomyocyte showing a rapid phase 0 depolarization and mild diastolic depolarization. **B:** Table summarizing hCMPC action potential parameters. **C:** Combined calcium-imaging and current clamp recording showing excitation-contraction coupling in a hCMPC-derived cardiomyocyte. **D:** Effects of  $\beta$ -adrenergic stimulation and modulation of L-type calcium channel activity on spontaneous beating rate; mean beats per minute. ISO: isoproterenol, NIF: nifedipine. Scale bars: horizontal 500 ms, vertical 50 mV.

PCs demonstrated that hCMPC-derived cardiomyocytes are amenable to pharmacological modulation and show a physiological response to  $\beta$ -adrenergic stimulation. They are therefore likely to be a suitable model for pharmacological, (patho)physiological, and developmental studies.

## Discussion

In this study, we characterized a progenitor cell population isolated from the human heart and defined these hCMPCs as immunophenotypically distinct from all cardiac stem and progenitor cells described previously (reviewed in (146; 149)). Most remarkable in our study was the isolation and culture of hCMPCs from atrial biopsies of adult patients undergoing cardiac surgery with an unexpectedly high success frequency. Recently, several groups have isolated cell populations from the rodent and human heart (153; 155; 156; 157; 154). All of these cardiac-derived stem cell populations appear to be distinct for one another as well as from the hCMPCs described here, based on gene expression profile and the expression of cell surface markers. However, they may all represent subpopulations of one major cardiac stem cell population, since it seems unlikely that an organ known for its lack of regenerative capacity would harbour so many different cardiomyocyte progenitors (165; 166). The diversity of isolation and culture conditions however precludes a direct comparison.

We have provided here the first evidence for robust expansion and functional and efficient differentiation of hCMPCs into cardiomyocytes. Importantly, none of the previously described human cardiac stem cell populations have been shown to be capable of differentiation into cardiomyocytes *in vitro*, except when co-cultured with neonatal cardiomyocytes. Messina et al. stimulated explants grown from cardiac biopsies with

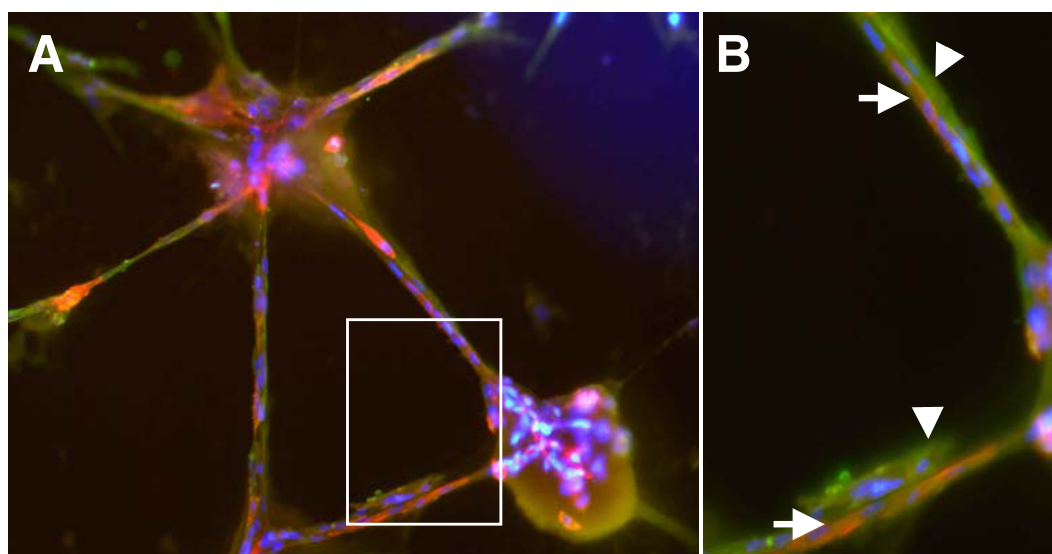


**Figure 6.4:** **A:** Immunolabeling of CMPCs grown on matrigel against endothelial cells (PECAM-1; red) and smooth muscle cells (SMA; green) and blue nuclei (Hoechst). **B:** Higher magnification of the box in A. Tube-like structures, harboring red endothelial cells (arrows) surrounded by a green layer of smooth muscle cells (arrowheads) can be appreciated.

cardiotropin and generated cardiospheres (157). While mouse cardiospheres spontaneously started to beat, with primitive cells located internally and beating myocytes at the edges, human cardiospheres only differentiated when co-cultured with rat cardiomyocytes. Isolated mouse *Isl-1*+ progenitor cells differentiated into cardiomyocytes when co-cultured with neonatal cardiomyocytes (155), as was also shown for mouse cardiac SP cells (167). Although *Isl-1*+ cells were also identified in human neonatal atrium, these cells have not been isolated and grown in culture to-date (155).

Analysis of the differentiation potential of the hCMPCs showed that addition of the demethylating agent 5'-azacytidine induced the expression of cardiac and contractile genes, assembly of sarcomeric bundles, formation of cardiac action potentials and spontaneous beating. Supplementing the differentiation medium with ascorbic-acid, known to enhance cardiomyocyte differentiation of ESCs (151; 160), improved the percentage of formed cardiomyocytes but it was still well below the one-to-one conversion that would be ideal. However, treatment with  $TGF\beta 1$  resulted in a highly significant improvement in efficiency and cultures almost entirely composed of relatively mature cardiomyocytes.  $TGF\beta 1$  phosphorylated Smad2 and caused earlier expression of contractile proteins, higher numbers of  $\alpha$ -actinin positive cells and more beating areas per dish. Recently,  $TGF\beta$  was found to induce the expression of cardiac genes in *c-kit*+ bone marrow cells (168), again indicating the important role for  $TGF\beta$  signaling in cardiomyogenic differentiation. It is quite likely that the cardiomyocyte co-culture effects on differentiation described for other stem cell populations is mediated by  $TGF\beta$  secreted by the neonatal cardiomyocytes (169). Analysis of hCMPC cardiomyocyte action potential shape showed a low maximal diastolic potential, compared to values we measured previously in hESC-derived cardiomyocytes and human fetal ventricular cardiomyocytes ( $-67 \pm 8$  mV compared to  $-48 \pm 2$  and  $-38.5 \pm 1.6$ , respectively (15; 32)). Furthermore, and possibly as a consequence, the maximal upstroke veloc-

ity is higher ( $39 \pm 4$  V/s compared to  $7.0 \pm 0.8$  and  $8.9 \pm 4.3$ ).  $APD_{90}$  of hCMPCs is comparable with values measured in hESC-derived cardiomyocytes and human fetal ventricular cardiomyocytes ( $483 \pm 51$  ms compared to  $436.4 \pm 55.3$  and  $370.0 \pm 45.8$ ). hCMPCs express high levels of gap junction proteins both in the differentiated and the undifferentiated state although after differentiation, they are almost exclusively found on the sarcolemma. In contrast to undifferentiated hES cells that express 18 out of 21 connexin isoforms (44), undifferentiated hCMPCs express only 6 connexin isoforms, suggesting commitment to a cardiac or endothelial lineage. The gap-junctions found in hCMPCs were also functional, mediating both metabolic and electrical coupling. Interestingly, hCMPC cardiomyocytes appear even more mature than cultured ventricular cardiomyocytes isolated from 16 week human fetuses from which the hCMPCs were generally isolated (15), showing that our differentiation strategy enhances maturation of the cardiomyocytes.

In this report we show that hCMPC-derived cardiomyocytes can be used to study cardiomyocyte physiology. Isolated rat primary cardiomyocytes are a widely used model for cardiomyocyte biology, however they differ significantly in physiology with human cardiomyocytes so that extrapolation of drug and toxicity data is by definition limited. hESC-derived cardiomyocytes may, in principle, be a better model than rodent cells, certainly for studying early differentiation of the human heart, but the heterogeneity of cultures after differentiation and the maximum of 20-25% cardiomyocytes present limits their development into high throughput in vitro models for compound screening. hCMPC-derived cardiomyocytes, differentiated efficiently in presence of TGF $\beta$ 1, are certainly the best option to-date for this purpose. The hCMPC-derived cardiomyocytes were responsive to  $\beta$ -adrenergic stimulation as well as pharmacological modulation of L-type calcium channel activity, illustrating their potential use in pharmacological testing, perhaps as an even better screen than the obligatory animal tests. This study identified a distinct population of CPCs that is for the first time scalable and nearly homogeneous, two of the most important criteria for development as a compound screen and as a source of cells for cardiomyocyte physiology.

## Acknowledgements

We are grateful to Cor Seinen, Bart Kok, Raimond Heukers and Malin Jonsson for technical assistance and Dr. D. de Kleijn for helpful discussions. This work was supported by a VIDI grant (016.056.319, MG) and a VENI grant (916.36.012, TvV) from the Netherlands Organization for Scientific Research (NWO), the Netherlands Heart Foundation (2003B07304, TdB, BK), the FP6 (Framework Program LSHB-CT-2004-502988) of the European Committee (BK), Van Ruyven Foundation, and BSIK program "Dutch Program for Tissue Engineering", grants #MKG5942 (MvdH) and UGT.6746 (TvV).

## Material and methods

*Isolation and culture of cardiomyocyte progenitor cells from human heart tissue* For human fetal tissue collection and atrial biopsies, individual permission using standard

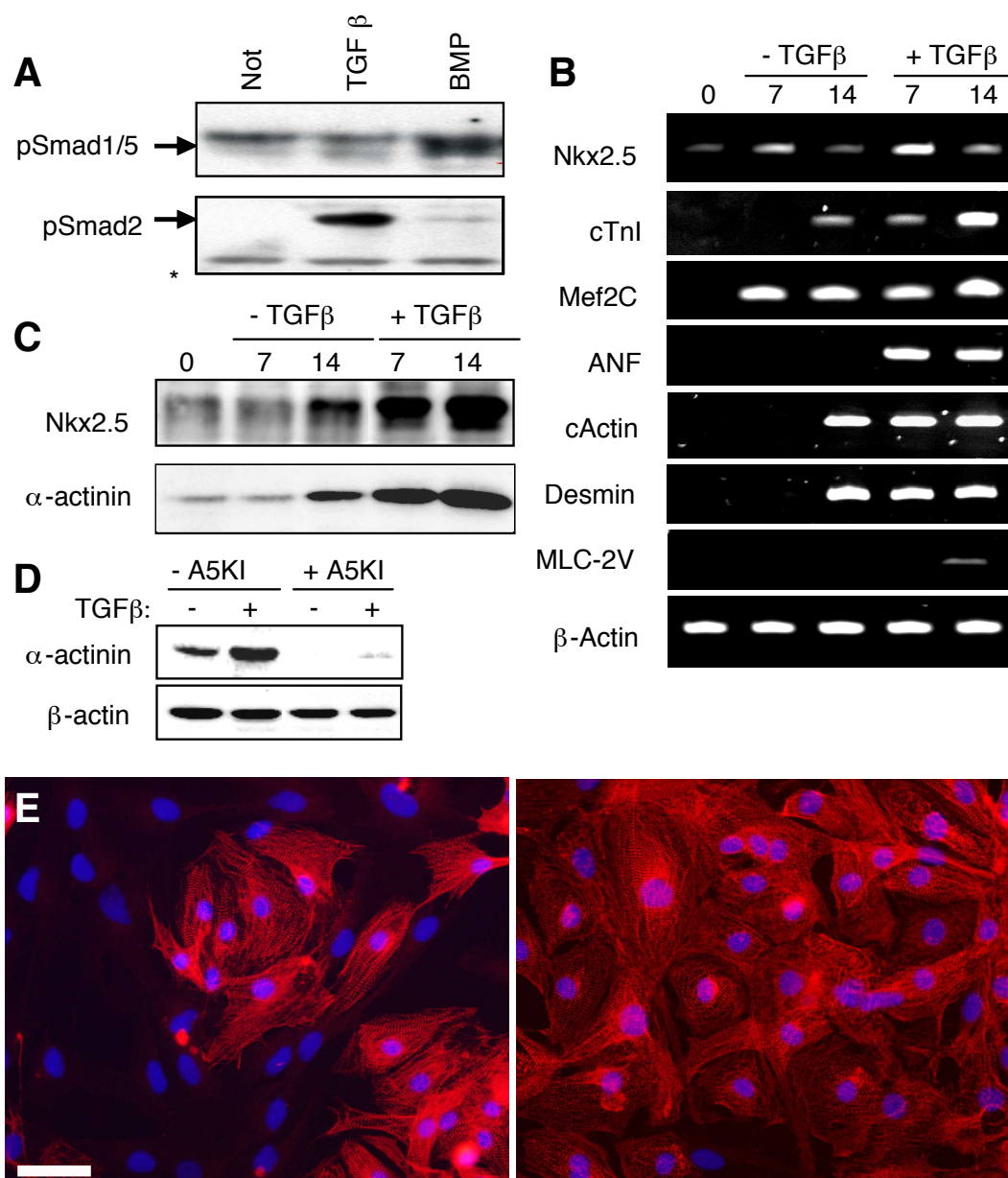


**Figure 6.5:** **A:** Western blot analysis of protein samples isolated from hCMPCs stimulated without or with 1 ng/ml TGF $\beta$ 1 or 25 ng/ml BMP-6 and probed for pSmad1 or pSmad2. Asterisk indicates a non-specific band showing equal loading. **B:** Semi-quantitative RT-PCR on RNA isolated from hCMPCs stimulated without or with 1 ng/ml TGF $\beta$ 1 for the indicated days probed for the expression of the early cardiac transcription factors Nkx2.5 and Mef2C, the contractile proteins cardiac actin, cardiac Troponin I, desmin, ANP and MLC2v.  $\beta$ -actin was used as a control for equal RNA input. **C:** Western blot analysis on protein samples from hCMPCs stimulated without or with 1 ng/ml TGF $\beta$ 1 for the indicated days, probed for Nkx2.5 or  $\alpha$ -actinin. **D:** Immunohistochemical labeling for  $\alpha$ -actinin shows the degree of differentiation into cardiomyocytes within the cultures without (left) or with (right) TGF $\beta$ 1 stimulation. Counterstaining of nuclei was performed using DAPI. Bar = 50  $\mu$ m.



informed consent procedures and prior approval of the ethics committee of the University Medical Center Utrecht were obtained. Fetal hearts were collected after elective abortion followed by Langendorff perfusion with Tyrode's solution, collagenase and protease. Atrial biopsies were minced into small pieces followed by collagenase treatment. After cardiomyocyte depletion of the cell suspension, clonal analysis was performed by limited-dilution. The cardiac cell suspension, containing dissociated single cells, was plated into the wells of a 96-well plate at a density of 0.5 cell per well in M199 (Gibco)/EGM (3:1) supplemented with 10% FCS (Gibco), 10 ng/ml basic Fibroblast growth factor (bFGF), 5 ng/ml epithelial growth factor (EGF), 5 ng/ml insulin like growth factor (IGF-1) and 5 ng/ml hepatocyte growth factor (HGF). The wells were analyzed for growing colonies twice weekly. Cardiomyocyte progenitor cells were also isolated by magnetic cell sorting (MACS, Miltenyl Biotec, Sunnyvale, CA) using Sca-1-coupled beads, following the manufacturers protocol. Sca-1-like+ cells were eluted from the column by washing with PBS supplemented with 2% fetal calf serum (FCS).

To induce differentiation, cells were treated with 5  $\mu$ M 5'-azacytidine (Sigma) for 72 hours in differentiation medium (Iscove's Modified Dulbecco's Medium /HamsF12 (1:1) (Gibco)) supplemented with L-Glutamine (Gibco), 2% horse serum, non-essential amino acids, Insulin-Transferrin-Selenium supplement, and  $10^{-4}$  M Ascorbic Acid (Sigma)). After induction, the medium was changed every 3 days.

For TGF $\beta$ 1 treatment, hCMPCs were cultured in differentiation medium, stimulated with 5  $\mu$ M 5'-azacytidine (Sigma) for 72 hours followed by TGF $\beta$ 1 stimulation (1ng/ml, Sigma). The medium was changed every 3 days.

*RNA isolation and reverse transcription PCR* RNA was isolated using of Trizol (Invitrogen, Breda, The Netherlands) and reverse transcribed using oligo-dT Superscript 3 (Invitrogen). Primer sequences are given in Table 6.1. The PCR reactions started with 2 min at 94°C followed by 35 cycles of: 15 s at 94°C, 30 s at 55°C and 45 s at 72°C. Products were analyzed on ethidium bromide-stained 1% agarose gel.  $\beta$ -tubulin or  $\beta$ -actin were used as RNA input control.

*Flow cytometric analysis* hCMPCs were either used freshly isolated or as trypsinized cells after culture. 200.000 cells per sample were used for FACS analysis. The cells were washed twice in wash-buffer (wb: 1% FCS/PBS/0.05M azide) and resuspended in 100  $\mu$ L wb containing 0.5% antibody. Antibodies used for FACS analysis were FITC- or PE-conjugated antibodies against CD14, CD31, CD34, CD105 (Endoglin), CD117 (c-kit), Sca-1, and isotype control IgGs, all from Pharmingen BD. The cells were incubated on ice in the dark for 30 minutes, washed 4 times with cold wb, resuspended in 250  $\mu$ L wb and analyzed using a Beckman Coulter Cytomics FC500 FACS.

*Karyomapping* Growing CMPC cultures (100.000 cells) were treated with 100 ng/ml colcemid (Karyomax, Gibco) for 1 hour at 37 °C. The cells were harvest the cells with 0.05% trypsin-EDTA, washed, and treated with hypotonic solution (0.6% Na-citrate) for 20 minutes at room temperature. After spinning at 300g for 5 minutes the cells were fixed using 5:1 methanol:glacial acetic acid. After fixing for 3 times, the cells were spinned down, resuspended in a small volume of fix and slides were made. The

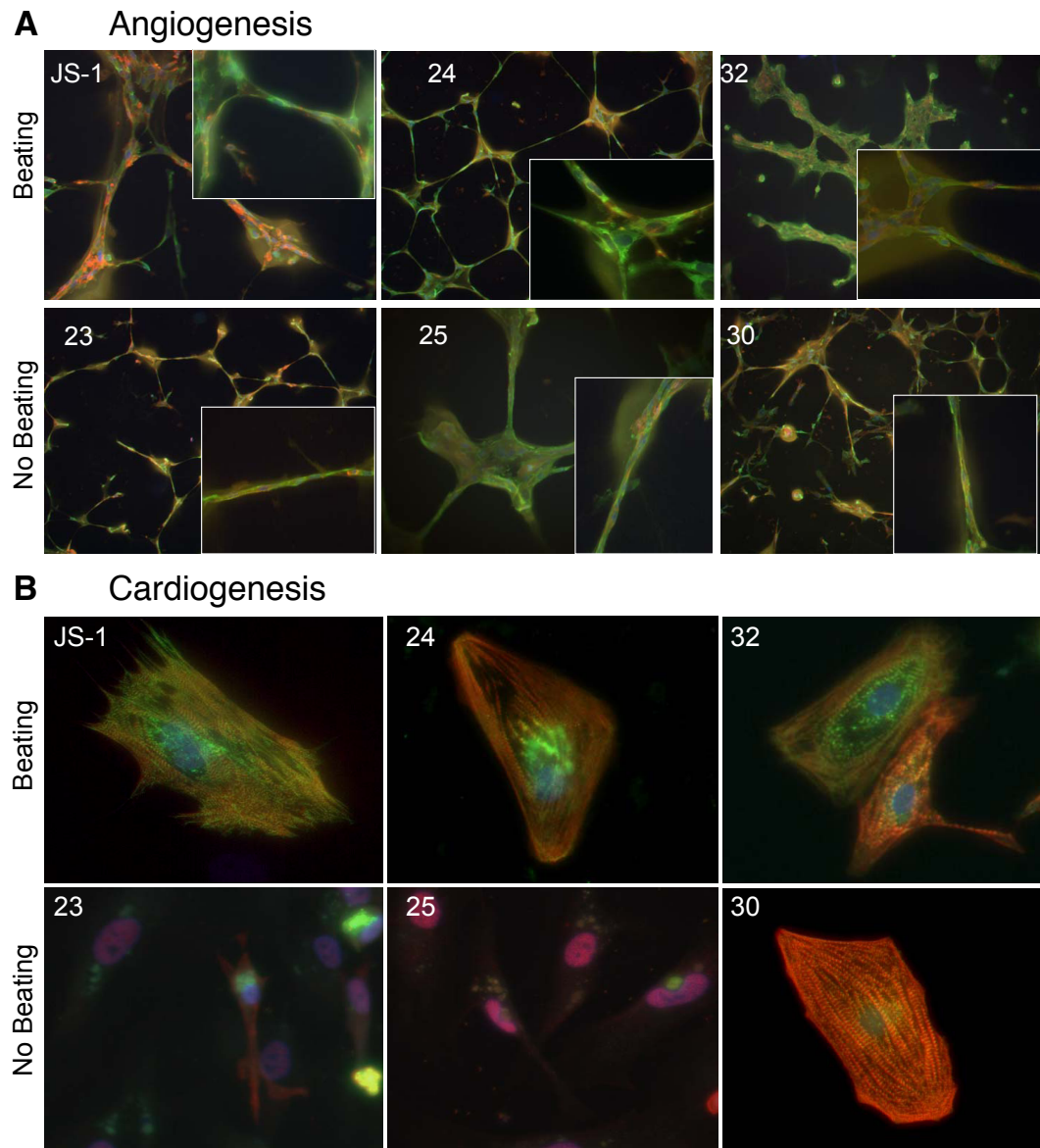


**Figure 6.6:** **A:** All CMPC clones, isolated by plating 1 cell per well, are able to form tube-like structures when cultured on matrigel. Cultures are stained with antibodies for endothelial cells (PECAM-1; red) and smooth muscle cells (SMA; green). **B:** CMPC clones were analyzed for their capacity to form striated cardiomyocytes. Cultures were stained with  $\alpha$ -actinin (red) and Troponin I (green). Although only 3 out of 6 clones differentiated into beating cultures, 4 out of 6 clones formed myocytes.



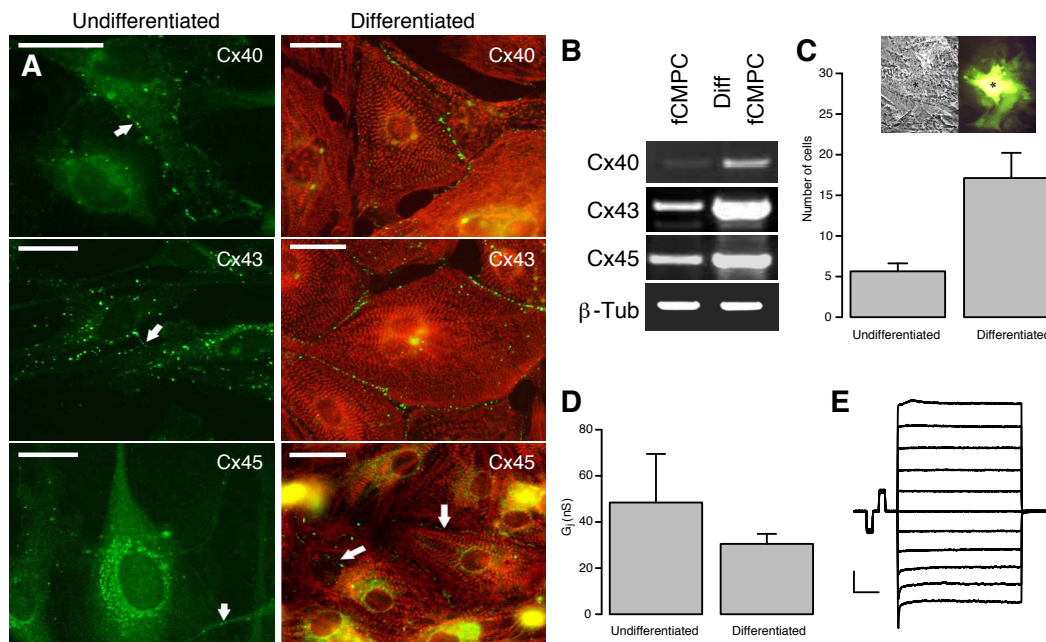


**Figure 6.7:** **A:** Immunolabeling against the connexin isoforms Cx40, Cx43 and Cx45 in undifferentiated hCMPCs (top panels) and hCMPCs differentiated into cardiomyocytes (bottom panels). Bar = 25  $\mu\text{m}$ . **B:** Semi-quantitative RT-PCR on RNA isolated from undifferentiated (undif) and differentiated (dif) hCMPCs for the expression of Cx40, Cx43 and Cx45.  $\beta$ -tubulin was used as a control for equal RNA input. **C:** Transfer of Lucifer Yellow from the injected cell to surrounding cells showing metabolic coupling. Dye spreading is significantly higher in differentiated hCMPCs compared to undifferentiated cells. Inset: photomicrograph of a representative Lucifer Yellow injection in differentiated hCMPCs, phase-contrast (left panel) and Lucifer Yellow fluorescence (right panel). Asterisk marks the injected cell. **D:** Quantification of electrical conductance in undifferentiated and differentiated hCMPC cell pairs. **E:** Representative recording or gap-junctional currents in a differentiated hCMPC cell pair. Scale bars: horizontal 200 ms, vertical 200 pA.

slides were treated with trypsin and stained. 50 mitotic cells were analyzed giving 95% confidence of detecting a mosaicism of 6%.

*Immunohistochemistry on cultured cells* Coverslips with cultured cells were rinsed in serum free medium, fixed in methanol ( $-20^{\circ}\text{C}$ ) or 4% paraformaldehyde, washed with PBS and permeabilized with 0.2% Triton X-100/PBS. Non-specific binding of antibodies was blocked with 2% bovine serum albumin (BSA). Incubation with primary antibodies was performed overnight in PBS/10% normal goat serum (NGS). Antibodies used recognized GATA-4 (Santa Cruz), Islet-1 (Hybridoma Bank), Cx40 (Chemicon), Cx43 (Zymed), Cx45 (kindly provided by Dr. T.H. Steinberg, Washington University, St.Louis, USA),  $\alpha$ -actinin (Sigma), Troponin I (Chemicon), desmin (Sanbio), titin (Sigma), MLC2v (Alexis),  $\beta$ -MHC (kindly provided by Dr. A.F.M. Moorman, AMC Amsterdam, Netherlands), N-cadherin (Sigma) and ZO-1 (Zymed). Immunolabeling was performed using Texas Red (TR)- or fluorescein isothiocyanate (FITC)-conjugated secondary antibodies (Jackson Laboratories). All incubation steps were performed at room temperature and in between all incubation steps, cells were washed with PBS. Finally, coverslips were mounted in Vectashield (Vector Laboratories) and examined with a Nikon Optiphot-2 light microscope equipped for epifluorescence.

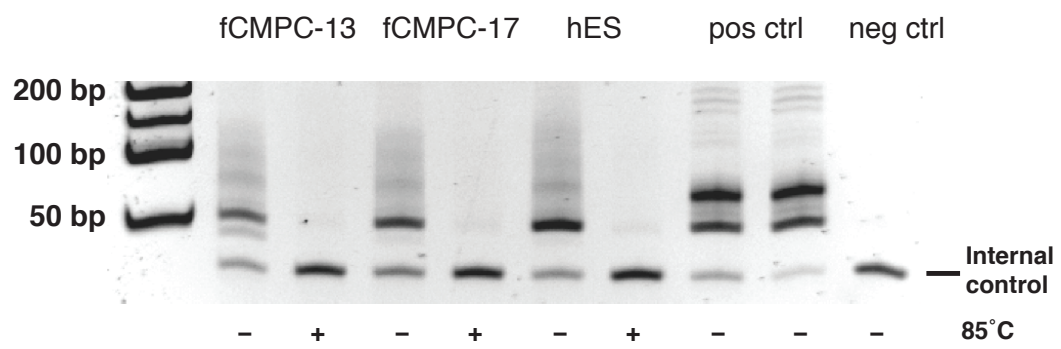


**Figure 6.8:** Telomerase activity analysis using a trapeze assay. We analyzed two CMPC cultures. Both CMPCs as well as the embryonic stem cells have telomerase activity.

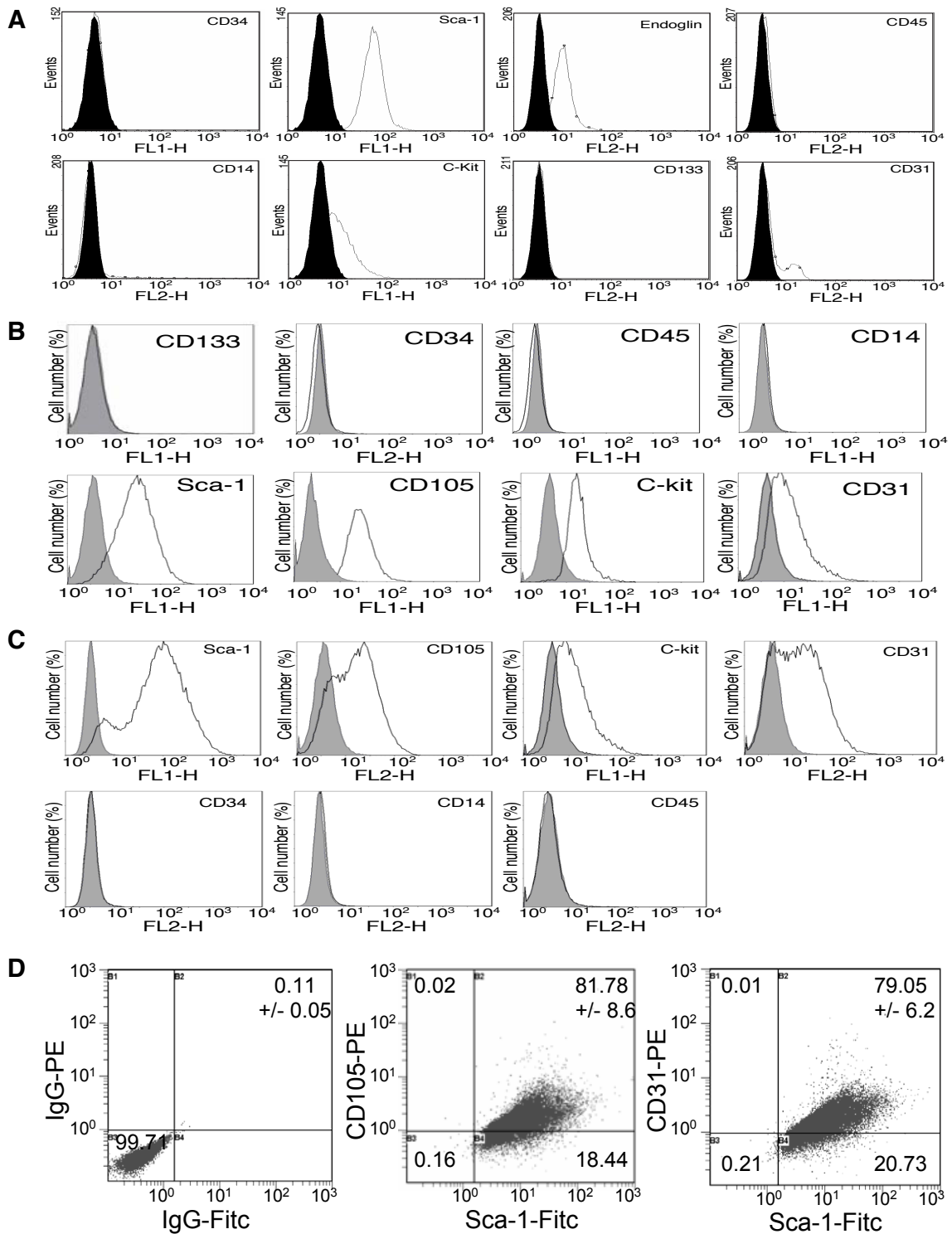


**Figure 6.9:** Flow cytometric analysis of (stem) cell markers expression on CMPCs. Histogram plots are shown with the isotype control in black and the specific signal in white.

**Matrigel assay** CMPCs, resuspended in EGM-2 medium containing an extra addition of 25 ng/ml VEGF (15.000 cells/well), were seeded into a matrigel coated 24 well plate (Chemicon ECM625), containing cover slips. After overnight culture, the cells were fixed using 4% paraformaldehyde, washed with PBS and blocked for 30 minutes using 0.1% saponin and 2% BSA (block buffer). Cover slips were stained with goat-anti-PECAM-1 (1:200 sc1505, Santa Cruz) and mouse-anti-SMA (1:40 (Clone 1A4, Dako)) in block buffer for 1 hour at RT. Immunolabelling was performed using Cy3 donkey-anti-goat (1:400, Dako), and 488nm goat-anti-mouse (1:400, invitrogen). Nuclei were stained using 0.2  $\mu$ g/ml Hoechst. The stained cells were embedded in mowiol and analyzed by fluorescence microscopy.

**Western blot analysis** Western blot analysis was performed as described previously (170). Detection was by ECL (Amersham). PSmad1 and PSmad2 rabbit polyclonal antibodies that specifically recognize phosphorylated Smad1/5 or Smad2 respectively were used 1:1000 (Cell Signaling), Nkx2.5 rabbit polyclonal 1:500 (Santa Cruz), and  $\alpha$ -actinin mouse monoclonal 1:5000 (Sigma).  $\beta$ -actin detection (1:10000, Chemicon) was used as a loading control.

**Table 6.1:** PCR primer pairs

Name	Forward/reverse 5'-3'	Product
MEF2C	AGATACCCACAACACACCACGCGCC ATCCTTCAGAGAGTCGCATGCGCTT	192
Isl-1	TAAGCCACCGTCGTGTCTC TGATGAAGCAACTCCAGCAG	107
GATA-4	GACAATCTGGTTAGGGGAAGC ACCAGCAGCAGCGAGGAGAT	105
NKX2.5	CGCCGCTCCAGTTCATAG GGTGGAGCTGGAGAAGACAGA	111
MLC2V	GTCAATGAAGCCATCCCTGT GCGCCAACTCCAACGTGTTCT	101
TropT	GTGGGAAGAGGCAGACTGAG ATAGATGCTCTGCCACAGC	131
$\beta$ -MHC	GAAGCCCAGCACATCAAAAG GATCACCAACAACCCCTACG	118
cActin	TCCTGATGCGCATTTTTTATTC AACACCACTGCTCTAGCCACG	123
Desmin	ACCTGCTCAACGTGAAGATG TGGTATGGACCTCAGAACC	159
MyoD	CGGCGGGGAACTGCTACGAA GGGGCGGGGGCGGAAACTT	458
c-kit	AAGTGGATGGCACCTGAAAG GAACTTAGAATCGACCGGCA	138
Cx40	GAGAAGAAGCAGCCAGAGTGTGAA GACATGCAGGGTGGTCAGGAAGATT	651
Cx43	AGCGTGAGGAAAGTACCAAACAGC AAGAAGGCCACCTCAAAGATAGAC	666
Cx45	CTAGACCCACTGAAAAGACC TGATTTGCTACTGGCAGTGC	494

*Electrophysiology* A symmetrical setup with two HEKA EPC-7 patch clamp amplifiers was used to measure action potentials and electrical coupling between cells. All signals were recorded using a custom data acquisition program (kindly provided by Dr. J.G. Zegers, AMC Amsterdam, The Netherlands) running on an Apple Macintosh computer equipped with a 12bit National Instruments PCI-MIO-16E-4 acquisition card. Current signals were low-pass filtered at 2.5 kHz and acquired at 10 kHz. Calcium imaging combined with action potential recording was done using a Cairn Research imaging system and an Axopatch 200B amplifier. All experiments were done using the whole cell patch clamp configuration. Action potential parameters measured from current clamp recordings were maximal diastolic potential, maximal upstroke velocity, action potential duration at 50 and 90 percent of repolarisation (APD<sub>50</sub> and APD<sub>90</sub>). Gap junctional macroscopic conductance in cell pairs was measured at a holding potential of  $-50$  mV using a voltage clamp protocol that included 50 ms square pulses with an amplitude of  $+10$  and  $-10$  mV, followed by a 1 second square pulse ranging between  $-50$  and  $+50$  mV. Gap junctional conductance ( $g_j$ ) is defined as  $g_j = I_j/V_j$ , where  $I_j$  and  $V_j$  denote junctional current and transjunctional voltage, respectively. By using the small prepulses for this calculation, gap junctional conductances were maximal and not inactivating. Offline analysis was done using MacDaq 8.0 (kindly provided by Dr. A.C.G. van Ginneken, AMC Amsterdam, The Netherlands) and R 2.0.1 (81). Experiments were done at  $20^\circ\text{C}$  or, for calcium imaging, at  $37^\circ\text{C}$ . For calcium imaging, cells were loaded with  $10\ \mu\text{M}$  Fluo-3 AM for 25 minutes at  $37^\circ\text{C}$ . Extracellular buffer used in all cases was a modified Tyrode's solution, containing (in mmol/L) NaCl 140, KCl 5.4, CaCl<sub>2</sub> 1, MgCl<sub>2</sub> 1, glucose 6, NaHCO<sub>3</sub> 17.5, HEPES 15, pH 7.20/NaOH. Action potentials were recorded using a pipette solution containing (in mmol/L) KCl 130, NaCl 10, HEPES 10, Mg<sub>2</sub>ATP 5, MgCl<sub>2</sub> 0.5, pH 7.20/KOH. Pipette buffer used for conductance measurements contained (in mmol/L) potassium gluconate 125, KCl 10, HEPES 5, EGTA 5, MgCl<sub>2</sub> 2, CaCl<sub>2</sub> 0.6, Na<sub>2</sub>ATP 4, pH 7.20/KOH. For dye injections, microelectrodes were filled with 4% w/v Lucifer Yellow in 150 mM LiCl<sub>2</sub>, 10 mM HEPES and cells were injected for 2 minutes. Cells stained with Lucifer Yellow were counted, excluding the injected cell. Patch pipettes were pulled on a Narishige PC-10 puller and fire-polished. When filled with pipette buffer, the pipette resistance ranged between 2-5 M $\Omega$ . Liquid junction potentials were calculated using Clampex (Axon Instruments) and used for offline correction.

*Measurement of beating rate in response to pharmacological stimuli* Cultures of differentiated fetal hCMPCs were superfused with DMEM/F12 (1:1), Gibco, Breda, The Netherlands) supplemented with 10% fetal calf serum (Gibco), 10 mM HEPES, 2 mM L-glutamine, 50 U/mL penicillin, 50  $\mu\text{g}/\text{mL}$  streptomycin, pH 7.40. All experiments were carried out at  $37 \pm 0.2^\circ\text{C}$ . Responses to  $0.1\ \mu\text{M}$  isoproterenol,  $1\ \mu\text{M}$  nifedipine and  $0.1\ \mu\text{M}$  BayK 8644 (all from Sigma) were recorded using a  $40\times$  objective for 1 minute.

*Statistics* Group comparisons were made using one-way ANOVA with the Holm-Sidak post-hoc test for multiple comparisons. Statistical significance was assumed if  $P < 0.05$ . All data are presented as mean  $\pm$  SEM.



## **Chapter 7**

# **Human fetal cardiac progenitor cells can be efficiently differentiated into cardiomyocytes expressing a cardiac electrical phenotype**

Teun P. de Boer, Toon A.B. van Veen, Bart J.M. Kok, Malin K.B. Jonsson, M.J. Goumans, P.A. Doevendans, J.M.T. de Bakker, Marcel A.G. van der Heyden

## Abstract

Cell replacement therapy using stem cell-derived cardiomyocytes is envisioned as a means to improve performance of diseased hearts. Thus far, only embryonic stem cells have an established cardiogenic potential, but the obtained cardiomyocytes have an immature phenotype, resulting in poor expression of connexin43 and rather depolarized resting membrane potentials. Recent studies identified cardiac progenitor cells in rodent and human hearts that can differentiate into cardiomyocytes in vitro. We isolated CPCs from human fetal hearts. Using a highly efficient differentiation protocol we obtained cultures containing up to 90 percent  $\alpha$ -actinin positive cardiomyocytes. Western blot experiments demonstrated upregulation upon differentiation of  $\alpha$ -actinin,  $\alpha$ -skeletal actin,  $\beta$ -catenin, N-cadherin, desmin and plakophilin2. Cx43 and Cx45 expression levels were similar in undifferentiated and differentiated cells, but we did observe increased phosphorylation of Cx43. RT-PCRs demonstrated upregulation of all major cardiac ion channels and transporters during differentiation. Patch clamp experiments showed that monolayers of differentiated cardiomyocytes have a stable resting membrane potential of  $-73.4 \pm 1.8$  mV. Infusion of 1 mM BaCl<sub>2</sub> resulted in a depolarization to  $-59.9 \pm 2.8$  mV, indicating functional expression of inward rectifying potassium channels. Subsequent voltage clamp experiments confirmed the presence of near mature  $I_{Na}$ ,  $I_{K1}$  and  $I_{Ca,L}$  current densities. Our experiments indicate that human fetal CPC-derived cardiomyocytes have a relatively mature electrical phenotype. Additionally, they express proteins involved in cardiac electro-mechanical integration. When compared with embryonic stem cell-derived cardiomyocytes, this new cell type may be used to generate cardiomyocytes with reduced pro-arrhythmogenic properties upon transplantation.

## Introduction

Cell replacement therapy is envisioned as a future approach to improve cardiac performance in patients suffering from heart failure. It involves transplantation of stem cell-derived cardiomyocytes into the myocardium. Clinical trials have however demonstrated that transplantation of cells can also have adverse effects. Transplantation of skeletal myoblasts resulted in ventricular tachyarrhythmias in some patients (11; 12). Factors involved in such pro-arrhythmic effects of cell replacement have been investigated by our group and others. Using an in vitro model composed of co-cultured spontaneously active immature and adult quiescent cardiomyocytes, we found that pro-arrhythmia depends on spontaneous activity, intercellular coupling and the size of the transplanted cluster (150). These findings emphasize that cells generated for cell replacement therapy should ideally possess no automaticity and have appropriate coupling capabilities.

Several stem cell types have been tested with respect to cardiogenic potential, including mesenchymal stem cells, skeletal myoblast and embryonic stem cells (149). Up to now, only embryonic stem cells have an undisputed cardiogenic potential. Human embryonic stem cells can be differentiated into cardiomyocytes (171; 14), either spontaneously or after induction with endoderm-derived factors. The electrical pheno-



type of human embryonic stem cell-derived cardiomyocytes has been studied by several groups.

Compared to the resting membrane potential of adult working cardiomyocytes ( $\sim -80$  mV), human embryonic stem cell-derived cardiomyocytes have a less negative membrane potential of ( $\sim -55$  mV) (13; 15; 36). Depolarization of mature cardiomyocytes predominantly relies on sodium current (SCN5A) and to a lesser extent on calcium currents ( $\alpha 1C$ ). In human embryonic stem cell-derived cardiomyocytes sodium channels are mostly inactivated due to the relatively depolarized membrane potential. This probably increases the role of calcium currents during the upstroke, but there is no consensus in literature whether spontaneous activity in hES-derived cardiomyocytes is determined by sodium or by calcium currents, possibly due to variations between cell lines (15; 37). After the plateau phase of the action potential which depends on calcium currents in adult and stem cell-derived cardiomyocytes, repolarization is caused by sequential activation of HERG, KvLQT1 and Kir2.*x* potassium currents. mRNA expression of these channels in human embryonic stem cell-derived cardiomyocytes has been reported, but no electrophysiological data are available on the current carried by KvLQT1 yet, whereas inward rectifier (Kir2.*x*) currents are absent or small (37; 36). While human embryonic stem cell-derived cardiomyocytes provide developmental biologists with a good model of early cardiogenesis, their immature electrical phenotype and limited expression of cardiac connexins complicates, at present, their use in cell replacement therapy. This is further complicated by factors as ethical objection and immunological rejection.

Recently, a new type of stem cells with cardiogenic potential has been identified in the heart itself. These so-called cardiac progenitor cells have been found in rodent and human hearts (153; 155; 157; 154; 172). As was demonstrated in a previous study by our group, cardiac progenitor cells can also be isolated from the human fetal heart (173). Fetal CPCs proliferate rapidly in culture and current differentiation protocols yield up to 90% cardiomyocytes displaying cross-striated  $\alpha$ -actinin expression. Interestingly, the newly generated cardiomyocytes have resting membrane potentials that are more negative than those measured in human embryonic stem cell-derived cardiomyocytes. Also the upstroke of the action potential is significantly faster, which indicates a more mature electrical phenotype when compared to human embryonic stem cell-derived cardiomyocytes.

In this study we set out to establish the electrical phenotype of differentiated human fetal CPCs on the level of ion currents and found that the rather mature electrical phenotype of these cells is explained by near-adult current densities of the major cardiac ion channels. In addition we observed expression of cardiac proteins involved in electrical and mechanical integration. These findings suggest that cardiomyocytes obtained from human fetal cardiac progenitor cells have reduced pro-arrhythmogenic properties as compared to contemporary stem cell-derived cardiomyocytes.

## Materials and Methods

*Cardiac progenitor cell isolation and differentiation* Cardiac progenitor cells were isolated from human fetal hearts obtained after elected abortion with prior informed con-

sent and approval of the ethical committee of the University Medical Center Utrecht, as published previously (see (173)). Briefly, hearts were isolated and perfused using a Langendorff perfusion setup. After digestion with collagenase and protease, CPCs were isolated from the cardiac cell suspension using magnetic beads coated with a Sca-1 antibody. Cells were cultured on 0.1% gelatin coated material, using SP++ medium (EBM-2 with EGM-2 additives, mixed 1:3 with M199) supplemented with 10% FCS (Gibco), 10 ng/ml basic Fibroblast growth factor (bFGF), 5 ng/ml epithelial growth factor (EGF), 5 ng/ml insuline like growth factor (IGF-1) and 5 ng/ml hepatocyte growth factor (HGF).

CPCs were differentiated in Iscove's Modified Dulbecco's Medium /Ham's F-12 (1:1) (Gibco) supplemented with L-Glutamine (Gibco), 2% horse serum, non-essential amino acids, Insulin-Transferrin-Selenium supplement, and  $10^{-4}$  M ascorbic acid (Sigma). First, CPCs were exposed to 5  $\mu$ M 5'-azacytidine for three days, followed by 1 ng/mL TGF- $\beta$ 1 every three days. For electrophysiological experiments, differentiated cultures were dissociated using collagenase and replated on gelatin coated coverslips in densities ranging from single cells to monolayers.

*Semi-quantitative RT-PCR* RNA was isolated using Trizol and 2  $\mu$ g total RNA was reverse transcribed using oligo-dT Superscript 3 (Invitrogen in a 20  $\mu$ l reaction volume. Subsequently, 1  $\mu$ l reaction volume (cDNA equivalent of 100 ng total RNA) was used in the PCR reaction. Primers, annealing temperature, product size, and optimized number of PCR cycles are depicted in Table 7.1. Products were analyzed in 1-1.5% agarose, ethidium bromide-stained gels.  $\beta$ -tubulin was used as an internal standard.

*Western blotting* Cells were lysed in Tripure and protein fraction was obtained using phase extraction according to the manufacturer's protocol. Twenty microgram protein lysate was mixed with Laemmli sample buffer and proteins were separated by 10% sodium dodecyl sulfate-polyacrylamide gel electrophoresis (SDS-PAGE) and subsequently electro-blotted onto a nitrocellulose membrane (Biorad, Veenendaal, the Netherlands). Equal loading was checked by reversible Ponceau staining. The antibodies used were Cx40 (Chemicon), Cx43 (Transduction), Cx45 (kindly provided by Dr. T.H. Steinberg, Washington University, St.Louis (120)),  $\alpha$ -skeletal-actin (Clement),  $\alpha$ -actinin (Sigma), desmin (Sanbio), N-cadherin (Sigma),  $\beta$ -catenin (Transduction) and plakophilin2 (Transduction). Proteins were visualized by using peroxidase-labeled secondary antibodies (Jackson) and standard ECL procedures (Amersham Bioscience).

*Immunohistochemistry* Cells were fixed with methanol at  $-20^{\circ}\text{C}$  for 2 min and rinsed three times in PBS. Immunolabelling was performed as described before (62). Primary antibodies used were anti- $\alpha$ -skeletal actin (Clement), anti- $\alpha$ -actinin (Sigma).

*Electrophysiological experiments and analysis* Measurements of ion currents and field stimulated action potentials were done using a HEKA EPC-10 Double Plus amplifier controlled by PatchMaster 2.20. Voltage clamp experiments were done using online correction of liquid junction potential, a minimal series resistance compensation of 70% was used and measurements were normalized to membrane capacitance. Data

**Table 7.1: PCR primer pairs**

Name	Forward/reverse 5'-3'	Product (bp)	Annealing (°C)
$\beta$ -Tubulin	TGGCTTTGCCCTCTCACCA CGGCGGAACATGGCAGTGAA	369	61
ANF	GAACCAGAGGGGAGAGACAGAG CCCTCAGCTTGCTTTTTAGGAG	406	61
$\alpha$ 1C	CTGGACAAGAACCAGCGACAGTGCG ATCACGATCAGGAGGGCCACATAGGG	406	61
$\alpha$ 1D	GCAAGATGACGAGCCTGAG ATGGTTATGATGGTTATGACAC	243	55
$\alpha$ 1H	CACTCATTCTACAACCTTCATC CTCTCCCGCTGCTTCGTC	118	55
Kv4.3	CTGGACAAGAACCAGCGACAGTGCG ATCACGATCAGGAGGGCCACATAGGG	322	55
KvLQT1	TTCTTGGCTCGGGTTTGCC TGTTGCTGCCGCGATCCTTG	723	58
SCN5a	ACCATCGTGAACAACAAGAGCC GGCAGCCAGCTTGACAATACAC	617	60
HERG	GACGTGCTGCCTGAGTACAAGC GCCGCGCCGTACTCTGAGTAG	497	63
NCX1	CATCATGGAGGTGAAAGTATTG CCTTTAGAAGCCTTTTATGTGG	1263	53
NCX2	TCCGACTACGAGTACAGCG TGCATCACGTAGTCAAAGCAC	856	58
Kir2.1	TTGAGTAAACAGGACATTGAC CTGGTTGTGAAGTCTATG	389	50
Kir2.2	GACCTGGAGACGGACGAC AGCCTGGAGTCTGTCAAAGTC	393	55
Cx40	GAGAAGAAGCAGCCAGAGTGTGAA GACATGCAGGGTGGTCAGGAAGATT	651	65
Cx43	AGCGTGAGGAAAGTACCAAACAGC AAGAAGGCCACCTCAAAGATAGAC	666	62
Cx45	CTAGACCCACTGAAAAGACC TGATTTGCTACTGGCAGTGC	494	53
HCN2	GAGGACAACACGGAGATCATC TTGATGGACACCCAGCAGT	397	57
HCN4	GAGGACAACACAGAGATCATC TTGATGGACACCCAGCAGT	400	57
SERCA2a	TCCTTCTACCAGCTGAGTCA GGAAGCGGTTACTCCAGTATT	410	55
SERCA2b	CTCATCTTCCAGATCACACCGC CAGGCTGCACACACTCTTTAC	141	55
SERCA2c	TCCTTCTACCAGCTGAGTCA CTTCCCCTCAAGCAGAGTACA	431	55
FKBP12.6	CTATGGGCGTGGAGATCGAG GTGGCATTGGGAGGGATGAC	292	60
RyR	CCTGCTTTGAGAGGAGAAGGT GAGTCAATGAGAGAAGCGTGG	644	55
TBX3	CAGCTTTCAACTGCTTCGCC GTTGAAGAAGTGTGGCCCGC	512	60

were further analysed using FitMaster and Kaleidagraph. Cells attached to coverslips were placed in a temperature controlled perfusion chamber (Cell Microcontrols) and kept at 37°C, except for sodium current measurements (20°C).

Inward rectifying potassium currents ( $I_{K1}$ ) were measured as barium-sensitive currents, elicited by 1 second voltage steps from +30 to -120 mV, with 10 mV increments, from a holding potential of -40 mV. The average normalized steady state current from 900 to 990 ms was plotted versus test potential. Inward sodium currents ( $I_{Na}$ ) were recorded by applying 750 ms pulses with 10 mV increments ranging between -110 and +30 mV, from a holding potential of -120 mV. Peak sodium current was plotted versus test potential. L-type calcium currents ( $I_{Ca,L}$ ) were elicited by 500 ms pulses with 10 mV increments ranging between -40 and +40 mV, from a holding potential of -80 mV. Residual sodium currents were inactivated by a 200 ms prepulse at -40 mV. Peak inward calcium currents were plotted versus test potential. Hyperpolarization activated cationic currents ( $I_f$ ) were measured with 1.5 second test pulses with 10 mV increments ranging between -50 and -120 mV, from a holding potential of -40 mV. Activating currents were fitted with mono-exponential curves and steady state current was normalized to the maximal current and subsequently plotted versus test potential.

Action potentials were evoked by bipolar field stimulation using two platinum electrodes and a Grass S88 stimulator. To measure effective refractory period, trains of eight pulses (basic cycle length 1 second) were followed by a premature pulse at coupling intervals from 500 to 250 ms (50 ms decrements). The effect of  $I_{Kr}$  block on action potential duration ( $APD_{90}$ ) was measured with a basic cycle length of 1 second.

*Solutions for electrophysiology* Extracellular buffer for measurements of  $I_{K1}$ ,  $I_f$  and action potentials contained (in mmol/L) NaCl 140, KCl 5.4,  $CaCl_2$  1,  $MgCl_2$  1, glucose 6,  $NaHCO_3$  17.5, HEPES 15, pH 7.4/NaOH. For measurements of  $I_f$ ,  $BaCl_2$  1,  $CdCl_2$  0.2,  $MnCl_2$  2 and 4-aminopyridine 0.5 were added. Pipette buffer contained potassium gluconate 125, KCl 10, HEPES 5, EGTA 5,  $MgCl_2$  2,  $CaCl_2$  0.6,  $Na_2ATP$  4, pH 7.20/KOH.

$I_{Na}$  and  $I_{Ca,L}$  measurements were done in NMDG 140, KCl 5.4,  $CaCl_2$  1,  $MgCl_2$ , glucose 6,  $NaHCO_3$  17.5, HEPES 15, pH 7.4/CsOH. Pipette buffer contained CsCl 120, TEACl 10,  $MgCl_2$  3,  $CaCl_2$  1,  $Na_2ATP$  2, EGTA 10, HEPES 5, pH 7.2/CsOH.

Pipettes were pulled using a Sutter P-2000 and patch pipettes had resistances of approximately 3 M $\Omega$  when fire-polished and filled with pipette solution. Microelectrodes had resistances of 8-12 M $\Omega$  when filled with 3M KCl.

*Statistics* All results are presented as mean  $\pm$  s.e.m. Differences between group averages were tested using Student's t-test or one-way ANOVA followed by a Holm-Sidak post-hoc test for multiple comparison, significance was assumed if  $p < 0.05$ .

## Results

### CPC-derived cardiomyocytes express cardiac proteins involved in electrical and mechanical integration

Differentiated CPCs present as synchronously beating monolayers in culture medium were indicative of efficient cardiac differentiation. Indeed, up to 90% of the cells were found to express  $\alpha$ -actinin in a cross-striated pattern, see Figure 6.4C. In a subpopulation of  $\alpha$ -actinin positive cells, we also found expression of  $\alpha$ -skeletal actin, combined with  $\alpha$ -actinin expression (Figure 7.1). Western Blotting experiments confirmed that upon differentiation, both  $\alpha$ -actinin and  $\alpha$ -skeletal-actin are upregulated, see Figure 7.2.

In vivo, cardiomyocytes form a functional, but not anatomical, electrical syncytium facilitating fast impulse propagation and mechanical integrity. Electrical coupling depends on expression of the cardiac connexins Cx40, Cx43 and Cx45. Western blot experiments showed that connexin expression in undifferentiated and differentiated CPCs is similar when considering expression level. No Cx40 could be detected, but Cx43 and -45 were expressed (see Fig. 7.2). While the total amount of Cx43 expressed in undifferentiated and differentiated CPCs appeared comparable, there was a clear increase in the P1 and P2 bands, indicating increased phosphorylation of Cx43 upon differentiation. Next, we tested the expression of several proteins involved in mechanical integration in the heart. N-cadherin was expressed in undifferentiated CPCs, but expression was further increased upon differentiation. The same pattern was observed for  $\beta$ -catenin, plakophilin2 and desmin, indicating increased mechanical integration upon differentiation.

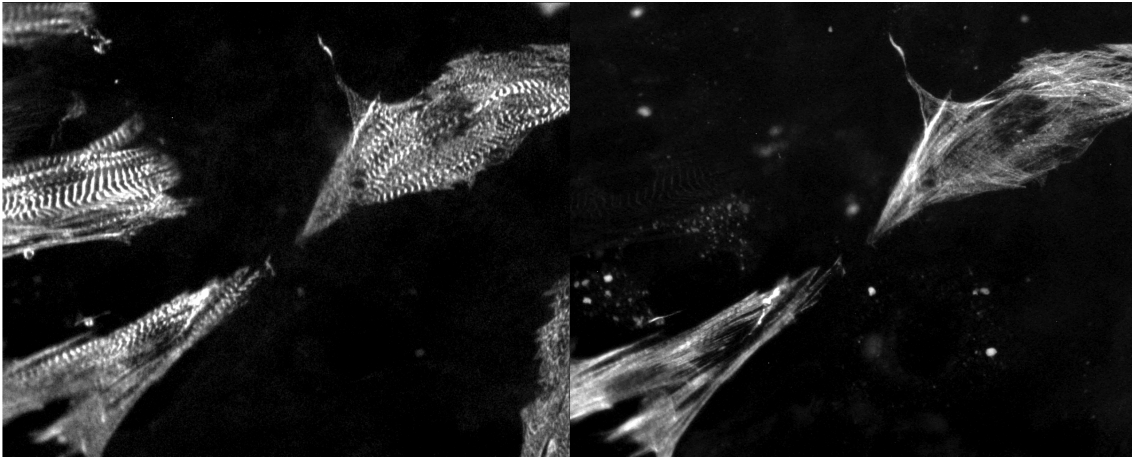


**Figure 7.1:** Human fetal CPC-derived cardiomyocytes stained for  $\alpha$ -actinin (left) or skeletal actin (right). Clear cross-striations can be seen in  $\alpha$ -actinin expression, while skeletal actin appears mostly organized in fibers with faint cross-striation. Cells were observed to express either  $\alpha$ -actinin, or skeletal actin and  $\alpha$ -actinin.

## Cardiomyocytes differentiating from CPCs show upregulation of cardiac ion channels and transporters

Expression of transcripts of major cardiac ion channels involved in depolarization and repolarization was determined during differentiation, see Figure 7.3. After 2 weeks of differentiation, we observed upregulated expression of HCN2 and 4, Kir2.1 and 2.2, SCN5A,  $\alpha$ 1C, Kv4.3, HERG and KvLQT1. Also upregulated were RyR2, SERCA2a, 2b and 2c, NCX-1, Cx40, 43 and 45 as well as ANF. At 4 weeks of differentiation, most transcripts were expressed at levels comparable to 2 weeks. Notably, we did see a downregulation of Kir2.1 with a concomitant upregulation of Kir2.2, which may be indicative of an isoform-switch. Furthermore we observed increased expression of  $\alpha$ 1C,  $\alpha$ 1H as well as RyR2, SERCA2c and NCX-1, indicating development of the excitation-contraction apparatus. Ion channels involved in repolarization, Kv4.3, HERG and KvLQT1 were also further upregulated. Taken together, our RT-PCR data demonstrate increased expression of the cardiac electronome during differentiation.

## CPC-derived cardiomyocytes have a negative membrane potential that can be attributed to functional $I_{K1}$ current

As established in an earlier study, CPC-derived cardiomyocytes have a rather negative membrane potential (173). Although cultures were spontaneously active in culture medium, they become quiescent in the absence of fetal calf serum. Nonetheless, cultures were still excitable, as they responded to field stimulation (Figure 7.4) by firing action potentials. Next, the membrane potential of cardiomyocytes in monolayers was measured and 1 mM BaCl<sub>2</sub>, a potent blocker of  $I_{K1}$ , was infused (174). Control measurements showed a resting membrane potential of  $-73.4 \pm 1.8$  mV, which reduced significantly to  $-59.9 \pm 2.8$  mV in the presence of BaCl<sub>2</sub> (N=5). These experiments indicate that the observed expression of Kir2.1 and 2.2 transcripts resulted in functional expression of  $I_{K1}$  channels, which contributed significantly to the resting membrane potential.

## Functional expression of cardiac ion channels in CPC-derived cardiomyocytes

Incited by the finding that Kir2.x expression in CPC-derived cardiomyocytes has a significant impact on membrane potential, we used single cell voltage clamp to assess the current densities of  $I_{K1}$  and other major cardiac currents ( $I_f$ ,  $I_{Na}$ ,  $I_{Ca,L}$ ).

We found that CPC-cardiomyocytes express large inward rectifying currents that could be blocked by 1 mM BaCl<sub>2</sub>.  $I_{K1}$  current density at  $-120$  mV was  $-14.2 \pm 2.5$  pA/pF (N=7) (Figure 7.5A), which is comparable to values we measured in adult dog cardiomyocytes ( $-15.1 \pm 2.6$  pA/pF, N=5, data not shown) and explains the stable and rather negative membrane potential observed earlier.

The actions of  $I_{K1}$  are opposed by the hyperpolarization-activated cationic current ( $I_f$ ). CPC-cardiomyocytes (N=7) displayed  $I_f$  currents with a mean steady state current density of  $-5.5 \pm 1.8$  pA/pF at  $-120$  mV. Currents were half-maximally activated

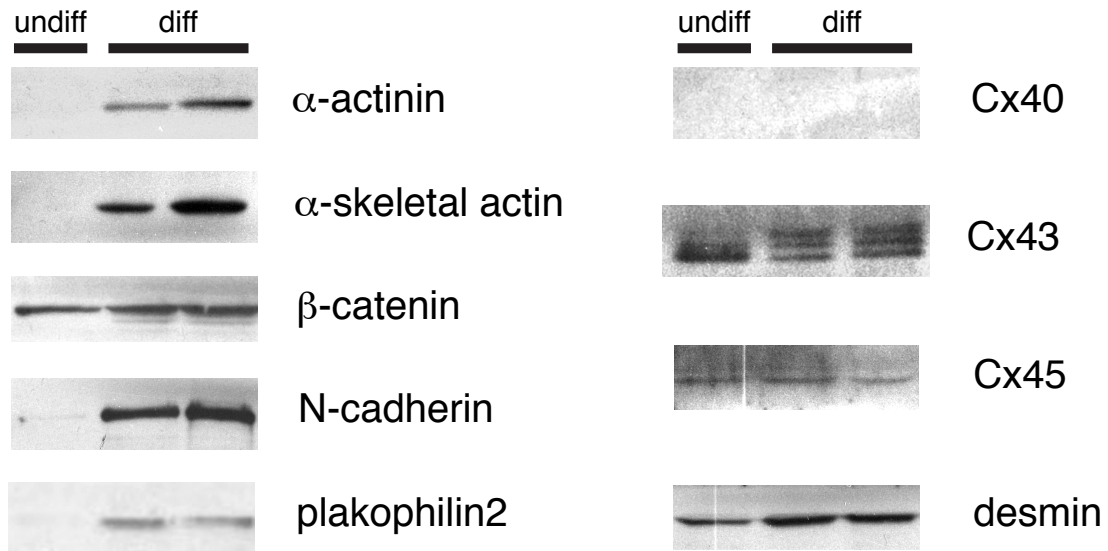


**Figure 7.2:** Western blot experiments demonstrating expression of proteins involved in contractile and electro-mechanical integration.

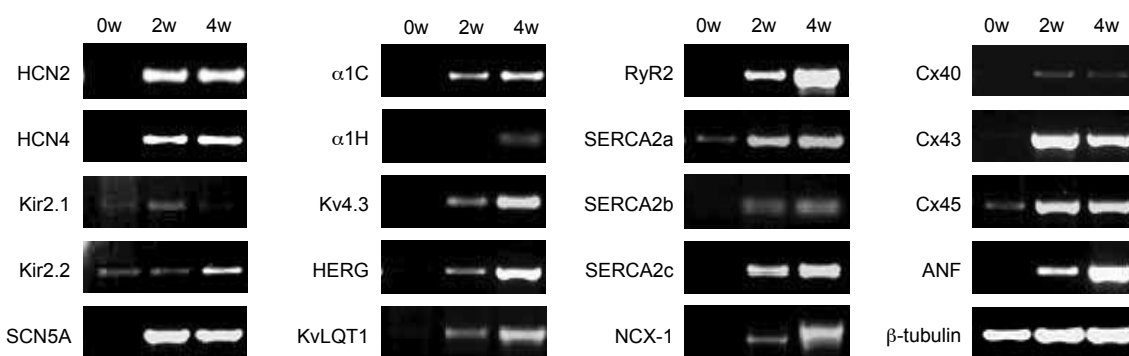


**Figure 7.3:** RT-PCR experiments demonstrating mRNA expression of ion channels and transporters. Upon differentiation, we observed upregulation of all major human cardiac ion channels and transporters. Also the cardiac connexins Cx43 and Cx45 are expressed. Increased expression of ANF demonstrated a progressive differentiation into cardiomyocytes.

at  $-93 \pm 8$  mV.

In our earlier study we found that the upstroke velocity of CPC-derived cardiomyocytes was high as compared to other immature cardiomyocytes, which is compatible with a significant expression of SCN5A. In voltage clamp experiments we observed large inward sodium currents that started to activate at  $-60$  mV. Mean maximal peak current density was  $-47.7 \pm 10.2$  pA/pF (N=7). This current could be blocked only partially by infusion of  $10 \mu\text{M}$  tetrodotoxin (N=6), which is characteristic for cardiac sodium channels encoded by SCN5A (175).

Also partially involved in upstroke velocity, but more prominent in the plateau phase of the action potential, is the inward calcium current. We measured inward currents that were maximally activated at  $0$  mV, with an average current density of  $-3.9 \pm 0.7$  pA/pF (N=7). Infusion of  $10 \mu\text{M}$  nifedipine completely blocked the inward current (N=7), confirming that it was conducted by L-type calcium channels.

### Blocking $I_{Kr}$ prolongs action potentials of CPC-derived cardiomyocytes

In order to assess the contribution of  $I_{Kr}$  to action potential duration, we tested the effects of the  $I_{Kr}$  blocker almokalant on field-stimulated monolayers (see Figure 7.6). In control buffer,  $\text{APD}_{90}$  was  $429.7 \pm 17.6$  ms, which was significantly prolonged by infusing  $2 \mu\text{M}$  almokalant to  $554.3 \pm 27.3$  ms (N=6).

## Discussion

In this study we investigated the electrical phenotype of cardiomyocytes derived from human fetal cardiac progenitor cells. Western blot experiments demonstrated expression of Cx43 and 45, adhesive proteins and  $\alpha$ -actinin and skeletal actin in differentiated cardiomyocytes. Upon differentiation we also observed upregulation of cardiac ion channels and transporters, which resulted in hyperpolarization of the membrane potential and excitability. Voltage clamp experiments showed functional expression of  $I_{K1}$ ,  $I_{Na}$ ,  $I_{Ca,L}$  and  $I_f$ . Action potentials were prolonged by  $I_{Kr}$  block.

The strategy to use stem cells to produce in vitro differentiated cells for transplantation into a patient's compromised heart in order to improve cardiac function can potentially be of use for future clinical practice. Attempts to use stem cells from various sources, e.g. bone marrow, peripheral blood or skeletal muscle, to repair hearts of patients suffering from cardiac disease have thus far not resulted in a clear-cut increase in muscle mass. Studies employing skeletal myoblasts demonstrated that transplantation of differentiated myoblasts can introduce an arrhythmogenic substrate leading to ventricular arrhythmias (11; 12). Use of mesenchymal stem cells did improve cardiac output temporarily in several studies, but this was probably caused primarily by factors secreted by the transplanted stem cells and/or through increased neovascularisation (7). Up to now, true cardiac differentiation has been demonstrated only using embryonic stem cells. However, embryonic stem cells are not a preferable source to use in clinical applications. Apart from ethical issues, practical problems as limited differentiation efficiency, pro-arrhythmogenic potential, risk of teratoma formation and



immune-rejection of the graft after transplantation make clinical application of embryonic stem cells a difficult task.

*Immunohistochemistry and WB* Differentiation of the fetal CPCs induced expression of  $\alpha$ -actinin in up to 90% of the cells, while a subset of cells also expressed  $\alpha$ -skeletal actin. Western blot experiments confirmed this finding, showing expression of both  $\alpha$ -skeletal actin and  $\alpha$ -actinin in samples from differentiated cultures. This is in line with previous publications that demonstrated that while both the cardiac and  $\alpha$ -skeletal actin isoforms are expressed in the human heart,  $\alpha$ -skeletal actin is the less abundant isoform (176) although both the cardiac and  $\alpha$ -skeletal actin isoforms are expressed in the human heart. During the early phases of cardiac differentiation of mouse embryonic stem cells, both isoforms are upregulated, but  $\alpha$ -skeletal actin expression is decreased in later phases while cardiac actin expression persists (177). This is similar to our finding that not all  $\alpha$ -actinin expressing cardiomyocytes co-express  $\alpha$ -skeletal actin. Detection of Cx43 and -45 confirms our earlier immunohistochemical findings (173). The absence of Cx40 probably can be explained by the fact that immunohistochemistry indicated that only a small amount of cells appeared to be Cx40 positive. The increase in phosphorylation of Cx43 upon differentiation is compatible with the enhanced Cx43 expression at the cell borders (121) and the high levels of intercellular coupling observed in our earlier study. Combined with expression of N-cadherin,  $\beta$ -catenin, desmin and plakophilin2, our data suggest that these newly generated cardiomyocytes are well-equipped to integrate in myocardial tissue. With respect to pro-arrhythmia upon transplantation, a previous in vitro modeling study by our group has indicated that the intercellular coupling is an important determinant of pro-arrhythmic risk (150). The levels of coupling found in CPC-derived cardiomyocytes will decrease the likelihood of developing arrhythmias after transplantation.

*Human fetal heart CPC-derived cardiomyocytes show robust functional expression of cardiac ion currents* In this study we observed a rather negative membrane potential in CPC-derived cardiomyocytes which was sensitive to  $I_{K1}$  block using barium. Subsequent voltage clamp experiments demonstrated barium-sensitive  $I_{K1}$  currents with a mean current density of  $-14.2 \pm 2.5$  pA/pF. This is comparable to current densities measured in adult dog and human ventricular cardiomyocytes (150; 178), which is remarkable since stem cell-derived cardiomyocytes from other sources (hES, mES) are known to express no or only low levels of functional  $I_{K1}$  (36; 32).

An interesting finding in this study, namely spontaneous activity in the presence of serum and quiescence in its absence, probably result from modulation of  $I_f$ . The observed current density of  $-5.5 \pm 1.8$  at  $-120$  mV is in between densities reported for human adult ventricular cardiomyocytes and human embryonic stem cell-derived cardiomyocytes ( $-1.9 \pm 0.3$  and  $-7.2 \pm 1.9$  pA/pF, respectively) (179; 37). The potential at which  $I_f$  was half-maximally activated ( $V_{0.5}$ ) was almost identical with that reported for human infant and adult cardiomyocytes (180; 179). Preliminary experiments showed that spontaneous activity in CPC-derived cardiomyocytes is not inhibited by high levels (10  $\mu$ M) of TTX and therefore probably does not involve window sodium currents. In contrast, observations in hES-derived cardiomyocytes showed that

spontaneous activity depends on a window sodium current that is triggered by their relatively depolarized membrane potential (37). These observations together with the fact that CPC-derived cardiomyocyte membrane potential is rather negative, suggest that spontaneous activity is more likely to be the result of activation of  $I_f$ . Alternatively, inhibition of  $I_{K1}$  could disturb the delicate balance between  $I_f$  and  $I_{K1}$ . This however seems unlikely since in preliminary experiments, resting membrane potentials were comparable under serum and serum-free conditions.

Expression of cardiac sodium channel mRNA (SCN5A) was correlated with large sodium currents (peak amplitude  $-47.4 \pm 10.2$  pA/pF). These current densities are somewhat larger than in reports on human adult atrial and ventricular cardiomyocytes (181; 182), which can be explained by a larger sodium gradient used in our study.

An previous finding that nifedipine silences beating of CPC-derived cardiomyocytes indicated functional expression of the L-type calcium channel (173). In this study we observed both mRNA expression and functional L-type calcium currents. The current density observed ( $-3.9 \pm 0.7$  pA/pF) is in the lower range of reported densities for human atrial ( $-2.2$  to  $-5.7$  pA/pF) and ventricular ( $-3.8$  to  $-5.1$  pA/pF) cardiomyocytes (183; 184; 185).

Inhibition of  $I_{Kr}$  with almokalant resulted in significant action potential prolongation. Besides demonstrating a functional role of  $I_{Kr}$  as a repolarizing current in CPC-derived cardiomyocytes, this also opens possibilities to use CPC-derived cardiomyocytes to test anti-arrhythmic drugs that prolong the cardiac action potential. The availability of an in vitro model of human origin could be beneficial in the starting phase of drug discovery and safety testing.

In summary, our cellular electrophysiological data provide evidence of near adult current densities of the primary cardiac ion currents. This results in a resting membrane potential that is more negative when compared to cardiomyocytes derived from human embryonic stem cells. As a consequence, and in combination with our observations of robust intercellular coupling, fetal CPC-derived cardiomyocytes likely possess less pro-arrhythmic potential as compared to other sources of immature cardiomyocytes.

## Acknowledgments

The authors would like to express their gratitude towards S.C.M. van Amersfoort, and dr. G.A. Antoons for excellent assistance and discussions. This study was supported by the Netherlands Heart Foundation (grant 2003B07304, TdB), the Technology Foundation (STW program DPTE, grant #MKG5942, MAGvdH and grant UGT.6746, TABvV) and the Netherlands Organization for Scientific Research (NWO, grant 916.36.012, TABvV).

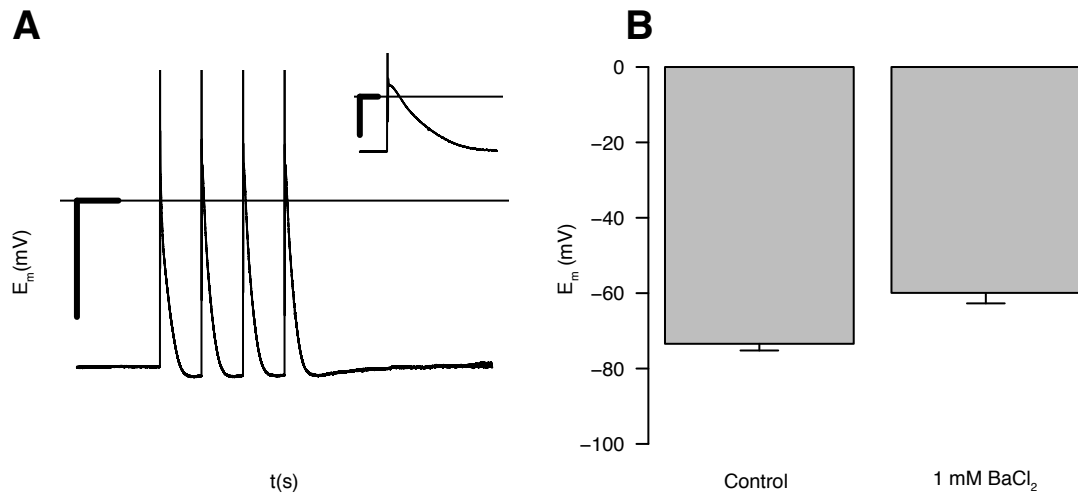


**Figure 7.4:** Action potentials and resting membrane potential of fetal CPC-derived cardiomyocytes. **A:** Representative recording of action potentials elicited by biphasic field stimulation, demonstrating excitability of the cardiomyocytes. In the absence of stimulation, resting membrane potential was stable. In the inset, an action potential is depicted at a smaller time scale. Horizontal scales: 1000 ms or 100 ms (inset). Vertical scale: 50 mV. **B:** Bar plot depicting the effect of infusion of 1 mM  $BaCl_2$  on mean resting membrane potential.

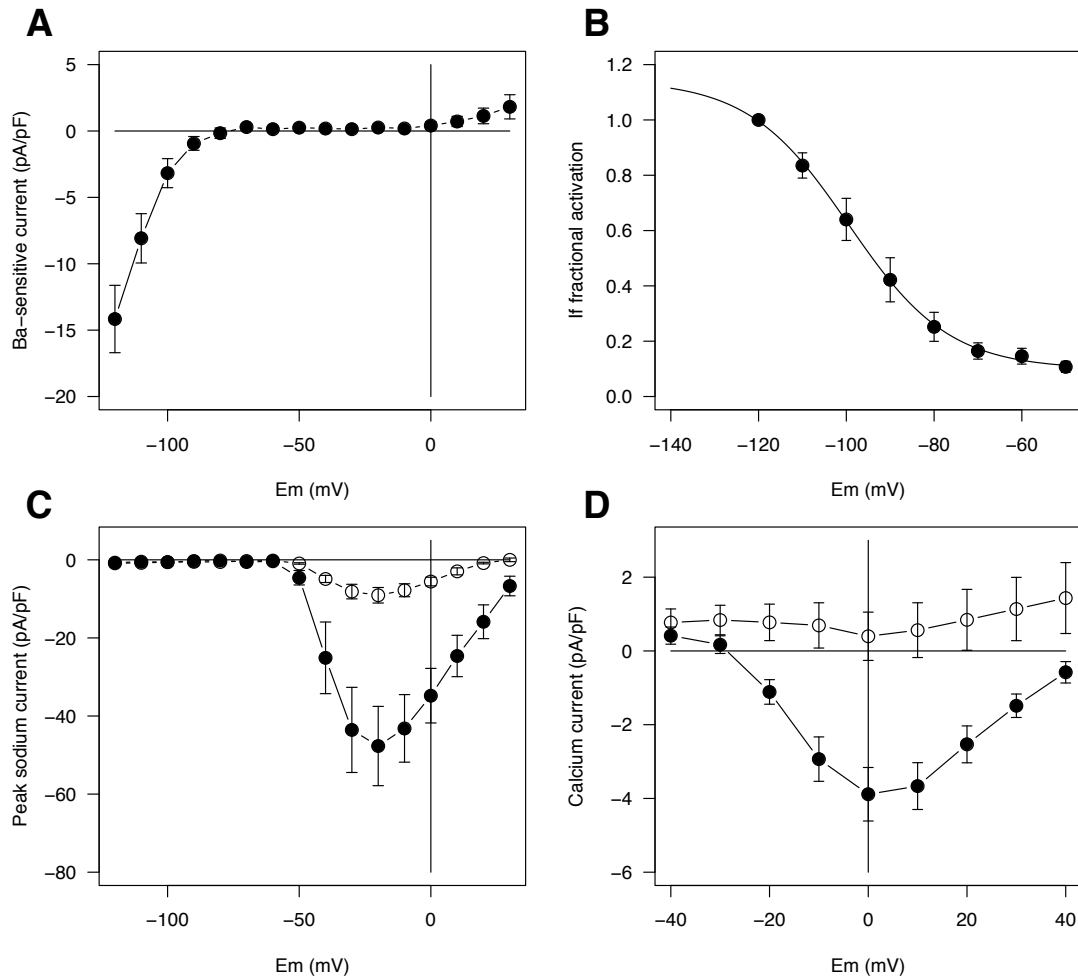


**Figure 7.5:** Voltage clamp experiments demonstrate large cardiac ion currents. **A:** CPC-derived cardiomyocytes expressed inward rectifying potassium currents ( $I_{K1}$ ). Plotted are barium-sensitive mean steady-state currents versus test potential. **B:** Plotting activation of hyperpolarization-activated current ( $I_f$ ) versus test potential revealed typical cardiac activation kinetics. **C:** Plot of mean peak sodium current ( $I_{Na}$ , closed symbols) versus test potential. The inward sodium currents could be partially blocked by application of  $10 \mu\text{M}$  TTX (open symbols). **D:** Mean peak inward calcium currents ( $I_{Ca,L}$ , closed symbols) plotted versus test potential. Application of  $10 \mu\text{M}$  nifedipine completely blocked the inward currents (open symbols), confirming that the currents were carried by the L-type calcium channel.

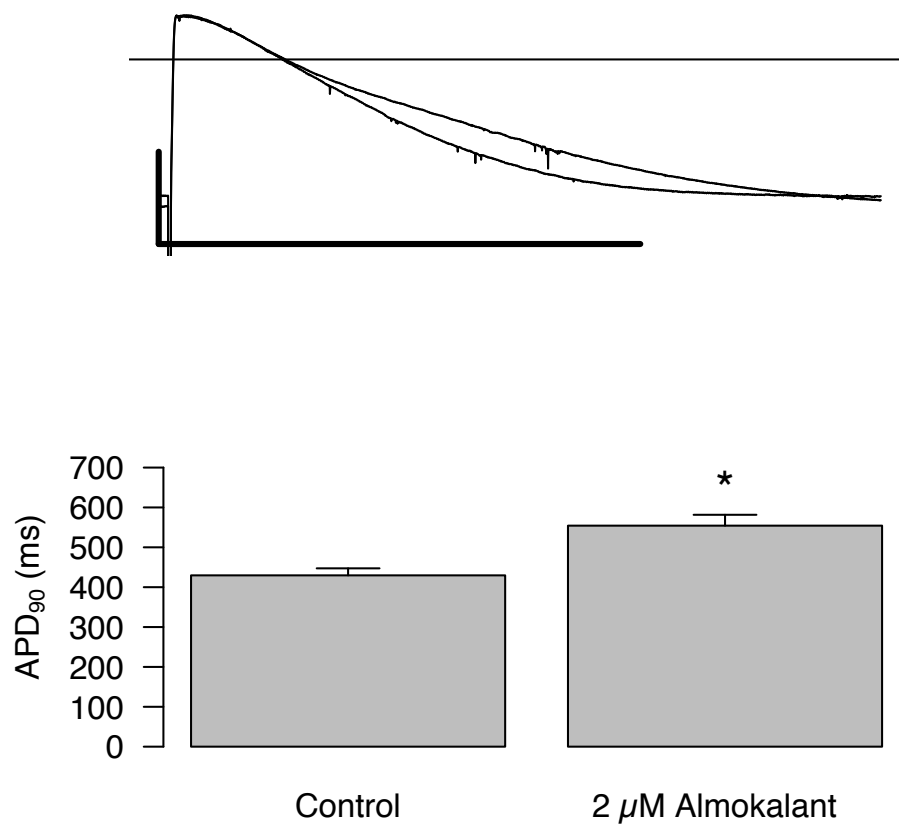


**Figure 7.6:** Infusion of almokalant to block  $I_{Kr}$  leads to prolongation of the action potentials. **A:** Typical recordings of action potentials recorded in absence and presence of 2  $\mu\text{M}$  almokalant. Vertical scale: 50 mV, horizontal scale: 500 ms. **B:** Bar graph depicting the effect of 2  $\mu\text{M}$  almokalant on mean APD<sub>90</sub>.



## **Chapter 8**

### **General discussion**

Teun P. de Boer

All chapters in this thesis center around the general theme, stem cells and their electrophysiological characteristics and capacity to induce pro-arrhythmia. A distinction can be made between chapters 1 to 4 and chapters 5 and 6. The first part of this thesis focusses on key aspects that are relevant to possible pro-arrhythmic effects of stem cell transplantation. An important factor in this context is intercellular coupling via gap junctions. Earlier studies by our group have implicated the transcription factor Snail1 in the regulation of connexin43 (the main cardiac connexin) expression in differentiating stem cells (76; 77).

Furthermore, spontaneous activity as observed in stem cell-derived cardiomyocytes is a clear indication of pro-arrhythmic potential. Studies by our group and others have demonstrated poor expression of the potassium inward rectifier current in stem cell-derived cardiomyocytes (32; 37; 36), suggesting that adding inward rectifying currents to stem cell-derived cardiomyocytes may control their pro-arrhythmic potential.

Both spontaneous activity and poor expression of connexin43 are reflections of the immature phenotype of stem cell-derived cardiomyocytes. Manipulation of Snail1 expression may help to enhance connexin43 expression and differentiation. The exposure to increasing levels of catecholamines during development exerts an important influence on maturing cardiomyocytes *in vivo*. It may be possible that adrenergic stimulation is also beneficial to differentiation of immature cardiomyocytes *in vitro*.

Evaluation of spontaneous activity and gap junctional communication between grafted cardiomyocytes and host myocardium is not feasible *in vivo*, therefore we devised an *in vitro* model that allowed us to integrate the key pro-arrhythmic aspects in an accessible model.

In the second part, we provide a description of a new human source for stem cell-derived cardiomyocytes, the human fetal cardiac progenitor cells. Given the fact that these cells originate from the heart, it is likely that they are committed to the mesodermal or cardiac lineage. We hypothesized that a better maturation of the cardiomyocytes can be achieved, leading to less spontaneous activity and a more robust expression of connexin43. In that case, human fetal cardiac progenitor cell-derived cardiomyocytes may have fewer pro-arrhythmic properties.

Differentiation of cardiomyocytes from embryonic stem cells recapitulates early cardiac development *in vivo*. One of the first steps in mesodermal differentiation is an epithelium-to-mesenchyme transition. In chapter 1, we have studied this process using two different embryonal carcinoma cell lines, F9 and P19. The main findings in this study were that connexin43 expression in embryonal carcinoma cells is repressed by the transcription factor Snail1, probably by direct interaction of Snail1 with E-box elements in the promoter of connexin43. siRNA experiments showed that reducing Snail1 expression leads to increased expression of connexin43 with a concomitant increase in functional coupling. Additionally, severe reduction of Snail1 induced a reverse EMT, since the mesenchymal mesodermal cells used in this experiments obtained an epithelial morphology. Whether upregulation of Snail1 is a common element in other EMTs during development is unclear, but it has recently been implicated in mesodermal differentiation of human embryonic stem cells. Ullmann et al. found that mesodermal specification is accompanied by downregulation of connexin43 and upregulation of the



transcription factors Snail and Slug (45). The position of Snail in the transcriptional network of differentiating stem cells is not fully understood. Possibly, an improved understanding of Snail and its up- and downstream partners will help to manipulate cardiac differentiation of stem cells *in vitro* in order to increase the expression of connexin43 and members of the cadherin family and thereby generate stem cell-derived cardiomyocytes that are better suited for transplantation strategies.

In chapter 2, we gave proof of concept of the possibility to control the beating frequency of spontaneously active cardiomyocytes by electrotonic application of  $I_{K1}$ . We demonstrated that beating frequency of neonatal rat cardiomyocyte cultures could be 'dose-dependently' modulated by co-culturing them with HEK-cells expressing Kir2.1 as increasing the fraction of co-cultured HEK cells decreased the beating frequency. Blocking  $I_{K1}$  conductance with barium partially tempered this suppressive effect. The concept described in chapter 2 bears relevance to application of biological pacemakers. Contemporary spontaneously active and immature cardiomyocytes express depolarizing currents, e.g. the sodium and calcium currents. However, they lack proper expression of the inward rectifier currents needed for stabilization of the membrane potential and control of automaticity. Therefore, inclusion of  $I_{K1}$ -expressing cells in populations of cells generated for transplantation may be necessary to temper the beating frequency and improve their usefulness. On the other side of the spectrum, our findings also permit to think about ways to quench ectopic foci in hearts of patients. Such foci can originate from changes in tissue architecture that alter conduction pathways, or are the result of increased automaticity. When present, these foci disturb the heart rhythm and pose a significant risk for the development of atrial or ventricular tachycardia. Currently applied techniques to treat patients involves resection of the focus, or radiofrequency ablation. Our study demonstrates that, in principle, transplantation of  $I_{K1}$  expressing cells can suppress the excess automaticity of the focus. This secondary finding, for which we coin the term biological ablation, will be subject of further investigation in our lab.

Release of adrenaline is a key factor of mammalian response to raised physiological demand, but is also involved in longterm processes. Both during maturation of the neonatal heart and in diseased adult hearts, changes in the levels of circulating catecholamines are accompanied by changes in the conduction velocity of the heart. In chapter 3 we studied the effect of persistent adrenergic stimulation on conduction in neonatal rat cardiomyocytes. Our primary finding was that  $\beta$ -adrenergic stimuli increase the impulse conduction velocity in geometrically defined cultures, while  $\alpha$ -adrenergic stimuli do not. Contrary to what has been reported by others, this could not be attributed to increased expression of connexin43. Instead, we observed increased expression of the cardiac sodium channel and even more of the L-type calcium channel (SCN5A and  $\alpha 1c$ , respectively) with a concomitant increase in upstroke velocity of the action potential. Based on our findings, it can be speculated that other immature heart cells, such as stem cell-derived cardiomyocytes, will respond in a similar way to adrenergic stimulation. In the context of immature cardiomyocytes, increased conduction velocity and expression of ion channels would constitute improved maturation. These data therefore suggest that adrenergic stimulation of cultured immature cardiomyocytes can further promote *in vitro* maturation. However, the cardiomyocytes in our study were exposed to adrenergic stimuli only for a limited time span. It can

not be excluded that further prolongation of exposure does elicit additional changes in intercellular coupling.

The study presented in chapter 4 focussed on the possible mechanism of pro-arrhythmia once immature spontaneously active cardiomyocytes are mixed with intrinsically quiescent adult cardiomyocytes. Using an *in vitro* model, we found that small clusters of immature cardiomyocytes are capable of pacing much larger, and normally quiescent, adult cardiomyocytes. This was shown to be facilitated by newly generated, but poor electrical coupling between the two cell types. Quantification of coupling efficiency and resting membrane potential was made possible by using our *in vitro* model. The modelling experiments allowed us to extrapolate these results to the tissue level. The outcome suggested that pro-arrhythmic consequences of implantation of a spontaneously active cluster in myocardium are determined by at least two factors, cluster size and level of electrical coupling between the cluster and myocardium. This is in line with the observations presented in the first three chapters of this thesis. Our findings underscore the necessity of sufficient functional expression of connexin43 in stem cell-derived cardiomyocytes. Furthermore they illustrate that cell replacement strategies should not promote clustering of grafted cells and that automaticity should be repressed. On the other hand, creation of a biological pacemaker is likely to benefit from such clustering and characteristics.

As outlined in the introduction to this thesis, thus far only embryonic stem cells have a well-established cardiogenic potential, while other, autologous, stem cells do not. Evidently, the availability of autologous stem cells capable of cardiac differentiation would be beneficial to clinical introduction of cell replacement therapies. In chapter 5, we provide evidence of the presence of cardiac progenitor cells in human fetal hearts. After isolation and proliferation, these cells can be differentiated with high efficiencies into cardiomyocytes *in vitro*. The electrophysiological properties of these cardiomyocytes are more mature than those of other stem cell-derived cardiomyocytes. If we apply our knowledge from the first part of this thesis, both the observed relatively negative resting membrane potential and high gap junctional conductances are likely to temper the pro-arrhythmic potential of these cells. The observation that beating frequency increases after addition of isoproterenol confirms that the cells are sensitive to  $\beta$ -adrenergic stimuli. It is possible that also cardiac progenitor cell-derived cardiomyocytes can be stimulated to mature further by persistent  $\beta$ -adrenergic stimuli.

While our findings constitute a major advance in terms of the amount of available cells and their phenotype, the use of fetal cardiac progenitor cells for clinical purposes is not ethically acceptable, as in case of human embryonic stem cells. In addition, application of both cell types will require immunosuppressive therapy. Therefore, isolation of cardiac progenitor cells from adult hearts will be more favourable. At present, adult cardiac progenitor cells are routinely isolated from human atrial appendages and current differentiation protocols yield large fractions of *in vitro* differentiated cardiomyocytes. Preliminary experiments in our lab have demonstrated an even more mature electrical phenotype than observed in fetal cardiac progenitor cell-derived cardiomyocytes. If these findings can be substantiated with more detailed electrophysiological data, human adult cardiac progenitor cells could be differentiated in the presence of autologous serum, which would bring clinical application within reach.

A further investigation of the electrophysiology of fetal cardiac progenitor cell-derived

cardiomyocytes is presented in chapter 6. Our data demonstrate presence of all major cardiac ion channels on the mRNA level, which results in expression of functional ion channels as determined by voltage clamp technique. The principal finding is that upon differentiation, fetal cardiac progenitor-derived cardiomyocytes express near adult levels of most ion channels. Compared to embryonic stem cell-derived cardiomyocytes, the most remarkable difference is the robust expression of  $I_{K1}$ , which is reflected in a rather negative resting membrane potential. Though we also recorded presence of  $I_f$ , no clear phase 4 depolarizations between action potentials were observed in the absence of serum. The fact that fetal cardiac progenitor cell-derived cardiomyocytes do display spontaneous activity when exposed to serum, may be attributable to activation of  $I_f$  by factors present in serum. Alternatively, serum components could inhibit  $I_{K1}$ , but in preliminary experiments we found no change in resting membrane potential in response to serum, suggesting that  $I_{K1}$  was not affected. If we reflect the properties of fetal cardiac progenitor cell-derived cardiomyocytes on the factors involved in pro-arrhythmia that we identified in the first part of this thesis, several points can be made. Firstly, the high levels of functional gap junction coupling observed may limit the risk of pro-arrhythmia. The gap junctional conductances reported in chapter 5 are comparable to the values reported for cultured adult dog cardiomyocytes in chapter 4. Robust expression of  $I_{K1}$  resulting in a rather negative resting membrane potential also decreases the likelihood of pro-arrhythmia. Their responsiveness to adrenergic stimulation will help to follow increasing heart rates during exercise. When compared to embryonic stem cell-derived cardiomyocytes that have a less negative membrane potential and poor expression of connexin43, a strong reduction in pro-arrhythmic potential can be expected. However, as with other cell types, it is possible that arrhythmias occur shortly after transplantation when intercellular coupling between graft and host is low and still developing. In preliminary experiments, injection of differentiated fetal cardiac progenitor cells into the AV-nodal region of one chronic AV-block dog resulted in a temporary change in ventricular activation and rhythm. The observed shift indicated activation from the injected region, but this was reversed to the initial pattern of AV-block when an ECG was recorded one week later. Telemetric experiments are required to further study the dynamics of changes in ECG morphology, but the observation might be explained by either loss of transplanted cells or the opposite, that the cells integrated well which caused them to be electrotonically silenced by surrounding cardiomyocytes.

Besides their potential in transplantation strategies, our characterization indicates that these cells can be regarded as a promising tool for pharmacological studies. The combination of highly efficient differentiation and near adult levels of ion current densities provides us with a homogenous human model that is more realistic than contemporary stem cell-based alternatives.

Conventional approaches to test drug effects on ion channels involve the use of adult cardiomyocytes that are isolated from dog or rodent hearts. Alternatively, cell lines expressing the ion channel of interest are used. Both methods have drawbacks, the first requires sacrifice of animals and resulting cardiomyocytes are obviously not human, thus may show responses different from those in human cells. The second option can be used to study human ion channels, but these may not be accompanied by their human, cardiac signalling partners. Using cardiac progenitor cell-derived cardiomyocytes, both limitations become irrelevant. Besides presence of the human ion channels, it is likely

that their cardiac signalling partners are also expressed even though this remains to be validated.

A common means to assess pro- or anti-arrhythmic properties of drugs is to determine the effect of a substance on the occurrence of early after depolarizations (EADs). EADs can be triggered in adult cells after creating susceptibility to development of EADs by decreasing their repolarization reserve with an  $I_{Kr}$  blocker or inducing depolarization by blocking  $I_{K1}$  with barium. Preliminary experiments have shown that cardiac progenitor cell-derived cardiomyocytes can also be pushed to develop EADs. This further increases the resemblance with adult cardiomyocytes and adds to their attractiveness as a model for drug testing.

The perspective of stem cell derived-cardiomyocytes in clinical applications is still difficult to foresee. Significant advances have been made in the past few years, but it appears that the first feasible application will not be cell replacement. In order to replace cardiomyocytes lost after myocardial infarction, enormous amounts of de novo generated cardiomyocytes are required. Moreover, these cardiomyocytes will have to be properly integrated in the host myocardium, which will only be possible after significant improvement of our tissue engineering skills. Therefore, it is more likely that biopacemaking will find its way to the clinic first. Generating spontaneously active cardiomyocytes is less problematic than generating quiescent cardiomyocytes and biopacemaking will only require a small fraction of the amount of cells required for cell replacement strategies. This smaller number of cells also decreases the complexity of tissue engineering involved. In the meantime, stem cells can help us to improve our understanding of cardiac differentiation. In that respect, especially cardiac progenitor cells are very intriguing. The mere presence of these cells in adult hearts raises questions about their purpose and about their role in cardiac physiology and pathophysiology. Regeneration of cardiac tissue in situ is possible in for instance zebrafish, so why not in mammalian hearts? Cardiac progenitor cells provide us with an excellent tool to search for factors that may induce in situ cardiac regeneration in patients. Besides  $TGF\beta$  signalling, one potential factor that has already been identified, preliminary experiments have demonstrated that hyperpolarization of undifferentiated fetal CPCs can induce differentiation, resulting in a more negative resting membrane potential and appearance of beating clusters. Since we have established that both undifferentiated and differentiated CPCs express high levels of connexin43, it is conceivable that CPCs can differentiate in vivo after coupling to adult cardiomyocytes. Following this line of reasoning, we probably need to induce both proliferation of resident CPCs and migration of the cells to infarcted regions in order to stimulate in situ regeneration.

One thing is beyond any doubt, stem cells will provide researchers all around the world with a subject that will keep renewing its appeal.

## Chapter 9

### Bibliography

- [1] Díaz, M.E., Graham, H.K., O'Neill, S.C., Trafford, A.W., and Eisner, D.A. *The control of sarcoplasmic reticulum Ca content in cardiac muscle*. *Cell Calcium*, 38(3-4):391–396, 2005.
- [2] Anderson, P.A. and Greenberg, R.M. *Phylogeny of ion channels: clues to structure and function*. *Comp Biochem Physiol B Biochem Mol Biol*, 129(1):17–28, 2001.
- [3] Söhl, G. and Willecke, K. *An update on connexin genes and their nomenclature in mouse and man*. *Cell Commun Adhes*, 10(4-6):173–180, 2003.
- [4] Coumel, P. *The management of clinical arrhythmias. an overview on invasive versus non-invasive electrophysiology*. *Eur Heart J*, 8(2):92–99, 1987.
- [5] Orlic, D., Kajstura, J., Chimenti, S., Jakoniuk, I., Anderson, S.M., Li, B., Pickel, J., McKay, R., Nadal-Ginard, B., Bodine, D.M., Leri, A., and Anversa, P. *Bone marrow cells regenerate infarcted myocardium*. *Nature*, 410(6829):701–705, 2001.
- [6] Murry, C.E., Soonpaa, M.H., Reinecke, H., Nakajima, H., Nakajima, H.O., Rubart, M., Pasumarthi, K.B., Virag, J.I., Bartelmez, S.H., Poppa, V., Bradford, G., Dowell, J.D., Williams, D.A., and Field, L.J. *Haematopoietic stem cells do not transdifferentiate into cardiac myocytes in myocardial infarcts*. *Nature*, 428(6983):664–668, 2004.
- [7] Laflamme, M.A. and Murry, C.E. *Regenerating the heart*. *Nat Biotechnol*, 23(7):845–856, 2005.
- [8] Ziegelhoeffer, T., Fernandez, B., Kostin, S., Heil, M., Voswinckel, R., Helisch, A., and Schaper, W. *Bone marrow-derived cells do not incorporate into the adult growing vasculature*. *Circ Res*, 94(2):230–238, 2004.
- [9] Hagege, A.A., Marolleau, J.P., Vilquin, J.T., Alhéritière, A., Peyrard, S., Duboc, D., Abergel, E., Messas, E., Mousseaux, E., Schwartz, K., Desnos, M., and Menasché, P. *Skeletal myoblast transplantation in ischemic heart failure: long-term follow-up of the first phase I cohort of patients*. *Circulation*, 114(1 Suppl):108–113, 2006.
- [10] Dib, N., Michler, R.E., Pagani, F.D., Wright, S., Kereiakes, D.J., Lengerich, R., Binkley, P., Buchele, D., Anand, I., Swingen, C., Di Carli, M.F., Thomas, J.D., Jaber, W.A., Opie, S.R., Campbell, A., McCarthy, P., Yeager, M., Dilsizian, V., Griffith, B.P., Korn, R., Kreuger, S.K., Ghazoul, M., MacLellan, W.R., Fonarow, G., Eisen, H.J., Dinsmore, J., and Diethrich, E. *Safety and feasibility of autologous myoblast transplantation in patients with ischemic cardiomyopathy: four-year follow-up*. *Circulation*, 112(12):1748–1755, 2005.

- [11] Menasché, P., Hagège, A.A., Vilquin, J.T., Desnos, M., Abergel, E., Pouzet, B., Bel, A., Sarateanu, S., Scorsin, M., Schwartz, K., Bruneval, P., Benbunan, M., Marolleau, J.P., and Duboc, D. *Autologous skeletal myoblast transplantation for severe postinfarction left ventricular dysfunction*. *J Am Coll Cardiol*, 41(7):1078–1083, 2003.
- [12] Smits, P.C., van Geuns, R.J., Poldermans, D., Bountiukos, M., Onderwater, E.E., Lee, C.H., Maat, A.P., and Serruys, P.W. *Catheter-based intramyocardial injection of autologous skeletal myoblasts as a primary treatment of ischemic heart failure: clinical experience with six-month follow-up*. *J Am Coll Cardiol*, 42(12):2063–2069, 2003.
- [13] He, J.Q., Ma, Y., Lee, Y., Thomson, J.A., and Kamp, T.J. *Human embryonic stem cells develop into multiple types of cardiac myocytes: action potential characterization*. *Circ Res*, 93(1):32–39, 2003.
- [14] Mummery, C., Ward, D., van den Brink, C.E., Bird, S.D., Doevendans, P.A., Opthof, T., Brutel de la Riviere, A., Tertoolen, L., van der Heyden, M., and Pera, M. *Cardiomyocyte differentiation of mouse and human embryonic stem cells*. *J Anat*, 200(Pt 3):233–242, 2002.
- [15] Mummery, C., Ward-van Oostwaard, D., Doevendans, P., Spijker, R., van den Brink, S., Hassink, R., van der Heyden, M., Opthof, T., Pera, M., de la Riviere, A.B., Passier, R., and Tertoolen, L. *Differentiation of human embryonic stem cells to cardiomyocytes: role of coculture with visceral endoderm-like cells*. *Circulation*, 107(21):2733–2740, 2003.
- [16] Kehat, I., Khimovich, L., Caspi, O., Gepstein, A., Shofti, R., Arbel, G., Huber, I., Satin, J., Itskovitz-Eldor, J., and Gepstein, L. *Electromechanical integration of cardiomyocytes derived from human embryonic stem cells*. *Nat Biotechnol*, 22(10):1282–1289, 2004.
- [17] Hodgson, D.M., Behfar, A., Zingman, L.V., Kane, G.C., Perez-Terzic, C., Alekseev, A.E., Pucéat, M., and Terzic, A. *Stable benefit of embryonic stem cell therapy in myocardial infarction*. *Am J Physiol Heart Circ Physiol*, 287(2):471–479, 2004.
- [18] Swijnenburg, R.J., Tanaka, M., Vogel, H., Baker, J., Kofidis, T., Gunawan, F., Lebl, D.R., Caffarelli, A.D., de Bruin, J.L., Fedoseyeva, E.V., and Robbins, R.C. *Embryonic stem cell immunogenicity increases upon differentiation after transplantation into ischemic myocardium*. *Circulation*, 112(9 Suppl):166–172, 2005.
- [19] Nussbaum, J., Minami, E., Laflamme, M.A., Virag, J.A., Ware, C.B., Masino, A., Muskheli, V., Pabon, L., Reinecke, H., and Murry, C.E. *Transplantation of undifferentiated murine embryonic stem cells in the heart: teratoma formation and immune response*. *FASEB J*, 21(7):1345–1357, 2007.
- [20] Kolossov, E., Bostani, T., Roell, W., Breitbach, M., Pillekamp, F., Nygren, J.M., Sasse, P., Rubenchik, O., Fries, J.W., Wenzel, D., Geisen, C., Xia, Y., Lu, Z., Duan, Y., Kettenhofen, R., Jovinge, S., Bloch, W., Bohlen, H., Welz, A., Hescheler, J., Jacobsen, S.E., and Fleischmann, B.K. *Engraftment of engineered es cell-derived cardiomyocytes but not bm cells restores contractile function to the infarcted myocardium*. *J Exp Med*, 203(10):2315–2327, 2006.
- [21] Christman, K.L. and Lee, R.J. *Biomaterials for the treatment of myocardial infarction*. *J Am Coll Cardiol*, 48(5):907–913, 2006.
- [22] Leor, J., Aboulafia-Etzion, S., Dar, A., Shapiro, L., Barbash, I.M., Battler, A., Granot, Y., and Cohen, S. *Bioengineered cardiac grafts: A new approach to repair the infarcted myocardium?* *Circulation*, 102(19 Suppl 3):III56–61, 2000.
- [23] Zimmermann, W.H., Melnychenko, I., Wasmeier, G., Didie, M., Naito, H., Nixdorff, U., Hess, A., Budinsky, L., Brune, K., Michaelis, B., Dhein, S., Schwoerer, A., Ehmke, H., and Eschenhagen, T. *Engineered heart tissue grafts improve systolic and diastolic function in infarcted rat hearts*. *Nat Med*, 12(4):452–458, 2006.

- [24] Huang, N.F., Yu, J., Sievers, R., Li, S., and Lee, R.J. *Injectable biopolymers enhance angiogenesis after myocardial infarction*. *Tissue Eng*, 11(11-12):1860–1866, 2005.
- [25] Christman, K.L., Vardanian, A.J., Fang, Q., Sievers, R.E., Fok, H.H., and Lee, R.J. *Injectable fibrin scaffold improves cell transplant survival, reduces infarct expansion, and induces neovasculature formation in ischemic myocardium*. *J Am Coll Cardiol*, 44(3):654–660, 2004.
- [26] Kofidis, T., Lebl, D.R., Martinez, E.C., Hoyt, G., Tanaka, M., and Robbins, R.C. *Novel injectable bioartificial tissue facilitates targeted, less invasive, large-scale tissue restoration on the beating heart after myocardial injury*. *Circulation*, 112(9 Suppl):1173–7, 2005.
- [27] Zhang, P., Zhang, H., Wang, H., Wei, Y., and Hu, S. *Artificial matrix helps neonatal cardiomyocytes restore injured myocardium in rats*. *Artif Organs*, 30(2):86–93, 2006.
- [28] Rubart, M., Soonpaa, M.H., Nakajima, H., and Field, L.J. *Spontaneous and evoked intracellular calcium transients in donor-derived myocytes following intracardiac myoblast transplantation*. *J Clin Invest*, 114(6):775–783, 2004.
- [29] Xue, T., Cho, H.C., Akar, F.G., Tsang, S.Y., Jones, S.P., Marbán, E., Tomaselli, G.F., and Li, R.A. *Functional integration of electrically active cardiac derivatives from genetically engineered human embryonic stem cells with quiescent recipient ventricular cardiomyocytes: insights into the development of cell-based pacemakers*. *Circulation*, 111(1):11–20, 2005.
- [30] Maltsev, V.A., Wobus, A.M., Rohwedel, J., Bader, M., and Hescheler, J. *Cardiomyocytes differentiated in vitro from embryonic stem cells developmentally express cardiac-specific genes and ionic currents*. *Circ Res*, 75(2):233–244, 1994.
- [31] Fijnvandraat, A.C., van Ginneken, A.C., Schumacher, C.A., Boheler, K.R., Lekanne Deprez, R.H., Christoffels, V.M., and Moorman, A.F. *Cardiomyocytes purified from differentiated embryonic stem cells exhibit characteristics of early chamber myocardium*. *J Mol Cell Cardiol*, 35(12):1461–1472, 2003.
- [32] van der Heyden, M.A., van Kempen, M.J., Tsuji, Y., Rook, M.B., Jongsma, H.J., and Opthof, T. *P19 embryonal carcinoma cells: a suitable model system for cardiac electrophysiological differentiation at the molecular and functional level*. *Cardiovasc Res*, 58(2):410–422, 2003.
- [33] Hescheler, J., Fleischmann, B.K., Lentini, S., Maltsev, V.A., Rohwedel, J., Wobus, A.M., and Adicks, K. *Embryonic stem cells: a model to study structural and functional properties in cardiomyogenesis*. *Cardiovasc Res*, 36(2):149–162, 1997.
- [34] van der Heyden, M.A. and Defize, L.H. *Twenty one years of p19 cells: what an embryonal carcinoma cell line taught us about cardiomyocyte differentiation*. *Cardiovasc Res*, 58(2):292–302, 2003.
- [35] Wang, K., Xue, T., Tsang, S.Y., Van Huizen, R., Wong, C.W., Lai, K.W., Ye, Z., Cheng, L., Au, K.W., Zhang, J., Li, G.R., Lau, C.P., Tse, H.F., and Li, R.A. *Electrophysiological properties of pluripotent human and mouse embryonic stem cells*. *Stem Cells*, 23(10):1526–1534, 2005.
- [36] Sartiani, L., Bettioli, E., Stillitano, F., Mugelli, A., Cerbai, E., and Jaconi, M.E. *Developmental changes in cardiomyocytes differentiated from human embryonic stem cells: a molecular and electrophysiological approach*. *Stem Cells*, 25(5):1136–1144, 2007.
- [37] Satin, J., Kehat, I., Caspi, O., Huber, I., Arbel, G., Itzhaki, I., Magyar, J., Schroder, E.A., Perlman, I., and Gepstein, L. *Mechanism of spontaneous excitability in human embryonic stem cell derived cardiomyocytes*. *J Physiol*, 559(Pt 2):479–496, 2004.
- [38] Dolnikov, K., Shilkrut, M., Zeevi-Levin, N., Gerech-Nir, S., Amit, M., Danon, A., Itskovitz-Eldor, J., and Binah, O. *Functional properties of human embryonic stem cell-derived cardiomyocytes: intracellular  $Ca^{2+}$  handling and the role of sarcoplasmic reticulum in the contraction*. *Stem Cells*, 24(2):236–245, 2006.

- [39] Oyamada, Y., Komatsu, K., Kimura, H., Mori, M., and Oyamada, M. *Differential regulation of gap junction protein (connexin) genes during cardiomyocytic differentiation of mouse embryonic stem cells in vitro*. *Exp Cell Res*, 229(2):318–326, 1996.
- [40] Bhattacharya, B., Miura, T., Brandenberger, R., Mejido, J., Luo, Y., Yang, A.X., Joshi, B.H., Ginis, I., Thies, R.S., Amit, M., Lyons, I., Condie, B.G., Itskovitz-Eldor, J., Rao, M.S., and Puri, R.K. *Gene expression in human embryonic stem cell lines: unique molecular signature*. *Blood*, 103(8):2956–2964, 2004.
- [41] Wong, R.C., Dottori, M., Koh, K.L., Nguyen, L.T., Pera, M.F., and Pébay, A. *Gap junctions modulate apoptosis and colony growth of human embryonic stem cells maintained in a serum-free system*. *Biochem Biophys Res Commun*, 344(1):181–188, 2006.
- [42] Cui, L., Johkura, K., Takei, S., Ogiwara, N., and Sasaki, K. *Structural differentiation, proliferation, and association of human embryonic stem cell-derived cardiomyocytes in vitro and in their extracardiac tissues*. *J Struct Biol*, 158(3):307–317, 2007.
- [43] Baharvand, H., Ashtiani, S.K., Taei, A., Massumi, M., Valojerdi, M.R., Yazdi, P.E., Moradi, S.Z., and Farrokhi, A. *Generation of new human embryonic stem cell lines with diploid and triploid karyotypes*. *Dev Growth Differ*, 48(2):117–128, 2006.
- [44] Huettner, J.E., Lu, A., Qu, Y., Wu, Y., Kim, M., and McDonald, J.W. *Gap junctions and connexon hemichannels in human embryonic stem cells*. *Stem Cells*, 24(7):1654–1667, 2006.
- [45] Ullmann, U., In't Veld, P., Gilles, C., Sermon, K., De Rycke, M., Van de Velde, H., Van Steirteghem, A., and Liebaers, I. *Epithelial-mesenchymal transition process in human embryonic stem cells cultured in feeder-free conditions*. *Mol Hum Reprod*, 13(1):21–32, 2007.
- [46] Kehat, I., Gepstein, A., Spira, A., Itskovitz-Eldor, J., and Gepstein, L. *High-resolution electrophysiological assessment of human embryonic stem cell-derived cardiomyocytes: a novel in vitro model for the study of conduction*. *Circ Res*, 91(8):659–661, 2002.
- [47] Dolnikov, K., Shilkrut, M., Zeevi-Levin, N., Danon, A., Gerech-Nir, S., Itskovitz-Eldor, J., and Binah, O. *Functional properties of human embryonic stem cell-derived cardiomyocytes*. *Ann N Y Acad Sci*, 1047:66–75, 2005.
- [48] Marbán, E. and Cho, H.C. *Creation of a biological pacemaker by gene- or cell-based approaches*. *Med Biol Eng Comput*, 2007.
- [49] Chang, M.G., Tung, L., Sekar, R.B., Chang, C.Y., Cysyk, J., Dong, P., Marban, E., and Abraham, M.R. *Proarrhythmic potential of mesenchymal stem cell transplantation revealed in an in vitro coculture model*. *Circulation*, 113(15):1832–1841, 2006.
- [50] Beeres, S.L., Atsma, D.E., van der Laarse, A., Pijnappels, D.A., van Tuyn, J., Fibbe, W.E., de Vries, A.A., Ypey, D.L., van der Wall, E.E., and Schalij, M.J. *Human adult bone marrow mesenchymal stem cells repair experimental conduction block in rat cardiomyocyte cultures*. *J Am Coll Cardiol*, 46(10):1943–1952, 2005.
- [51] Pijnappels, D.A., Schalij, M.J., van Tuyn, J., Ypey, D.L., de Vries, A.A., van der Wall, E.E., van der Laarse, A., and Atsma, D.E. *Progressive increase in conduction velocity across human mesenchymal stem cells is mediated by enhanced electrical coupling*. *Cardiovasc Res*, 72(2):282–291, 2006.
- [52] Beeres, S.L., Zeppenfeld, K., Bax, J.J., Dibbets-Schneider, P., Stokkel, M.P., Fibbe, W.E., van der Wall, E.E., Atsma, D.E., and Schalij, M.J. *Electrophysiological and arrhythmogenic effects of intramyocardial bone marrow cell injection in patients with chronic ischemic heart disease*. *Heart Rhythm*, 4(3):257–265, 2007.



- [53] Abraham, M.R., Henrikson, C.A., Tung, L., Chang, M.G., Aon, M., Xue, T., Li, R.A., O' Rourke, B., and Marbán, E. *Antiarrhythmic engineering of skeletal myoblasts for cardiac transplantation*. *Circ Res*, 97(2):159–167, 2005.
- [54] Fouts, K., Fernandes, B., Mal, N., Liu, J., and Laurita, K.R. *Electrophysiological consequence of skeletal myoblast transplantation in normal and infarcted canine myocardium*. *Heart Rhythm*, 3(4):452–461, 2006.
- [55] Saez, J.C., Berthoud, V.M., Branes, M.C., Martinez, A.D., and Beyer, E.C. *Plasma membrane channels formed by connexins: their regulation and functions*. *Physiol Rev*, 83(4):1359–1400, 2003.
- [56] Stout, C., Goodenough, D.A., and Paul, D.L. *Connexins: functions without junctions*. *Curr Opin Cell Biol*, 16(5):507–512, 2004.
- [57] Wei, C.J., Xu, X., and Lo, C.W. *Connexins and cell signaling in development and disease*. *Annu Rev Cell Dev Biol*, 20:811–838, 2004.
- [58] Jongen, W.M., Fitzgerald, D.J., Asamoto, M., Piccoli, C., Slaga, T.J., Gros, D., Takeichi, M., and Yamasaki, H. *Regulation of connexin 43-mediated gap junctional intercellular communication by  $ca_2^+$  in mouse epidermal cells is controlled by e-cadherin*. *J Cell Biol*, 114(3):545–555, 1991.
- [59] Ohsugi, M., Larue, L., Schwarz, H., and Kemler, R. *Cell-junctional and cytoskeletal organization in mouse blastocysts lacking e-cadherin*. *Dev Biol*, 185(2):261–271, 1997.
- [60] Giepmans, B.N. *Gap junctions and connexin-interacting proteins*. *Cardiovasc Res*, 62(2):233–245, 2004.
- [61] Wong, R.C., Pébay, A., Nguyen, L.T., Koh, K.L., and Pera, M.F. *Presence of functional gap junctions in human embryonic stem cells*. *Stem Cells*, 22(6):883–889, 2004.
- [62] van Kempen, M., van Ginneken, A., de Grijis, I., Mutsaers, N., Opthof, T., Jongasma, H., and van der Heyden, M. *Expression of the electrophysiological system during murine embryonic stem cell cardiac differentiation*. *Cell Physiol Biochem*, 13(5):263–270, 2003.
- [63] van der Heyden, M.A., Rook, M.B., Hermans, M.M., Rijksen, G., Boonstra, J., Defize, L.H., and Destrée, O.H. *Identification of connexin43 as a functional target for wnt signalling*. *J Cell Sci*, 111 ( Pt 12):1741–1749, 1998.
- [64] Boheler, K.R., Czyz, J., Tweedie, D., Yang, H.T., Anisimov, S.V., and Wobus, A.M. *Differentiation of pluripotent embryonic stem cells into cardiomyocytes*. *Circ Res*, 91(3):189–201, 2002.
- [65] van Kempen, M.J., Fromaget, C., Gros, D., Moorman, A.F., and Lamers, W.H. *Spatial distribution of connexin43, the major cardiac gap junction protein, in the developing and adult rat heart*. *Circ Res*, 68(6):1638–1651, 1991.
- [66] Van Kempen, M.J., Vermeulen, J.L., Moorman, A.F., Gros, D., Paul, D.L., and Lamers, W.H. *Developmental changes of connexin40 and connexin43 mrna distribution patterns in the rat heart*. *Cardiovasc Res*, 32(5):886–900, 1996.
- [67] Delorme, B., Dahl, E., Jarry-Guichard, T., Briand, J.P., Willecke, K., Gros, D., and Théveniau-Ruissy, M. *Expression pattern of connexin gene products at the early developmental stages of the mouse cardiovascular system*. *Circ Res*, 81(3):423–437, 1997.
- [68] Weitzer, G. *Embryonic stem cell-derived embryoid bodies: an in vitro model of eutherian pregastrulation development and early gastrulation.*, volume 174 of *Handbook of Experimental Pharmacology*. Springer, 2006.

- [69] Behr, R., Heneweer, C., Viebahn, C., Denker, H.W., and Thie, M. *Epithelial-mesenchymal transition in colonies of rhesus monkey embryonic stem cells: a model for processes involved in gastrulation*. *Stem Cells*, 23(6):805–816, 2005.
- [70] Thiery, J.P. *Epithelial-mesenchymal transitions in development and pathologies*. *Curr Opin Cell Biol*, 15(6):740–746, 2003.
- [71] Barrallo-Gimeno, A. and Nieto, M.A. *The snail genes as inducers of cell movement and survival: implications in development and cancer*. *Development*, 132(14):3151–3161, 2005.
- [72] Radisky, D.C. *Epithelial-mesenchymal transition*. *J Cell Sci*, 118(Pt 19):4325–4326, 2005.
- [73] Cano, A., Pérez-Moreno, M.A., Rodrigo, I., Locascio, A., Blanco, M.J., del Barrio, M.G., Portillo, F., and Nieto, M.A. *The transcription factor snail controls epithelial-mesenchymal transitions by repressing e-cadherin expression*. *Nat Cell Biol*, 2(2):76–83, 2000.
- [74] Ikenouchi, J., Matsuda, M., Furuse, M., and Tsukita, S. *Regulation of tight junctions during the epithelium-mesenchyme transition: direct repression of the gene expression of claudins/occludin by snail*. *J Cell Sci*, 116(Pt 10):1959–1967, 2003.
- [75] Vandewalle, C., Comijn, J., De Craene, B., Vermassen, P., Bruyneel, E., Andersen, H., Tulchinsky, E., Van Roy, F., and Berx, G. *Sip1/zeb2 induces emt by repressing genes of different epithelial cell-cell junctions*. *Nucleic Acids Res*, 33(20):6566–6578, 2005.
- [76] van der Heyden, M.A., Veltmaat, J.M., Hendriks, J.A., Destrée, O.H., and Defize, L.H. *Dynamic connexin43 expression and gap junctional communication during endoderm differentiation of f9 embryonal carcinoma cells*. *Eur J Cell Biol*, 79(4):272–282, 2000.
- [77] Veltmaat, J.M., Orelia, C.C., Ward-Van Oostwaard, D., Van Rooijen, M.A., Mummery, C.L., and Defize, L.H. *Snail is an immediate early target gene of parathyroid hormone related peptide signaling in parietal endoderm formation*. *Int J Dev Biol*, 44(3):297–307, 2000.
- [78] Mummery, C.L., Feijen, A., van der Saag, P.T., van den Brink, C.E., and de Laat, S.W. *Clonal variants of differentiated p19 embryonal carcinoma cells exhibit epidermal growth factor receptor kinase activity*. *Dev Biol*, 109(2):402–410, 1985.
- [79] Mummery, C.L., Feijen, A., Moolenaar, W.H., van den Brink, C.E., and de Laat, S.W. *Establishment of a differentiated mesodermal line from p19 ec cells expressing functional pdgf and egf receptors*. *Exp Cell Res*, 165(1):229–242, 1986.
- [80] Berstine, E.G., Hooper, M.L., Grandchamp, S., and Ephrussi, B. *Alkaline phosphatase activity in mouse teratoma*. *Proc Natl Acad Sci U S A*, 70(12):3899–3903, 1973.
- [81] R Development Core Team. *R: A Language and Environment for Statistical Computing*. R Foundation for Statistical Computing, Vienna, Austria, 2006.
- [82] van de Wetering, M., Oving, I., Muncan, V., Pon Fong, M.T., Brantjes, H., van Leenen, D., Holstege, F.C., Brummelkamp, T.R., Agami, R., and Clevers, H. *Specific inhibition of gene expression using a stably integrated, inducible small-interfering-rna vector*. *EMBO Rep*, 4(6):609–615, 2003.
- [83] Pfeifer, I., Anderson, C., Werner, R., and Oltra, E. *Redefining the structure of the mouse connexin43 gene: selective promoter usage and alternative splicing mechanisms yield transcripts with different translational efficiencies*. *Nucleic Acids Res*, 32(15):4550–4562, 2004.
- [84] Batlle, E., Sancho, E., Francí, C., Domínguez, D., Monfar, M., Baulida, J., and García De Herreros, A. *The transcription factor snail is a repressor of e-cadherin gene expression in epithelial tumour cells*. *Nat Cell Biol*, 2(2):84–89, 2000.

- [85] Kalimi, G.H. and Lo, C.W. *Communication compartments in the gastrulating mouse embryo*. *J Cell Biol*, 107(1):241–255, 1988.
- [86] Kalimi, G.H. and Lo, C.W. *Gap junctional communication in the extraembryonic tissues of the gastrulating mouse embryo*. *J Cell Biol*, 109(6 Pt 1):3015–3026, 1989.
- [87] Dahl, E., Winterhager, E., Reuss, B., Traub, O., Butterweck, A., and Willecke, K. *Expression of the gap junction proteins connexin31 and connexin43 correlates with communication compartments in extraembryonic tissues and in the gastrulating mouse embryo, respectively*. *J Cell Sci*, 109 ( Pt 1):191–197, 1996.
- [88] Wang, Y. and Rose, B. *An inhibition of gap-junctional communication by cadherins*. *J Cell Sci*, 110 ( Pt 3):301–309, 1997.
- [89] Fujimoto, K., Nagafuchi, A., Tsukita, S., Kuraoka, A., Ohokuma, A., and Shibata, Y. *Dynamics of connexins, e-cadherin and  $\alpha$ -catenin on cell membranes during gap junction formation*. *J Cell Sci*, 110 ( Pt 3):311–322, 1997.
- [90] Boyett, M.R., Honjo, H., and Kodama, I. *The sinoatrial node, a heterogeneous pacemaker structure*. *Cardiovasc Res*, 47(4):658–687, 2000.
- [91] Sato, R. and Koumi, S. *Modulation of the inwardly rectifying  $k^+$  channel in isolated human atrial myocytes by  $\alpha_1$ -adrenergic stimulation*. *J Membr Biol*, 148(2):185–191, 1995.
- [92] Dhamoon, A.S. and Jalife, J. *The inward rectifier current ( $i_{K1}$ ) controls cardiac excitability and is involved in arrhythmogenesis*. *Heart Rhythm*, 2(3):316–324, 2005.
- [93] Zaritsky, J.J., Redell, J.B., Tempel, B.L., and Schwarz, T.L. *The consequences of disrupting cardiac inwardly rectifying  $k^+$  current ( $i_{K1}$ ) as revealed by the targeted deletion of the murine kir2.1 and kir2.2 genes*. *J Physiol*, 533(Pt 3):697–710, 2001.
- [94] Raab-Graham, K.F. and Vandenberg, C.A. *Tetrameric subunit structure of the native brain inwardly rectifying potassium channel kir 2.2*. *J Biol Chem*, 273(31):19699–19707, 1998.
- [95] Zobel, C., Cho, H.C., Nguyen, T.T., Pekhletski, R., Diaz, R.J., Wilson, G.J., and Backx, P.H. *Molecular dissection of the inward rectifier potassium current ( $i_{K1}$ ) in rabbit cardiomyocytes: evidence for heteromeric co-assembly of kir2.1 and kir2.2*. *J Physiol*, 550(Pt 2):365–372, 2003.
- [96] McLerie, M., Lopatin, A.N., and Lopatin, A. *Dominant-negative suppression of  $i_{K1}$  in the mouse heart leads to altered cardiac excitability*. *J Mol Cell Cardiol*, 35(4):367–378, 2003.
- [97] Li, J., McLerie, M., and Lopatin, A.N. *Transgenic upregulation of  $i_{K1}$  in the mouse heart leads to multiple abnormalities of cardiac excitability*. *Am J Physiol Heart Circ Physiol*, 287(6):2790–2802, 2004.
- [98] Plaster, N.M., Tawil, R., Tristani-Firouzi, M., Canún, S., Bendahhou, S., Tsunoda, A., Donaldson, M.R., Iannaccone, S.T., Brunt, E., Barohn, R., Clark, J., Deymeer, F., George, A.L., Fish, F.A., Hahn, A., Nitu, A., Ozdemir, C., Serdaroglu, P., Subramony, S.H., Wolfe, G., Fu, Y.H., and Ptáček, L.J. *Mutations in kir2.1 cause the developmental and episodic electrical phenotypes of andersen's syndrome*. *Cell*, 105(4):511–519, 2001.
- [99] Tristani-Firouzi, M., Jensen, J.L., Donaldson, M.R., Sansone, V., Meola, G., Hahn, A., Bendahhou, S., Kwiecinski, H., Fidzianska, A., Plaster, N., Fu, Y.H., Ptacek, L.J., and Tawil, R. *Functional and clinical characterization of kcnj2 mutations associated with lqt7 (andersen syndrome)*. *J Clin Invest*, 110(3):381–388, 2002.
- [100] Miake, J., Marbán, E., and Nuss, H.B. *Biological pacemaker created by gene transfer*. *Nature*, 419(6903):132–133, 2002.

- [101] Potapova, I., Plotnikov, A., Lu, Z., Danilo, P., Valiunas, V., Qu, J., Doronin, S., Zuckerman, J., Shlapakova, I.N., Gao, J., Pan, Z., Herron, A.J., Robinson, R.B., Brink, P.R., Rosen, M.R., and Cohen, I.S. *Human mesenchymal stem cells as a gene delivery system to create cardiac pacemakers. Circ Res*, 94(7):952–959, 2004.
- [102] Teunissen, B.E., van Amersfoort, S.C., Opthof, T., Jongasma, H.J., and Bierhuizen, M.F. *Sp1 and sp3 activate the rat connexin40 proximal promoter. Biochem Biophys Res Commun*, 292(1):71–78, 2002.
- [103] Lange, P.S., Er, F., Gassanov, N., and Hoppe, U.C. *Andersen mutations of kcnj2 suppress the native inward rectifier current  $i_{K1}$  in a dominant-negative fashion. Cardiovasc Res*, 59(2):321–327, 2003.
- [104] Masuda, H. and Sperelakis, N. *Inwardly rectifying potassium current in rat fetal and neonatal ventricular cardiomyocytes. Am J Physiol*, 265(4 Pt 2):1107–1111, 1993.
- [105] Schram, G., Melnyk, P., Pourrier, M., Wang, Z., and Nattel, S. *Kir2.4 and kir2.1  $k^+$  channel subunits co-assemble: a potential new contributor to inward rectifier current heterogeneity. J Physiol*, 544(Pt 2):337–349, 2002.
- [106] Koumi, S., Backer, C.L., Arentzen, C.E., and Sato, R.  *$\beta$ -adrenergic modulation of the inwardly rectifying potassium channel in isolated human ventricular myocytes. alteration in channel response to  $\beta$ -adrenergic stimulation in failing human hearts. J Clin Invest*, 96(6):2870–2881, 1995.
- [107] Panama, B.K. and Lopatin, A.N. *Differential polyamine sensitivity in inwardly rectifying kir2 potassium channels. J Physiol*, 571(Pt 2):287–302, 2006.
- [108] Takano, M. and Kuratomi, S. *Regulation of cardiac inwardly rectifying potassium channels by membrane lipid metabolism. Prog Biophys Mol Biol*, 81(1):67–79, 2003.
- [109] Xie, L.H., John, S.A., Ribalet, B., and Weiss, J.N. *Long polyamines act as cofactors in pip2 activation of inward rectifier potassium (kir2.1) channels. J Gen Physiol*, 126(6):541–549, 2005.
- [110] Harvey, D.M. and Caskey, C.T. *Inducible control of gene expression: prospects for gene therapy. Curr Opin Chem Biol*, 2(4):512–518, 1998.
- [111] Renick, S.E., Seidler, F.J., McCook, E.C., and Slotkin, T.A. *Neuronal control of cardiac and hepatic macromolecule synthesis in the neonatal rat: effects of sympathectomy. Pediatr Res*, 41(3):359–363, 1997.
- [112] Claycomb, W.C. *Biochemical aspects of cardiac muscle differentiation. possible control of deoxyribonucleic acid synthesis and cell differentiation by adrenergic innervation and cyclic adenosine 3':5'-monophosphate. J Biol Chem*, 251(19):6082–6089, 1976.
- [113] Vaidya, D., Tamaddon, H.S., Lo, C.W., Taffet, S.M., Delmar, M., Morley, G.E., and Jalife, J. *Null mutation of connexin43 causes slow propagation of ventricular activation in the late stages of mouse embryonic development. Circ Res*, 88(11):1196–1202, 2001.
- [114] Willecke, K., Eiberger, J., Degen, J., Eckardt, D., Romualdi, A., Guldenagel, M., Deutsch, U., and Söhl, G. *Structural and functional diversity of connexin genes in the mouse and human genome. Biol Chem*, 383(5):725–737, 2002.
- [115] Delorme, B., Dahl, E., Jarry-Guichard, T., Marics, I., Briand, J.P., Willecke, K., Gros, D., and Théveniau-Ruissy, M. *Developmental regulation of connexin 40 gene expression in mouse heart correlates with the differentiation of the conduction system. Dev Dyn*, 204(4):358–371, 1995.
- [116] Alcoléa, S., Théveniau-Ruissy, M., Jarry-Guichard, T., Marics, I., Tzouanacou, E., Chauvin, J.P., Briand, J.P., Moorman, A.F., Lamers, W.H., and Gros, D.B. *Downregulation of connexin 45 gene products during mouse heart development. Circ Res*, 84(12):1365–1379, 1999.

- [117] van Veen, A.A., van Rijen, H.V., and Opthof, T. *Cardiac gap junction channels: modulation of expression and channel properties*. *Cardiovasc Res*, 51(2):217–229, 2001.
- [118] de Bakker, J.M., van Capelle, F.J., Janse, M.J., Tasseron, S., Vermeulen, J.T., de Jonge, N., and Lahpor, J.R. *Slow conduction in the infarcted human heart. 'zigzag' course of activation*. *Circulation*, 88(3):915–926, 1993.
- [119] Rohr, S., Schölly, D.M., and Kléber, A.G. *Patterned growth of neonatal rat heart cells in culture. morphological and electrophysiological characterization*. *Circ Res*, 68(1):114–130, 1991.
- [120] Lecanda, F., Towler, D.A., Ziambaras, K., Cheng, S.L., Koval, M., Steinberg, T.H., and Civitelli, R. *Gap junctional communication modulates gene expression in osteoblastic cells*. *Mol Biol Cell*, 9(8):2249–2258, 1998.
- [121] Musil, L.S., Cunningham, B.A., Edelman, G.M., and Goodenough, D.A. *Differential phosphorylation of the gap junction protein connexin43 in junctional communication-competent and -deficient cell lines*. *J Cell Biol*, 111(5 Pt 1):2077–2088, 1990.
- [122] Morgan, H.E. and Baker, K.M. *Cardiac hypertrophy. mechanical, neural, and endocrine dependence*. *Circulation*, 83(1):13–25, 1991.
- [123] Schlaich, M.P., Kaye, D.M., Lambert, E., Sommerville, M., Socratous, F., and Esler, M.D. *Relation between cardiac sympathetic activity and hypertensive left ventricular hypertrophy*. *Circulation*, 108(5):560–565, 2003.
- [124] Oyama, N., Urasawa, K., Kaneta, S., Sakai, H., Saito, T., Takagi, C., Yoshida, I., Kitabatake, A., and Tsutsui, H. *Chronic  $\beta$ -adrenergic receptor stimulation enhances the expression of g-protein coupled receptor kinases, grk2 and grk5, in both the heart and peripheral lymphocytes*. *Circ J*, 69(8):987–990, 2005.
- [125] Kwak, B.R., van Kempen, M.J., Théveniau-Ruissy, M., Gros, D.B., and Jongasma, H.J. *Connexin expression in cultured neonatal rat myocytes reflects the pattern of the intact ventricle*. *Cardiovasc Res*, 44(2):370–380, 1999.
- [126] Takeuchi, S., Akita, T., Takagishi, Y., Watanabe, E., Sasano, C., Honjo, H., and Kodama, I. *Disorganization of gap junction distribution in dilated atria of patients with chronic atrial fibrillation*. *Circ J*, 70(5):575–582, 2006.
- [127] Salameh, A., Frenzel, C., Boldt, A., Ressler, B., Glawe, I., Schulte, J., Mühlberg, K., Zimmer, H.G., Pfeiffer, D., and Dhein, S. *Subchronic  $\alpha$ - and  $\beta$ -adrenergic regulation of cardiac gap junction protein expression*. *FASEB J*, 20(2):365–367, 2006.
- [128] van Rijen, H.V., Eckardt, D., Degen, J., Theis, M., Ott, T., Willecke, K., Jongasma, H.J., Opthof, T., and de Bakker, J.M. *Slow conduction and enhanced anisotropy increase the propensity for ventricular tachyarrhythmias in adult mice with induced deletion of connexin43*. *Circulation*, 109(8):1048–1055, 2004.
- [129] Thomas, S.P., Kucera, J.P., Bircher-Lehmann, L., Rudy, Y., Saffitz, J.E., and Kléber, A.G. *Impulse propagation in synthetic strands of neonatal cardiac myocytes with genetically reduced levels of connexin43*. *Circ Res*, 92(11):1209–1216, 2003.
- [130] Cheng, Q., Ross, R.S., and Walsh, K.B. *Overexpression of the integrin  $\beta_{1A}$  subunit and the  $\beta_{1A}$  cytoplasmic domain modifies the  $\beta$ -adrenergic regulation of the cardiac l-type  $Ca^{2+}$  current*. *J Mol Cell Cardiol*, 36(6):809–819, 2004.
- [131] Maki, T., Gruver, E.J., Davidoff, A.J., Izzo, N., Toupin, D., Colucci, W., Marks, A.R., and Marsh, J.D. *Regulation of calcium channel expression in neonatal myocytes by catecholamines*. *J Clin Invest*, 97(3):656–663, 1996.

- [132] Joyner, R.W. and van Capelle, F.J. *Propagation through electrically coupled cells. how a small sa node drives a large atrium. Biophys J*, 50(6):1157–1164, 1986.
- [133] Gutstein, D.E., Morley, G.E., Vaidya, D., Liu, F., Chen, F.L., Stuhlmann, H., and Fishman, G.I. *Heterogeneous expression of gap junction channels in the heart leads to conduction defects and ventricular dysfunction. Circulation*, 104(10):1194–1199, 2001.
- [134] Oyamada, M., Oyamada, Y., Kaneko, T., and Takamatsu, T. *Regulation of gap junction protein (connexin) genes and function in differentiating es cells. Methods Mol Biol*, 185:63–69, 2002.
- [135] Stengl, M., Volders, P.G., Thomsen, M.B., Spätjens, R.L., Sipido, K.R., and Vos, M.A. *Accumulation of slowly activating delayed rectifier potassium current (iks) in canine ventricular myocytes. J Physiol*, 551(Pt 3):777–786, 2003.
- [136] Burt, J.M. and Spray, D.C. *Volatile anesthetics block intercellular communication between neonatal rat myocardial cells. Circ Res*, 65(3):829–837, 1989.
- [137] Wilders, R., Jongsma, H.J., and van Ginneken, A.C. *Pacemaker activity of the rabbit sinoatrial node. a comparison of mathematical models. Biophys J*, 60(5):1202–1216, 1991.
- [138] Verheijck, E.E., Wilders, R., Joyner, R.W., Golod, D.A., Kumar, R., Jongsma, H.J., Bouman, L.N., and van Ginneken, A.C. *Pacemaker synchronization of electrically coupled rabbit sinoatrial node cells. J Gen Physiol*, 111(1):95–112, 1998.
- [139] Luo, C.H. and Rudy, Y. *A dynamic model of the cardiac ventricular action potential. i. simulations of ionic currents and concentration changes. Circ Res*, 74(6):1071–1096, 1994.
- [140] Wilders, R., Wagner, M.B., Golod, D.A., Kumar, R., Wang, Y.G., Goolsby, W.N., Joyner, R.W., and Jongsma, H.J. *Effects of anisotropy on the development of cardiac arrhythmias associated with focal activity. Pflugers Arch*, 441(2-3):301–312, 2000.
- [141] Jongsma, H.J. and Wilders, R. *Channelopathies: Kir2.1 mutations jeopardize many cell functions. Curr Biol*, 11(18):747–750, 2001.
- [142] Rook, M.B., Jongsma, H.J., and van Ginneken, A.C. *Properties of single gap junctional channels between isolated neonatal rat heart cells. Am J Physiol*, 255(4 Pt 2):770–782, 1988.
- [143] Van Rijen, H.V., Wilders, R., Rook, M.B., and Jongsma, H.J. *Dual patch clamp. Methods Mol Biol*, 154:269–292, 2001.
- [144] van der Heyden, M.A., van Eijk, M., Wilders, R., de Bakker, J.M., and Opthof, T. *Connexin43 orthologues in vertebrates: phylogeny from fish to man. Dev Genes Evol*, 214(5):261–266, 2004.
- [145] Pumir, A., Arutunyan, A., Krinsky, V., and Sarvazyan, N. *Genesis of ectopic waves: role of coupling, automaticity, and heterogeneity. Biophys J*, 89(4):2332–2349, 2005.
- [146] Emanuelli, C., Lako, M., Stojkovic, M., and Madeddu, P. *In search of the best candidate for regeneration of ischemic tissues: are embryonic/fetal stem cells more advantageous than adult counterparts? Thromb Haemost*, 94(4):738–749, 2005.
- [147] van Laake, L.W., Hassink, R., Doevendans, P.A., and Mummery, C. *Heart repair and stem cells. J Physiol*, 577(Pt 2):467–478, 2006.
- [148] Leri, A., Kajstura, J., and Anversa, P. *Cardiac stem cells and mechanisms of myocardial regeneration. Physiol Rev*, 85(4):1373–1416, 2005.
- [149] Smits, A.M., van Vliet, P., Hassink, R.J., Goumans, M.J., and Doevendans, P.A. *The role of stem cells in cardiac regeneration. J Cell Mol Med*, 9(1):25–36, 2005.

- [150] de Boer, T.P., van der Heyden, M.A., Rook, M.B., Wilders, R., Broekstra, R., Kok, B., Vos, M.A., de Bakker, J.M., and van Veen, T.A. *Pro-arrhythmogenic potential of immature cardiomyocytes is triggered by low coupling and cluster size*. *Cardiovasc Res*, 71(4):704–714, 2006.
- [151] Passier, R., Oostwaard, D.W., Snapper, J., Kloots, J., Hassink, R.J., Kuijk, E., Roelen, B., de la Riviere, A.B., and Mummery, C. *Increased cardiomyocyte differentiation from human embryonic stem cells in serum-free cultures*. *Stem Cells*, 23(6):772–780, 2005.
- [152] Xu, C., Police, S., Rao, N., and Carpenter, M.K. *Characterization and enrichment of cardiomyocytes derived from human embryonic stem cells*. *Circ Res*, 91(6):501–508, 2002.
- [153] Beltrami, A.P., Barlucchi, L., Torella, D., Baker, M., Limana, F., Chimenti, S., Kasahara, H., Rota, M., Musso, E., Urbanek, K., Leri, A., Kajstura, J., Nadal-Ginard, B., and Anversa, P. *Adult cardiac stem cells are multipotent and support myocardial regeneration*. *Cell*, 114(6):763–776, 2003.
- [154] Oh, H., Bradfute, S.B., Gallardo, T.D., Nakamura, T., Gaussin, V., Mishina, Y., Pocius, J., Michael, L.H., Behringer, R.R., Garry, D.J., Entman, M.L., and Schneider, M.D. *Cardiac progenitor cells from adult myocardium: homing, differentiation, and fusion after infarction*. *Proc Natl Acad Sci U S A*, 100(21):12313–12318, 2003.
- [155] Laugwitz, K.L., Moretti, A., Lam, J., Gruber, P., Chen, Y., Woodard, S., Lin, L.Z., Cai, C.L., Lu, M.M., Reth, M., Platoshyn, O., Yuan, J.X., Evans, S., and Chien, K.R. *Postnatal *isl1* + cardioblasts enter fully differentiated cardiomyocyte lineages*. *Nature*, 433(7026):647–653, 2005.
- [156] Pfister, O., Mouquet, F., Jain, M., Summer, R., Helmes, M., Fine, A., Colucci, W.S., and Liao, R. **Cd31*- but not *cd31* + cardiac side population cells exhibit functional cardiomyogenic differentiation*. *Circ Res*, 97(1):52–61, 2005.
- [157] Messina, E., De Angelis, L., Frati, G., Morrone, S., Chimenti, S., Fiordaliso, F., Salio, M., Battaglia, M., Latronico, M.V., Coletta, M., Vivarelli, E., Frati, L., Cossu, G., and Giacomello, A. *Isolation and expansion of adult cardiac stem cells from human and murine heart*. *Circ Res*, 95(9):911–921, 2004.
- [158] Behfar, A., Zingman, L.V., Hodgson, D.M., Rauzier, J.M., Kane, G.C., Terzic, A., and Pucéat, M. *Stem cell differentiation requires a paracrine pathway in the heart*. *FASEB J*, 16(12):1558–1566, 2002.
- [159] Slager, H.G., Van Inzen, W., Freund, E., Van den Eijnden-Van Raaij, A.J., and Mummery, C.L. *Transforming growth factor- $\beta$  in the early mouse embryo: implications for the regulation of muscle formation and implantation*. *Dev Genet*, 14(3):212–224, 1993.
- [160] Takahashi, T., Lord, B., Schulze, P.C., Fryer, R.M., Sarang, S.S., Gullans, S.R., and Lee, R.T. *Ascorbic acid enhances differentiation of embryonic stem cells into cardiac myocytes*. *Circulation*, 107(14):1912–1916, 2003.
- [161] Sachinidis, A., Fleischmann, B.K., Kolossov, E., Wartenberg, M., Sauer, H., and Hescheler, J. *Cardiac specific differentiation of mouse embryonic stem cells*. *Cardiovasc Res*, 58(2):278–291, 2003.
- [162] Ménard, C., Hagege, A.A., Agbulut, O., Barro, M., Morichetti, M.C., Brasselet, C., Bel, A., Messas, E., Bissery, A., Bruneval, P., Desnos, M., Pucéat, M., and Menasché, P. *Transplantation of cardiac-committed mouse embryonic stem cells to infarcted sheep myocardium: a preclinical study*. *Lancet*, 366(9490):1005–1012, 2005.
- [163] ten Dijke, P. and Hill, C.S. *New insights into *tgf*- $\beta$ -*smad* signalling*. *Trends Biochem Sci*, 29(5):265–273, 2004.

- [164] Inman, G.J., Nicolás, F.J., Callahan, J.F., Harling, J.D., Gaster, L.M., Reith, A.D., Laping, N.J., and Hill, C.S. *Sb-431542 is a potent and specific inhibitor of transforming growth factor- $\beta$  superfamily type I activin receptor-like kinase (alk) receptors alk4, alk5, and alk7*. *Mol Pharmacol*, 62(1):65–74, 2002.
- [165] Kattman, S.J., Huber, T.L., and Keller, G.M. *Multipotent flk-1+ cardiovascular progenitor cells give rise to the cardiomyocyte, endothelial, and vascular smooth muscle lineages*. *Dev Cell*, 11(5):723–732, 2006.
- [166] Moretti, A., Caron, L., Nakano, A., Lam, J.T., Bernshausen, A., Chen, Y., Qyang, Y., Bu, L., Sasaki, M., Martin-Puig, S., Sun, Y., Evans, S.M., Laugwitz, K.L., and Chien, K.R. *Multipotent embryonic isl1+ progenitor cells lead to cardiac, smooth muscle, and endothelial cell diversification*. *Cell*, 127(6):1151–1165, 2006.
- [167] Mouquet, F., Pfister, O., Jain, M., Oikonomopoulos, A., Ngoy, S., Summer, R., Fine, A., and Liao, R. *Restoration of cardiac progenitor cells after myocardial infarction by self-proliferation and selective homing of bone marrow-derived stem cells*. *Circ Res*, 97(11):1090–1092, 2005.
- [168] Li, T.S., Hayashi, M., Ito, H., Furutani, A., Murata, T., Matsuzaki, M., and Hamano, K. *Regeneration of infarcted myocardium by intramyocardial implantation of ex vivo transforming growth factor- $\beta$ -preprogrammed bone marrow stem cells*. *Circulation*, 111(19):2438–2445, 2005.
- [169] Flanders, K.C., Holder, M.G., and Winokur, T.S. *Autoinduction of mrna and protein expression for transforming growth factor- $\beta$ s in cultured cardiac cells*. *J Mol Cell Cardiol*, 27(2):805–812, 1995.
- [170] Goumans, M.J., Valdimarsdottir, G., Itoh, S., Rosendahl, A., Sideras, P., and ten Dijke, P. *Balancing the activation state of the endothelium via two distinct tgf- $\beta$  type I receptors*. *EMBO J*, 21(7):1743–1753, 2002.
- [171] Kehat, I., Kenyagin-Karsenti, D., Snir, M., Segev, H., Amit, M., Gepstein, A., Livne, E., Binah, O., Itskovitz-Eldor, J., and Gepstein, L. *Human embryonic stem cells can differentiate into myocytes with structural and functional properties of cardiomyocytes*. *J Clin Invest*, 108(3):407–414, 2001.
- [172] Tateishi, K., Ashihara, E., Honsho, S., Takehara, N., Nomura, T., Takahashi, T., Ueyama, T., Yamagishi, M., Yaku, H., Matsubara, H., and Oh, H. *Human cardiac stem cells exhibit mesenchymal features and are maintained through akt/gsk-3 $\beta$  signaling*. *Biochem Biophys Res Commun*, 352(3):635–641, 2007.
- [173] Goumans, M.J., de Boer, T.P., Smits, A.M., Van Laake, L.W., Sluijter, J.P.G., van Vliet, P., Van der Heyden, M.A.G., Pasterkamp, G., Mummery, C.L., Van Veen, T.A.B., and Doevendans, P.A. *Tgf $\beta$ 1 induces efficient differentiation of human cardiomyocyte progenitor cells into functional cardiomyocytes in vitro*. *In review*, 2007.
- [174] de Boer, T.P., Kok, B., Roël, G., van Veen, T.A., Destrée, O.H., Rook, M.B., Vos, M.A., de Bakker, J.M., and van der Heyden, M.A. *Cloning, embryonic expression, and functional characterization of two novel connexins from xenopus laevis*. *Biochem Biophys Res Commun*, 349(2):855–862, 2006.
- [175] Verkerk, A.O., van Ginneken, A.C., van Veen, T.A., and Tan, H.L. *Effects of heart failure on brain-type na+ channels in rabbit ventricular myocytes*. *Europace*, 2007.
- [176] Ilkovski, B., Clement, S., Sewry, C., North, K.N., and Cooper, S.T. *Defining  $\alpha$ -skeletal and  $\alpha$ -cardiac actin expression in human heart and skeletal muscle explains the absence of cardiac involvement in acta1 nemaline myopathy*. *Neuromuscul Disord*, 15(12):829–835, 2005.
- [177] Clément, S., Stouffs, M., Bettiol, E., Kampf, S., Krause, K.H., Chaponnier, C., and Jaconi, M. *Expression and function of  $\alpha$ -smooth muscle actin during embryonic-stem-cell-derived cardiomyocyte differentiation*. *J Cell Sci*, 120(Pt 2):229–238, 2007.



- [178] Schram, G., Pourrier, M., Wang, Z., White, M., and Nattel, S. *Barium block of kir2 and human cardiac inward rectifier currents: evidence for subunit-heteromeric contribution to native currents.* *Cardiovasc Res*, 59(2):328–338, 2003.
- [179] Zorn-Pauly, K., Schaffer, P., Pelzmann, B., Bernhart, E., Lang, P., Zink, M., Mächler, H., Rigler, B., and Koidl, B. *A hyperpolarization activated inward current (if) is present in infant ventricular myocytes.* *Basic Res Cardiol*, 98(6):362–366, 2003.
- [180] Lonardo, G., Cerbai, E., Casini, S., Giunti, G., Bonacchi, M., Battaglia, F., Fiorani, B., Stefano, P.L., Sani, G., and Mugelli, A. *Pharmacological modulation of the hyperpolarization-activated current (i<sub>f</sub>) in human atrial myocytes: focus on g protein-coupled receptors.* *J Mol Cell Cardiol*, 38(3):453–460, 2005.
- [181] Sakakibara, Y., Wasserstrom, J.A., Furukawa, T., Jia, H., Arentzen, C.E., Hartz, R.S., and Singer, D.H. *Characterization of the sodium current in single human atrial myocytes.* *Circ Res*, 71(3):535–546, 1992.
- [182] Sakakibara, Y., Furukawa, T., Singer, D.H., Jia, H., Backer, C.L., Arentzen, C.E., and Wasserstrom, J.A. *Sodium current in isolated human ventricular myocytes.* *Am J Physiol*, 265(4 Pt 2):H1301–9, 1993.
- [183] Schroder, F., Handrock, R., Beuckelmann, D.J., Hirt, S., Hullin, R., Priebe, L., Schwinger, R.H., Weil, J., and Herzig, S. *Increased availability and open probability of single l-type calcium channels from failing compared with nonfailing human ventricle.* *Circulation*, 98(10):969–976, 1998.
- [184] Gassanov, N., Brandt, M.C., Michels, G., Lindner, M., Er, F., and Hoppe, U.C. *Angiotensin ii-induced changes of calcium sparks and ionic currents in human atrial myocytes: potential role for early remodeling in atrial fibrillation.* *Cell Calcium*, 39(2):175–186, 2006.
- [185] Mewes, T. and Ravens, U. *L-type calcium currents of human myocytes from ventricle of non-failing and failing hearts and from atrium.* *J Mol Cell Cardiol*, 26(10):1307–1320, 1994.



## Hoofdstuk 10

### Nederlandse samenvatting

Stamcellen zijn cellen met een aantal bijzondere eigenschappen. Ten eerste kunnen ze zichzelf vernieuwen, wat als consequentie heeft dat ze ongedifferentieerd kunnen blijven. De dochtercellen die na deling ontstaan kunnen vervolgens differentiëren, wat wil zeggen dat ze zich ontwikkelen tot een bepaald weefseltype met specifieke eigenschappen. De capaciteit tot zelfvernieuwing en de soorten weefsel die kunnen ontstaan uit de dochtercellen hangen af van het type stamcel. Embryonale stamcellen, die te vinden zijn in zeer jonge embryo's, kunnen alle drie primaire weefseltypen die in een embryo te vinden zijn maken; endoderm, ectoderm en mesoderm. Hieruit ontstaan respectievelijk (grofweg) de darmen en interne organen, de huid en hersenen, en het spierweefsel en botten. Andere stamcellen, zoals bijvoorbeeld volwassen beenmergcellen, of skeletspier myoblasten, hebben een meer beperkte plasticiteit; zij kunnen slechts differentiëren tot bloedcellen of skeletspiercellen.

De isolatie van embryonale stamcellen, en de mogelijkheid om deze in kweek te houden, heeft ontwikkelingsbiologen een belangrijk instrument gegeven om de vroege embryonale ontwikkeling te bestuderen. Deze cellen zijn bij uitstek geschikt om de signalen te ontdekken die de vorming van de drie weefseltypen sturen. Daarnaast zouden stamcellen gebruikt kunnen worden om nieuwe weefsels te genereren in een laboratorium, die mogelijk gebruikt kunnen worden om slecht functionerende weefsels in patiënten te repareren. Een van de toepassingen is de behandeling van patiënten met hartfalen met nieuwe hartspiercellen. De toevoeging van nieuwe spierkracht zou in principe de slechte hartfunctie kunnen verbeteren. Klinische studies waarin diverse soorten stamcellen in de harten van patiënten zijn gespoten hebben echter tot bedenkingen geleid. Het bleek namelijk dat sommige patiënten na de behandeling ernstige kamerritmestoornissen ontwikkelden die zonder verder ingrijpen levensbedreigend zijn. Het ontstaan van dit soort hartritmestoornissen en de onderliggende mechanismen zijn het centrale thema van dit proefschrift.

Om een beter inzicht te krijgen in de betrokken mechanismen hebben we experimenten gedaan die de situatie op verschillende niveau's belichten. Verschillende factoren kunnen het ontstaan van ritmestoornissen in het hart in de hand werken. Ten eerste kunnen hartspiercellen onder bepaalde omstandigheden ongepaste spontane activiteit ontwikkelen. Ten tweede kan een verminderde elektrische koppeling tussen hartspiercellen zorgen voor vertraging van de impulsgeleiding, wat het ontstaan van ritmestoornissen kan bevorderen. Tenslotte kunnen veranderingen in de weefselstructuur, als gevolg van het ontstaan van fibrose, de impulsgeleiding verstoren.

In het eerste hoofdstuk van dit proefschrift hebben wij onderzocht hoe elektrische koppeling door middel van gap junction-eiwitten (connexines) gereguleerd wordt in zich differentiërende stamcellen. Uit onze experimenten bleek dat connexine-43, het belangrijkste connexine-eiwit in het hart, onderdrukt wordt door Snail1, een zogenaamde transcriptiefactor. Transcriptiefactoren zijn eiwitten die de activiteit van genen op een directe wijze kunnen beïnvloeden. Wanneer we de expressie van Snail1 onderdrukten, resulteerde dit in toegenomen expressie van connexine-43, hetgeen de rol van Snail1 bevestigde. Tevens hebben we een verband kunnen leggen tussen activiteit van Snail1 en de morfologie van de cellen. Het bleek dat remming van Snail1 een verandering in het weefselverband op gang bracht. Deze experimenten geven aan dat Snail1 betrokken is bij de regulatie van connexine-43 expressie en een rol speelt bij mesodermale differentiatie van stamcellen.

Vervolgens hebben we in hoofdstuk 2 onderzocht of de ongewenste spontane activiteit van immature hartspiercellen te reguleren is. Hiertoe hebben we immature hartspiercellen gekweekt en daar HEK-cellen aan toegevoegd die Kir2.1 tot expressie brengen. Kir2.1 is het eiwit dat het  $I_{K1}$ -kanaal vormt, het belangrijkste kaliumkanaal in het hart dat de membraanpotentiaal stabiliseert. Het zorgt er voor dat volwassen hartspiercellen een rustmembraanpotentiaal hebben in de orde van  $-85$  mV en mede daardoor niet spontaan actief zijn. Uit onze experimenten bleek dat de stabiliserende werking van het  $I_{K1}$ -kanaal in de HEK-cellen overgedragen kon worden op de immature hartspiercellen. Dit ondersteunt ons concept waarin we beogen spontane activiteit van getransplanteerde stamcelafgeleide hartspiercellen te remmen door toevoeging van cellen die  $I_{K1}$  tot expressie brengen. Tevens biedt dit concept mogelijkheden voor de bestrijding van gelokaliseerde aritmogene regio's in harten van patiënten. Wellicht kan aritmogenese vanuit deze regio's voorkomen worden door via celtransplantatie lokaal  $I_{K1}$  toe te voegen.

Een belangrijke invloed op zich ontwikkelende hartspiercellen na de geboorte wordt uitgeoefend door adrenaline. Deze stof speelt tevens een belangrijke rol bij de veranderingen die optreden in harten van patiënten met hartfalen. Omdat veranderingen in adrenalinespiegels gerelateerd zijn aan veranderingen in de impulsgeleidingssnelheid in het hart, hebben wij de invloed van adrenerge stimuli op immature hartspiercellen onderzocht (hoofdstuk 3). Uit onze experimenten bleek, in tegenstelling tot eerdere onderzoeken, dat de toename in geleidingssnelheid na  $\beta$ -adrenerge stimulatie niet toe te schrijven was aan een toegenomen intercellulaire koppeling. Wat echter bleek was dat de hartspiercellen sneller depolariseerden, sneller activeerden en hun activiteit zo eerder doorgaven aan de naastliggende cellen. Verhoging van impulsgeleidingssnelheid duidt op toegenomen ontwikkeling van de cellen, wat betekent dat  $\beta$ -adrenerge stimulatie wellicht ook de differentiatie van stamcelafgeleide hartspiercellen kan bevorderen.

Het is vrijwel onmogelijk om de interacties tussen getransplanteerde immature hartspiercellen en mature hartcellen in het ontvangende hart in vivo te bestuderen. Om deze interacties toch te kunnen onderzoeken hebben we een in vitro model gemaakt, bestaande uit volwassen, niet spontaan actieve hartspiercellen en immature, spontaan actieve hartspiercellen (hoofdstuk 4). Het bleek dat de immature hartspiercellen in staat waren om de volwassen cellen te activeren, wat samen bleek te hangen met een inefficiënte elektrische koppeling tussen de twee celtypen. Door de electrofysiologische para-

meters van de cellen in ons in vitro model te gebruiken in computersimulaties, konden we onze bevindingen extrapoleren naar het weefselniveau. Dit leidde tot de conclusie dat normaal inactieve adulte hartspiercellen door immature cellen geactiveerd kunnen worden als deze relatief slecht gekoppeld zijn met de adulte cellen en in voldoende grote clusters aanwezig zijn. Dit geeft ons richtlijnen waaraan hartspiercellen bedoeld voor transplantatie moeten voldoen om niet aritmogeen te zijn; ze moeten voldoende connexine-43 tot expressie brengen en niet spontaan actief zijn. Verder dient clustering voorkomen te worden, wat vooral eisen stelt aan de wijze van transplantatie.

In de laatste twee hoofdstukken hebben we een nieuw soort stamcel onderzocht die tot hartspiercellen kan differentiëren. In hoofdstuk 5 hebben wij laten zien dat deze zogenaamde hartprogenitorcellen (voorlopercellen), afkomstig uit foetale harten, zich in kweek sterk kunnen vermenigvuldigen. Na een differentiatieprotocol waarin TGF $\beta$ 1, een groeifactor, een belangrijke rol speelt, verkregen we hartspiercellen met een relatief goed ontwikkeld fenotype. Dit uitte zich in een vrij negatieve membraan potentiaal, sterke elektrische koppeling tussen de cellen en expressie van hartspecifieke eiwitten. Verder bleek dat de cellen reageerden op  $\beta$ -adrenerge stimuli, wat wellicht mogelijkheden biedt voor een verdere ontwikkeling in vitro. De combinatie van eigenschappen geeft aan dat deze nieuwe stamcel na differentiatie meer volwassen is dan bijvoorbeeld hartspiercellen gedifferentieerd uit embryonale stamcellen.

De elektrofysiologische eigenschappen van de hartspiercellen gevormd uit foetale hartprogenitorcellen hebben we verder bestudeerd in hoofdstuk 6. De negatieve rustmembraanpotentiaal van deze hartspiercellen die we eerder gemeten hadden, suggereerde dat de cellen het  $I_{K1}$ -kanaal tot expressie brengen. De expressie van ionkanalen en -transporters hebben we op mRNA-niveau bestudeerd en uit deze experimenten bleek dat alle belangrijke hartspecifieke kanalen en transporters tot expressie komen in gedifferentieerde hartprogenitorcellen. Met behulp van de voltage clamp techniek hebben we gecontroleerd of deze mRNA-expressie ook daadwerkelijk leidde tot functionerende ionkanalen. Hieruit bleek dat de cellen de kanalen verantwoordelijk voor  $I_{Na}$ ,  $I_{Ca,L}$ ,  $I_{K1}$  en  $I_f$  tot expressie brachten met niveau's die niet veel afwijken van de niveau's die aanwezig zijn in adulte hartspiercellen. Andere experimenten wezen uit dat de belangrijkste eiwitten betrokken bij mechanische en elektrische integratie van cellen in het hart ook tot expressie komen in de gedifferentieerde hartprogenitorcellen. In combinatie met de bevindingen in hoofdstuk 5 geven onze experimenten aan dat foetale hartprogenitorcellen gebruikt kunnen worden om hartspiercellen te maken die betere eigenschappen hebben in relatie tot pro-aritmogenese dan voorheen bekende stamcellen. Klinische toepassing van hartprogenitorcellen uit foetale harten stuit echter op een aantal problemen. Deze zijn ethisch van aard, maar ook zijn problemen te verwachten met immunologische afstoting. Onder andere om die redenen hebben we ook hartprogenitorcellen geïsoleerd uit harttoortjes van volwassen patiënten. Deze cellen moeten nog nader bestudeerd worden, maar het is wel duidelijk dat ook met behulp van de adulte hartprogenitorcellen op uiterst efficiënte wijze nieuwe hartspiercellen gegenereerd kunnen worden. De eerste elektrofysiologische experimenten wijzen erop dat de hartspiercellen die op deze wijze verkregen zijn zelfs nog verder ontwikkeld zijn dan wanneer foetale hartprogenitorcellen gebruikt worden. Verder onderzoek zal moeten uitwijzen wat de klinische toepasbaarheid zal zijn wanneer deze cellen op autologe wijze geproduceerd worden.



# Chapter 11

## List of publications

### *Peer-reviewed publications*

J.C. Moore, R. Spijker, A.C. Martens, T.P. de Boer, M.B. Rook, M.A.G. van der Heyden, L.G.J. Tertoolen, C.L. Mummery. *A P19Cl6 GFP reporter line to quantify cardiomyocyte differentiation of stem cells*. *Int J Dev Biol*. 2004 Feb ; 48(1): 47-55.

T.P. de Boer, G.J.M. Kok, K.I. Neuteboom, N. Spieker, J. de Graaf, O.H.J. Destrée, M.B. Rook, T.A.B. van Veen, H.J. Jongsma, M.A. Vos, J.M.T. de Bakker, M.A.G. van der Heyden. *Cloning and functional characterization of a novel connexin expressed in somites of Xenopus laevis*. *Dev Dyn*. 2005 Jul ; 233(3): 864-71.

T.P. de Boer, M.A.G. van der Heyden. *Xenopus connexins: how frogs bridge the gap*. *Differentiation*. 2005 Sep ; 73(7): 330-40.

T.P. de Boer, T.A.B. van Veen, M.J. Houtman, J.A. Jansen, S.C.M. van Amersfoort, P.A. Doevendans, M.A. Vos, M.A.G. van der Heyden. *Inhibition of cardiomyocyte automaticity by electrotonic application of inward rectifier current from Kir2.1 expressing cells*. *Med Biol Eng Comput*. 2006 Jul ; 44(7): 537-42.

T.P. de Boer, M.A.G. van der Heyden, M.B. Rook, R. Wilders, R. Broekstra, G.J.M. Kok, M.A. Vos, J.M.T. de Bakker, T.A.B. van Veen. *Pro-arrhythmogenic potential of immature cardiomyocytes is triggered by low coupling and cluster size*. *Cardiovasc Res*. 2006 Sep 1; 71(4): 704-14.

T.P. de Boer, G.J.M. Kok, G. Roël, T.A.B. van Veen, O.H.J. Destrée, M.B. Rook, M.A. Vos, J.M.T. de Bakker, M.A.G. van der Heyden. *Cloning, embryonic expression, and functional characterization of two novel connexins from Xenopus laevis*. *Biochem Biophys Res Commun*. 2006 Oct 20; 349(2): 855-62.

T.P. de Boer, T.A.B. van Veen, M.F.A. Bierhuizen, G.J.M. Kok, M.B. Rook, K.J.M. Boonen, M.A. Vos, P.A. Doevendans, J.M.T. de Bakker, M.A.G. van der Heyden. *Connexin43 repression following epithelium-to-mesenchyme transition in embryonal carcinoma cells requires Snail1 transcription factor*. *Differentiation*. 2007 Mar ; 75(3): 208-18.

T.P. de Boer, H.V.M. van Rijen, M.A.G. van der Heyden, G.J.M. Kok, T. Opthof, M.A. Vos, H.J. Jongasma, J.M.T. de Bakker, T.A.B. van Veen.  *$\beta$ -, not  $\alpha$ -adrenergic stimulation enhances conduction velocity in cultures of neonatal cardiomyocytes.* *Circ J.* 2007 Jun ; 71(6): 973-81.

#### *Chapters in books*

J.C. Moore, T.P. de Boer, M.A.G. van der Heyden, L.G.J. Tertoolen, C.L. Mummery. *Stem cells and cardiomyocytes.* Chapter in: *Cardiovascular research: new technologies methods and applications.* Editors G. Pasterkamp and D.P. Kleijn (2006).

C.L. Mummery, M.A.G. van der Heyden, T.P. de Boer, R. Passier, D. Ward, C.E. van den Brink, M.A. van Rooijen, A. van de Stolpe. *ES derived cardiomyocytes.* Chapter in: *Methods in Molecular Medicine Tissue engineering 2nd edition.* Editors H. Hauser and M. Fussenegger (2007).

T.P. de Boer, T.A.B. van Veen, M.J. Houtman, J.A. Jansen, S.C.M. van Amersfoort, P.A. Doevendans, M.A. Vos, M.A.G. van der Heyden. *Inhibition of cardiomyocyte automaticity by electrotonic application of inward rectifier current from Kir2.1 expressing cells.* Chapter in: *Biopacemaking.* Editors J.M.T. de Bakker and A. Zaza (2007).

#### *Abstracts*

T.P. de Boer, G.J.M. Kok, G. Roel, N. Spieker, O.H.J. Destrée, M.B. Rook, T.A.B. van Veen, M.A. Vos, J.M.T. de Bakker, M.A.G. van der Heyden. *Cloning, characterization and expression of three novel connexins from Xenopus Laevis.* *Cell Commun. Adhes.* 12 (3&4): 127-216 May 2005

T.P. de Boer, M.A.G. van der Heyden, M.B. Rook, R. Broekstra, M.A. Vos, J.M.T. de Bakker, T.A.B. van Veen. *A co-culture model for stem cell transplantation related arrhythmogenesis.* *J. Mol. Cell. Cardiol.* 39 (1): 195-196 75 JUL 2005

M.A.G. van der Heyden, T.P. de Boer, G.J.M. Kok, A.A.B. van Veen, M.F.A. Bierhuizen, M.B. Rook, K.J.M. Boonen, M.A. Vos, P.A. Doevendans, J.M.T. de Bakker *Connexin43 inversely correlates with snail transcription factor during stem cell differentiation.* *J. Mol. Cell. Cardiol.* 39 (1): 188-188 55 JUL 2005

M.J. Goumans, T.P. de Boer, A. Smits, L.W. van der Laake, P. van Vliet, M.A.G. van der Heyden, T.A.B. van Veen, P.A. Doevendans. *Human cardiac progenitor cells are able to differentiate into cardiomyocytes in vitro.* *Circulation* 112 (17): U106-U106 337 Suppl. 2 Oct 25 2005

T.P. de Boer, T.A.B. van Veen, G.J.M. Kok, M.F.A. Bierhuizen, M.B. Rook, K.J.M. Boonen, M.A. Vos, P.A. Doevendans, J.M.T. de Bakker, M.A.G. van der Heyden. *Connexin isoform switching in stem cells undergoing epithelium-to-mesenchyme transition: connexin43 is a direct target of Snail1 transcription factor.* *J. Mol. Cell. Cardiol.* 40 (2006) 989



T.P. de Boer, T.A.B. van Veen, M.K.B. Jonsson, G.J.M. Kok, J.P.G. Sluiter, M.J. Goumans, P.A. Doevendans, J.M.T. de Bakker, M.A.G. van der Heyden. *The functional electrophysiology of cardiomyocytes differentiated from human cardiac progenitor cell*. Heart Rhythm (2007) 4, S3

P. van Vliet, T.P. de Boer, J.P.G. Sluiter, M.A.G. van der Heyden, P.A. Doevendans, M.J. Goumans *Potassium inward rectifier expression is regulated by TGF $\beta$  and BMP and increases during differentiation of cardiomyocyte progenitor cells*. European Heart Journal (2007) 28 (Abstract Supplement), 3

P. van Vliet, T.P. de Boer, J.P.G. Sluiter, M.A.G. van der Heyden, P.A. Doevendans, M.J. Goumans *Potassium Inward Rectifier Expression Is Regulated By TGF $\beta$  And BMP In Human Cardiomyocyte Progenitor Cells*. Scientific Sessions 2007, American Heart Association (in press)



## Hoofdstuk 12

### Dankwoord

Elektrofysiologische experimenten, en dan vooral de cellulaire soort, worden meestal niet door groepen mensen uitgevoerd. Sterker nog, je zit vaak de hele dag in je eentje achter je microscoop. Dit lijkt misschien saai of eenzaam voor de toeschouwer, maar het werk is leuk en in de praktijk zit je er toch niet helemaal alleen. Met enige regelmaat waait er iemand het lab binnen, zwaaiend met een mooi experiment, een mislukking of gewoon een kop koffie. En af en toe, wanneer je net een mooie proef aan het doen bent, komt juist dan iemand binnen met wie je dit kunt delen. Deze contacten zijn een belangrijke reden geweest dat ik het vier jaar vol heb gehouden achter mijn microscoop, en ik wil iedereen daar hartelijk voor bedanken!

Bijzondere aandacht verdienen mijn twee co-promotoren. Begeleiding door een duo zou in principe aanleiding kunnen zijn voor een hoop conflicten en gedoe waar je als promovendus klem tussen komt te zitten. Daarvan is bij Toon en Marcel absoluut geen sprake, vanaf de eerste dag hebben ze er zich gezamenlijk voor ingezet om mij te helpen een zelfstandig onderzoeker te worden. In welke mate dit gelukt is zal moeten blijken, maar voor mij is duidelijk dat ze het geweldig gedaan hebben. Verder is het in het academische wereldje waarin we zitten erg makkelijk om je te beperken tot zakelijkheden, maar Marcel en Toon hebben dat niet gedaan. Daardoor heb ik altijd in een prettige sfeer kunnen werken, ook als het buiten het werk even tegenzat. Of natuurlijk samen blij zijn als je in Bristol op een congres bent en van daaruit een huis gekocht hebt met je vriendin!

Mijn promotor, Jacques, verdient alle lof voor zijn deskundige commentaren, enthousiasme en ondersteuning. Ik denk met plezier terug aan de experimenten in Amsterdam met een prof die ook echt proeven doet. (Voor de mensen die niet vaak in een lab komen; dit is tamelijk uitzonderlijk). Marc, die faciliteren van onderzoek als een belangrijke taak ziet, heeft dit uitstekend gedaan. De sprong in de toekomst die ons cellulaire lab gemaakt heeft was niet mogelijk geweest zonder zijn adequate handelen, maar ook zijn inzichten in fysiologie, reviewprocessen en de hogere politiek in de wetenschap hebben mij een hoop geleerd.

Er zijn natuurlijk nog veel meer mensen die een belangrijke bijdrage hebben geleverd aan dit proefschrift. Bart heeft een enorme moleculaire berg verzet, Shirley heeft er telkens voor gezorgd dat de experimenten in Amsterdam prima voorbereid waren. Jet zorgde telkens weer voor verse hondemyocyten, samen met Morten en Marien. Gudrun heeft dat natuurlijk ook gedaan, maar daarbij was ze ook nog een uitstekende (en grappige) discussiepartner op het gebied van de cellulaire elektrofysiologie. Ik

hoop dat we elkaar nog vaak tegenkomen, al ga je straks naar België!. Ook Martin heeft mij een hoop bijgebracht over de cellulaire elektrofysiologie en was ook altijd in voor wat knutselaarij (of bolbliksems maken). Daarnaast wil ik ook Harold, Marti, Tobias, en Maria bedanken voor hun hulp, kritiek of experimentele input in dit proefschrift. Dit geldt ook voor de collega's van Experimentele Cardiologie, Marie-José, Pieter, Anke, Piet, Joost, Linda en Corina. Laten we hopen dat ons harde werk goed terecht komt!

Mijn kamergenoten, Mèra en Stephan wil ik bedanken voor hun gezelligheid en tolerantie jegens mijn bureauindeling en agressieve planten. Ook de andere AIO's (Mohamed, Peter, John, Avram, Birgit en Linda) wil ik bedanken voor hun bijdragen en ze succes wensen. John, ik zal proberen wat minder grappen over Tiel te maken, maar ik beloof niets... Alle studenten die in onze stamcelclub hebben gewerkt wil ik bedanken, en dan speciaal Malin en Raimond. Tonny, behalve een competente secretaresse ben je het sociale middelpunt van onze afdeling, bedankt daarvoor!

Dit proefschrift had niet tot stand kunnen komen zonder de steun van de liefste vrouw die ik ken, Roos. Ik heb veel tijd gestoken in mijn werk, wat nogal eens ten koste is gegaan is van ons leven samen en toch ben je me blijven steunen. Daarvoor kan ik je niet genoeg bedanken! Ik hoop dat ik nog heel erg lang kan genieten van je warme en sprankelende karakter.

Teun

## **Chapter 13**

### **Curriculum vitae**

Born on the sixth of April, 1978, Teun de Boer was raised in Raalte. Starting in 1990, he attended atheneum at Zwijsen College, Veghel, from which he graduated in 1996. After an inspiring period of studying technical physics at the Technical University Eindhoven, he started with new enthusiasm in Utrecht in 1998. In this city he commenced Medical Biology at the medical faculty. He did his first internship supervised by dr. Leon Tertoolen at the Hubrecht Laboratory where he studied the electrophysiology of murine and human embryonic stem cells. Inspired by developmental biology, he did his second internship supervised by dr. Robbert Notenboom at the Rudolf Magnus Institute of Neuroscience. Here he focussed on an animal model of febrile seizures, childhood seizures that appeared to alter brain development. After writing his masters thesis on 'Spatial specificity of cAMP signaling in the heart', again supervised by dr. Leon Tertoolen, he started his PhD-training as displayed in this thesis on stem cell electrophysiology in the laboratory of Medical Physiology, under supervision of dr. Marcel van der Heyden and dr. Toon van Veen.